ANL-6862

Argonne National Laboratory

TWO-PHASE HEAT TRANSFER WITH GAS INJECTION THROUGH A POROUS BOUNDARY SURFACE

by

A. A. Kudirka

ANL-6862
Engineering and Equipment
(TID-4500, 31st Ed.)
AEC Research and
Development Report

ARGONNE NATIONAL LABORATORY
9700 South Cass Avenue
Argonne, Illinois 60440

TWO-PHASE HEAT TRANSFER WITH GAS INJECTION THROUGH A POROUS BOUNDARY SURFACE

by

A. A. Kudirka

Reactor Engineering Division, ANL
and
Associated Midwest Universities

Reproduced from a Thesis Submitted in Partial Fulfillment of the Requirements for the Degree of Doctor of Philosophy of Nuclear Engineering in the Graduate School of Purdue University.

March 1964

Operated by The University of Chicago
under
Contract W-31-109-eng-38
with the
U. S. Atomic Energy Commission

FOREWORD

This report is one of a series that describes heat-transfer and fluid-flow studies performed at Argonne under a program sponsored jointly by the Associated Midwest Universities and the Argonne National Laboratory.

The earlier reports in this series are:

ANL-6625 Local Parameters in Cocurrent Mercury-Nitrogen Flow
L. G. Neal

ANL-6667 A Study of the Flow of Saturated Freon-11 through Apertures and Short Tubes
Hans K. Fauske and Tony C. Min

ANL-6674 Reduction of Vapor Carryunder in Simulated Boiling
P. L. Miller and C. P. Armstrong

ANL-6710 Transient Behavior of a Natural-Circulation Loop Operating Near the Thermodynamic Critical Point
Darrel G. Harden

ANL-6734 Two-phase (Gas-liquid) System: Heat Transfer and Hydraulics. An Annotated Bibliography
Robert R. Kepple and Thomas V. Tung

ANL-6738 Development of an Electrical Resistivity Probe for Void-fraction Measurements in Air-Water Flow
George P. Nassos

ANL-6754 An Experimental Investigation of Two-phase, Two-component Flow in a Horizontal, Converging-diverging Nozzle
Joseph A. Vogrin, Jr.

ANL-6755 Two-component Two-phase Flow Parameters for Low Circulation Rates
Georges E. Smissaert

ANL-6779 Two-phase Critical Flow with Application to Liquid-Metal Systems (Mercury, Cesium, Rubidium, Potassium, Sodium, and Lithium)
Hans K. Fauske

ANL-6796 The Slug-annular Flow Regime Transition at Elevated Pressure
Peter Griffith

ANL-6854 Effect of a Transverse Magnetic Field on Vertical Two-phase Flow through a Rectangular Channel
Richard J. Thome

TABLE OF CONTENTS

TABLE OF CONTENTS

TABLE OF CONTENTS

LIST OF FIGURES

LIST OF FIGURES

LIST OF TABLES

LIST OF SYMBOLS

TWO-PHASE HEAT TRANSFER WITH GAS INJECTION THROUGH A POROUS BOUNDARY SURFACE

by

A. A. Kudirka

ABSTRACT

Hydrodynamic aspects of two-phase heat transfer were studied experimentally in a forced-circulation system for the low-quality range. The role and influence of nucleation and convective mechanisms in enhancing heat transfer, the nature of the nucleation mechanism, including the influence of flow pattern, mass velocity, void fraction, and quality on the rate and nature of heat transfer were investigated.

These aspects of two-phase heat transfer were studied not with an actual boiling system, but with a two-component system where the hydrodynamic aspects of boiling were simulated by bubbling air through the wall of a porous heated tube into water and by ethylene glycol flowing upward inside the tube at room temperature and atmospheric pressure. The porous tube was $\frac{5}{8}$-in. I.D., with an 11-in. long electrically heated section and an 11-in. long unheated section preceding it.

Since one objective of this study was to verify experimentally the hydrodynamic similarity between boiling and bubbling of air from a porous surface, comparisons with boiling systems were made. A photographic comparison of bubbling and boiling from identical tubes in a tank of "Freon-11" showed the processes to be similar.

Void fractions for air-water flowing in the tube, obtained with the gamma-ray attenuation technique, could be correlated in terms of slip ratio versus volumetric gas/liquid ratio. Heat-transfer results could be correlated better using volumetric gas/liquid ratios than void fractions. Phase distributions with and without gas injection at the walls were different due to influence of gas bubbling, but heat-transfer results could be explained better in terms of local conditions at the heated wall instead of the overall phase distributions in the tube.

Correlation of two-phase heat-transfer results with no gas bubbling from the walls showed that dependence of heat-transfer coefficient on mass velocity and volumetric gas/liquid ratio at low qualities was much smaller than is usually associated with higher qualities.

The influence of gas-bubbling rate on heat transfer was additive, but algebraically rather than arithmetically as was previously claimed. While the heat-transfer coefficient always increased with increasing bubbling rate for air-ethylene glycol, it sometimes decreased for air-water. A simplified superposition type model based on microconvection, vapor-liquid exchange, and "convection area reduction" mechanisms predicted the trends of bubbling rate on heat transfer satisfactorily.

Gas-injection results at low and moderate bubbling rates compared quite well with nucleate pool boiling when convective heat-transfer rates were relatively low. This agreement indicated that the high heat-transfer rates at low and moderate boiling-heat fluxes in circulation as well as pool systems are caused mainly by microconvection and vapor-liquid exchange action of bubbles. Hence, the enhancement in heat transfer is hydrodynamic in nature, making latent heat transport unimportant as a heat-transfer mechanism.

For forced-circulation air-water results with gas injection, convection was dominant, and increases in heat-transfer rate with gas addition were mainly due to increased convection rates. Hence, air-water results could not be represented in terms of pool boiling. Examination of various systems indicated that the diameter of air bubbles may be important in determining the influence of air-injection rate.

INTRODUCTION

It is important to be able to remove the large amounts of heat produced in nuclear power reactors rapidly and efficiently, so that the maximum advantages and economies inherent in these high-power density systems can be realized. One of the most attractive methods that produces high heat-transfer rates at low temperature differences involves vaporization of liquid flowing through the reactor core. To make effective use of this two-phase heat-transfer process in designing efficient yet safe reactor-heat-removal systems, reliable prediction methods for heat transfer and flow behavior under various operating conditions are needed.

A recent analysis (1) of available two-phase heat-transfer prediction methods showed that no reliable method exists for predicting two-phase heat-transfer coefficients for a general range of conditions. This situation exists because the two-phase heat-transfer process is complicated; different boiling, or evaporation, regimes exist that are influenced in different ways by many variables. Two-phase flow patterns and local conditions also affect the two-phase heat-transfer coefficient in important ways. To arrive at more reliable and more accurate predictions requires a better understanding of the complex processes and mechanisms involved in two-phase heat transfer.

The purpose of this study is to investigate some of the hydrodynamic aspects of two-phase heat transfer in the lower quality range. Such aspects as the role and influence of nucleation and convective mechanisms in enhancing heat transfer, influence of flow pattern, mass-flow rate, and quality on the nature and rate of heat transfer are investigated. The importance of thermal and hydrodynamic influences of nucleation in enhancing heat transfer, and how nucleation applies to heat transfer in a forced-circulation system are also studied. The results of this study should contribute to a better and more thorough understanding of the processes and mechanisms affecting two-phase heat transfer, and in this way help in improving its prediction.

The above-mentioned aspects of two-phase heat transfer are investigated, not with an actual boiling system but with an analogous two-component system, where the hydrodynamic aspects of boiling are simulated by bubbling gas through the wall of a porous heated tube into a liquid flowing inside the tube. These investigations are performed with air-water and air-ethylene glycol two-phase mixtures.

Previous studies[2-4] have shown that this system simulates the hydrodynamic effects of boiling quite well theoretically, and that the initial and boundary conditions are the same. In this study, one of the aims was also to examine the analogy experimentally. Similarity between boiling and bubbling systems exists only where the boiling process (i.e., nucleation) takes place in the single-component system. This limits the range of study to lower qualities according to the presently accepted interpretation of two-phase, single-component heat-transfer processes.

The two-component gas-bubbling system offers advantages in studying boiling because gas-bubbling rate, liquid-flow rate, and gas quality can be controlled independently. Therefore, the hydrodynamic aspects of boiling can be conveniently studied at low temperatures and pressures for many conditions.

SURVEY OF THE LITERATURE

Two-phase flow and heat transfer have been studied extensively during recent years because of their increasing importance in engineering applications. Several excellent reviews summarized the work in this field. Collier[5] reviewed the literature published up to 1957, and Lottes et al.[6] reviewed the status of two-phase heat transfer and hydraulics in 1962. Zuber and Fried[1] evaluated information available in 1962 for predicting heat-transfer rates, and Westwater[7] discussed recent research in nucleate boiling. Other reviews of note are by Bennett,[8] Gresham et al.[9] and Jacobs.[10]

Since these reviews summarize the work in this field thoroughly and include extensive bibliographies, only articles that have a direct bearing on the present investigation will be reviewed.

Gas Injection and Generation

Several studies have appeared where electrolytic gas generation or gas bubbling from a porous sintered surface were used for studying or analyzing certain aspects of two-phase flow and heat transfer. Zuber,[4] in his investigation of hydrodynamic aspects of boiling-heat transfer, analyzed the hydrodynamic characteristics of nucleate and transitional boiling, critical heat flux, and bubble growth. The similarity between bubble formation at an orifice and in nucleate boiling was investigated. It was found that the types of bubbles and bubble formations appeared to be similar in both systems. Initiation, generation, and appearances of bubbling processes in nucleate boiling and from a porous plate were similar.

Wallis[2,3] presented a detailed analytical comparison of the hydrodynamic aspects of nucleate boiling and bubbling of air from sintered porous media into water. His analysis showed that:

1. The distribution of both nucleation and pore sites and sizes was statistical.
2. In both boiling and bubbling experiments, nucleation phenomena could be described by the same basic equations.
3. The hydrodynamic phenomena in both bubbling and boiling-bubble growth appeared to be the same, and growth time was controlled by statistical variations due to agitation.

Wallis also pointed out that the further growth of a steam bubble after leaving the heating surface had no analogue in the two-component gas-liquid system.

Wallis[11] also performed experiments of air-bubble generation from a porous tube submerged in water. Three different flow patterns,

"bubbly," "patchy," and "blanketed," were observed depending on the air-flow rate from the tube surface. The bubbly flow pattern was analogous to nucleate boiling, and the blanketed pattern to transition boiling. Transition from the patchy to the blanketed regime may be likened to the "burnout" transition in pool boiling.

Mixon et al.[12] studied the effect of electrolytic gas evolution on natural convection and surface (subcooled) boiling-heat transfer from a horizontal copper block. The heated block, immersed in a dilute aqueous NaOH electrolyte, served as a cathode for generating hydrogen bubbles on the top heated surface. The authors found that enhancement of heat transfer similar to that under boiling conditions could be obtained by their method of gas bubble generation. Mixon et al. maintained that these results indicated that high heat-transfer coefficients in surface boiling may be attributed to agitation action of the bubbles, and not latent heat effects. Although the size of electrolytic bubbles generated in their tests was not reported, they appeared to be much smaller than surface-boiling bubbles.

Gose et al.[13] simulated nucleate boiling in their heat-transfer study by bubbling gas through porous heated surfaces. The influence on heat transfer of bubbling gas from sintered porous and drilled plates into a pool of liquid was investigated in vertical and horizontal plate positions. Several viscous oils, ethylene glycol, and water were used in the experiments. Limited experiments were also performed with a porous tube geometry, where gas was bubbled into liquid flowing inside the porous heated tube. In these forced circulation experiments, however, the effects of gas bubbling and stream velocity increase (due to introduction of the gas phase) on heat transfer were not separated, making it difficult to evaluate the individual influences. The authors found that the effect of gas injection or h_{TP} was independent of gross geometry of the heated surface, and that the properties of the gas were not important. It was also concluded that the size and number of pores did not influence the injection effect but were a function of surface porosity. That is, high-porosity surfaces (of the sintered type) yielded higher h_{TP}'s at low injection rates, and low-porosity surfaces (of the drilled type) yielded higher h_{TP}'s at high injection rates. On the basis of comparison with pool boiling data, Gose et al. concluded that the large heat-transfer coefficients in nucleate boiling were largely due to the boundary-layer disturbance produced by the vapor bubbles.

Sims et al.[14] analyzed Gose's pool-boiling data and compared them to Kutateladze's[15] saturated-pool boiling-heat transfer and hydrodynamic-burnout theories. They found that Kutateladze's pool-boiling relationship for moderate heat fluxes, which predicts boiling-heat transfer rates quite reasonably, correlated gas-bubbling results for porous plates satisfactorily for moderate injection rates. The drilled-plate heat-transfer results, however, could not be correlated. The authors, therefore, concluded that porous plate systems appeared to simulate boiling at saturation temperature, but that drilled plates were not satisfactory for simulation of boiling.

Two-phase Flow Patterns

Gas and liquid phases flowing simultaneously in a duct or a pipe may assume various flow configurations, or so-called "flow patterns." Two-phase flow pattern studies up to 1960 have been reviewed by Vohr[16] for two-component, one-component, adiabatic, and nonadiabatic flows in both horizontal and vertical systems. Flow-pattern observations were usually made visually, but sometimes with the aid of stroboscopic lights and still or motion picture photography. Although investigators differed in the description and subdivision of various flow patterns, the same basic flow pattern types were found to occur in most of the investigations. The basic vertical flow patterns observed, as discussed by Vohr, can be summarized as follows:

1. Bubble Flow. Liquid flows with gas bubbles dispersed in it.
2. Slug Flow. Gas flows up in periodic slugs between a liquid phase continuous at the walls and discontinuous in the core (in form of dispersed liquid plugs).
3. Froth Flow. Gas and liquid phases flow in an evenly dispersed mixture which has the appearance of an emulsion.
4. Annular Flow. Liquid flows in an annular film around the walls, and gas flows in the central core.
5. Spray Flow. Liquid flows in the form of dispersed droplets carried along by a continuous gas phase.

The transitions between these basic flow patterns are usually not well defined, and the transition regions are sometimes quite lengthy.

The transition region between slug and annular flows is sometimes extensive and quite complicated and is described in such terms as dispersed plug flow, cycling flow, turbulent flow, slug-annular flow, and semi-annular flow.

Vohr found that flow-pattern regime maps of several investigators for horizontal two-phase flows did not agree very well. This was attributed to unknown effects that various parameters had on the stability of flow patterns. Very little analytical work on the stability of flow patterns was found. Many of the flow-pattern studies reviewed by Vohr were performed with two-component adiabatic systems. Flow patterns developed in these two-component adiabatic systems may differ from flow patterns in boiling systems because of the influence of nucleation on the fluid boundary conditions.

Hsu and Graham,[17] in their study of bubble and slug flow in vertical heated glass tubes, found that heat flux did affect flow patterns. The glass

tubes were coated with a thin transparent conducting film, and used as electrical resistance heaters to study the flow of steam-water. This investigation by Hsu and Graham showed that boiling two-phase flow had some characteristics not encountered in adiabatic two-phase flow. Bubble flow changed to slug flow as the heat flux was decreased, or the length of heating section increased, when the total heat input was kept constant. Bubble flow was more prevalent when active nucleation sites were more numerous, such as in aged glass tubes.

In a preliminary report, Hosler[18] discussed the steam-water flow patterns obtained in a rectangular, vertical channel heated on one side and fitted with two quartz side prisms and a quartz front window for observation. The flow patterns observed included inception of nucleate boiling, bubble flow, slug flow, and annular flow. Effects of pressure, mass velocity, and inlet temperature on flow-pattern transitions were observed. Although the effects of inlet temperature and heat flux could not be separated, it was noted that decreasing the inlet temperature caused the transitions to occur at lower bulk enthalpy. Hosler observed bubble generation on the heated wall in the bubble and slug type flows, but did not note any in the annular-flow regime.

Wallis and Griffith[19] investigated air-water flow patterns in an adiabatic, vertical, rectangular channel, where heat addition was simulated by a continuous bubbling of air into the section through two opposing porous bronze side plates. Observations were made through the other two glass side panels. They observed bubbly, transition, annular, and dropwise flows with continuous injection at the walls, and noted that the rate of bubble generation strongly influenced flow distribution and transition regions.

Wallis[11] used the porous-wall analogy to boiling to investigate the hydrodynamics of two-phase flow in horizontal tubes. He used porous tubes to obtain a continuous addition of air into a flowing water stream, and so to simulate the generation of steam bubbles on a heated wall in forced-circulation flow. The flow patterns observed at the tube outlet were described as bubbly, breakdown of bubbly, drop-annular, and dropwise. Past history of the flow and especially air injection rate at the wall were shown to be important in determining the flow type.

This review of flow pattern studies has shown that boundary conditions are important in determining distribution and type of two-phase flow, and that adiabatic, solid wall boundary conditions are not necessarily the same as actual or simulated boiling-boundary conditions.

Two-phase, Two-component Heat Transfer

Not many investigations have been devoted to measuring heat-transfer coefficients in two-phase, two-component flow systems. In studies

on this subject, average heat-transfer coefficients were usually measured for co-current gas-liquid flows in pipes. Test liquid temperatures were ordinarily kept well below boiling-point temperatures to minimize mass-transfer effects.

Verschoor and Stemerding[20] used a 0.55-in.-I.D. vertical tube, with 15.75 in. heated by condensing steam on the outside diameter, to investigate two-phase heat transfer for upward flow of air and water. The authors found that h_{TP} increased with increasing volumetric air/water ratio at constant liquid-flow rate, and that introduction of air was most effective in increasing heat-transfer rate at the lowest liquid-flow rate. It was observed that h_{TP} values dipped at an air/water ratio of about two, and passed through a maximum at about 200. This behavior was attributed to flow-regime transitions from bubble to slug, and from slug to annular, respectively.

Heat-transfer coefficients for upward flow of air/water and air/oil mixtures in a 0.55-in.-I.D. vertical tube, with a $7\frac{7}{8}$-in. condensing steam heated length, were measured by Groothuis and Hendal.[21] The authors found that introduction of the first amount of air caused a rapid increase in heat-transfer coefficient, but that further additions of air increased h_{TP} much more gradually. The influence of air was most pronounced at the lowest Reynolds numbers. This was explained by noting that resistance to heat transfer was mainly due to the viscous sublayer at the wall, and that eddies produced in the wake of the rising air bubbles reduced the effective thickness of the wall, thus enhancing the heat-transfer rate. The thicker the original laminar layer, the more pronounced the effect from this extra source of turbulence. A satisfactory correlation of results in the annular-flow region was obtained by relating the Nusselt, Prandtl, and "volumetric mean" two-phase Reynolds numbers. In general, the trends observed agreed well with the results by Verschoor and Stemerding, including the observation of a maximum in h_{TP} at high air/liquid ratios. This phenomenon was explained by the appearance of "dry patches" (i.e., breakdown of annular flow) on the heated wall.

In 1959, Knott et al.[22] made an experimental study of heat transfer to nitrogen gas-viscous oil mixtures flowing upward in a 0.506-in.-I.D. tube. The 5-ft-long stainless steel tube was used as a resistance heater to provide constant heat-flux boundary conditions. Very little increase in heat-transfer coefficient was found up to a gas/liquid volumetric ratio of 0.2. As the quantity of nitrogen was increased at a given oil-flow rate, h_{TP} increased up to 150% above its liquid value. No mass-flow rate effects on h_{TP} were observed. The authors correlated their results satisfactorily on the basis of the Sieder-Tate equation for laminar flow, when the increase in flow velocity caused by the gas phase was taken into account. The results of the experiments by Knott et al. indicated a much lower effect of the gas

phase on h_{TP} increase than did the results by Verschoor and Stemerding or Groothuis and Hendal, which were for higher initial-liquid Reynolds numbers.

In addition, two-phase, two-component heat transfer was investigated in horizontal tubes by Johnson and Abou-Sabe[23] for turbulent flow of water-air mixtures, and by Johnson[24] for viscous-turbulent oil-air mixtures. Heat-transfer rates increased with addition of air. The authors pointed out, however, that two-phase heat transfer in horizontal systems cannot really be compared on an equal basis to heat transfer in vertical systems because of the different flow patterns developed in the two orientations.

Boiling-liquid Heat Transfer

Although boiling-liquid heat transfer has been the topic of numerous studies, complete understanding is still lacking about the mechanisms and processes involved, and the parameters influencing it. Several mechanisms, some of which are incompatible with others, have been proposed to explain the high heat-transfer rates found in boiling. They are usually proposed for pool boiling, and then extended sometimes to forced-circulation boiling.

Jakob[25] first proposed that the rising bubbles exert a stirring effect on the liquid which enormously increases boundary-layer turbulence and hence heat transfer. He postulated that only a small part of the heat produced is directly transferred to the interior of the bubbles on the heated surface and that the main part of the energy is transferred through the liquid.

Based on a photographic study of subcooled boiling, Gunther and Kreith[26] considered that the high heat-transfer rates were caused by the mixing and stirring action of growing and collapsing bubbles, and that transport of latent heat by the vapor bubbles was of minor importance. A similar conclusion was also reached by Rohsenow and Clark[27] from their photographic study of subcooled boiling in forced convection.

Zuber[28] analyzed the turbulence created by vapor bubbles in the isolated bubble-flow regime for pool boiling in terms of turbulent natural convection. He considered the buoyant forces created by the density differences to be equivalent in the two systems, therefore producing the same heat-transfer effects. This type of natural convection analysis of nucleate boiling was also used by Nishikawa and Yamagata[29] to predict heat-transfer rates in pool and circulation boiling.

A different model was proposed by Engelberg-Forster and Greif[30] based on vapor-liquid exchange action of bubbles. They showed that the subcooled boiling data of Gunther and Kreith[26] could be explained satisfactorily in terms of energy transfer taking place when hot liquid is displaced from the surface by vapor bubbles into the cold bulk, and an equal

amount of cold liquid is then drawn in as a replacement. They also considered microconvection and latent heat-transport mechanisms, but claimed that while they were qualitatively present, quantitatively they could provide only a small portion of the heat flux in nucleate boiling. On the other hand, Ivey and Morris[31] showed that the vapor-liquid exchange mechanism was invalid for high pressures.

Moore and Mesler[32] measured surface-temperature fluctuations during nucleate boiling of saturated water. They interpreted the rapid temperature drops observed as being due to rapid removal of heat from the surface. This rapid heat removal was then attributed to vaporization of a liquid microlayer at the base of a vapor bubble, and thus the microlayer vaporization mechanism was established.

In 1962, Bankoff[33] examined available data on the importance of latent-heat transport in boiling-heat transfer, and concluded that latent-heat transport accounted for most of the heat transferred at high heat fluxes in subcooled boiling.

Because of the complexity of boiling-heat transfer, compounded even more when circulation is superimposed, it is difficult to investigate separately the various influences that determine the rate and nature of heat transfer. Therefore, most studies of boiling-circulation heat transfer have been concerned with arriving at a correlation for the system investigated, which is not necessarily applicable to other systems. In some studies, however, individual influences were investigated, either to learn more about the process, or to arrive at a correlation by combining the individual effects.

Mumm,[34] for example, investigated effects of mass velocity, heat flux, and quality for forced circulation boiling of water in an electrically heated, horizontal tube (0.465-in. I.D. and 7 ft long). These data were correlated by combining these effects into a dimensionless equation

$$\frac{h_{TP}D}{k_\ell} = \left[4.3 + 5.0 \times 10^{-4} \left(\frac{\rho_\ell}{\rho_\ell - \rho_g}\right)^{1.64} X\right] \left(\frac{q''}{Gh_{fg}}\right)^{0.464} \left(\frac{GD}{\mu_\ell}\right)^{0.808}.$$

Bogdanov[35] studied the effect of inlet velocity on heat-transfer coefficient for boiling of water in inclined tubes (45°) of 0.787-in. I.D. Inlet velocities were varied from 1.5 to 13.0 ft/sec, and the maximum heat flux used was 74,000 Btu/(hr)(ft^2). The author presented the average velocity effect on heat transfer in terms of

$$h_{TP} = \text{Const. } p^n (q'')^m + 100\, U_\ell,$$

where n and m are constants having different values at various heat fluxes, and U_ℓ is the liquid-inlet velocity.

Influence of vapor quality on heat-transfer coefficients for different mass-flow rates of water in a vertical tube (0.630 in. I.D.) was investigated by Sterman at 2 atmospheres[36] and at 7 atmospheres.[37] In the 2-atmosphere tests, as reported by Collier,[5] heat-transfer coefficients were independent of quality at a constant inlet velocity for low steam qualities. The heat-transfer coefficients increased with increasing mass velocity, and approached h_{TP} values calculated from the Dittus-Boelter equation for liquid flow at the same temperature. The effect of mass velocity at 7 atmospheres was qualitatively the same as at 2 atmospheres. The 7-atmosphere study,[37] where the 2-atmosphere results were also discussed, showed, however, that the range of flow rates over which h_{TP}'s are considerably higher than h_L's and the effect of mass velocity is small, widens as the pressure is increased at a given heat flux. The author stated that this explained why no mass-flow-rate effect is observed at high pressures and low liquid-inlet velocities.

Local heat-transfer coefficient values were presented by Anderson et al.[38] for water evaporating in a 6-ft-long tube (0.530 in. I.D.) at low pressures. The feed rate was varied from 200 to 1000 lb/hr for heat fluxes of 3500 to 95,000 Btu/(hr)(ft^2). Inflections observed in the curves for heat-transfer coefficient versus tube L/D were attributed to change in flow pattern and nature of heat transfer from nucleate boiling to convective. The influence of feed rate and pressure on h_{TP} was found to be complicated, and it was observed that while h_{TP} remained fairly constant with increasing quality at low heat fluxes, it increased more rapidly at higher heat fluxes.

A two-phase heat-transfer correlation that appears to predict h_{TP}'s fairly well in the "convective" regime, when the constants are adjusted for a specific system, is

$$\frac{h_{TP}}{h_L} = C_1 \left(\frac{1}{X_{TT}}\right)^{C_2},$$

where C_1 and C_2 are empirical constants, and X_{TT} is the Martinelli parameter for two-phase flow. This correlation was first proposed by Guerrieri and Talty,[39] who used it to correlate two-phase heat-transfer coefficients for boiling organic liquids with natural circulation in vertical tubes. Since then it has been used in different forms, recently by Collier and Pulling,[40] to correlate two-phase heat-transfer data at higher volumetric gas/liquid flow ratios.

Collier and Pulling[40] reviewed this correlation and applied it to their own two-phase, steam-water results for vertical annuli. The authors found that while h_{TP}'s in the "convective" region could be correlated within ±20% for a given test series, the best-fit values of the constants varied by as much as ±30% for different geometries and different systems. A nucleate boiling region existed at lower qualities where h_{TP}'s were independent of the Martinelli parameter.

Void Fractions in Two-phase Flow

A problem associated with two-phase flow and heat-transfer study is knowing the fraction of cross-sectional area occupied by each phase. The void fraction (fraction of cross-sectional area occupied by the gas phase) cannot be calculated from mass-flow rates because it is generally accepted that gas and liquid phases do not flow at the same average velocity. Because of the laboriousness and difficulty of obtaining void-fraction data, its use in two-phase hydrodynamic and heat-transfer analyses has been limited.

Lottes et al.[6] summarized most of the void-fraction data available up to 1962. Marchaterre and Hoglund[41] prepared a correlation for void fractions in terms of velocity ratio between phases (slip ratio), Froude number, and volumetric flow ratio.

Petrick[42] analyzed and discussed phase distributions obtained by him for upward flow of air-water in an adiabatic channel. Christensen[43] also illustrated phase-distribution development in a channel with increasing quality in his system for upward flow of steam-water.

Bankoff[44] proposed a variable-density model to predict void fractions for two-phase flow, where he assumed that locally there is no slip between phases. The average velocity of the gaseous phase was explained as being greater than that of the liquid phase only because gas is concentrated in the region of higher velocities.

Although Isbin et al.[45] tried a void-model correlation of the type

$$\frac{h_{TP}}{h_L} = \left[\frac{(1 - X)}{(1 - \bar{\alpha})}\right]^{0.8}$$

for their heat-transfer results for flow of steam-water in a horizontal pipe, they found that experimental values were about 50% higher than their void correlation predicted. Their correlation was obtained by starting with the Dittus-Boelter equation for single-phase flow, using liquid properties, and liquid velocity

$$V_\ell = \frac{(1 - X)W_T}{(1 - \bar{\alpha})A_T}$$

to obtain the ratio of two-phase to single-phase heat-transfer coefficients.

The literature survey presented indicates that a better understanding of the complex processes and mechanisms involved in two-phase boiling-heat transfer is needed. Equipment that simulates the hydrodynamic aspects of boiling-heat transfer was designed to investigate some of these influences and mechanisms involved experimentally.

DESCRIPTION OF APPARATUS

A forced-circulation loop was designed and built with a heated test section of porous bronze tubing for the forced-convection heat-transfer tests. Equipment was also built to perform the descriptive comparison experiments of pool boiling and pool-gas bubbling. Since the overall system is rather complex, the principal aspect of the equipment will be described and discussed individually.

Forced-circulation Loop-flow System

The flow schematic of the loop is presented in Fig. 1, and a general view of the loop is shown in Fig. 2. Demineralized water and commercial ethylene glycol (Union Carbide Co., iron and chloride free type with 0.3% maximum water content) were the liquids used in the tests. The test liquids were stored in a 40-gal. stainless steel tank of 2-ft diameter, from which they were pumped through the heat exchangers and metering orifices into the air-liquid mixing section. Air was injected along the length of the porous tube in the mixing section, and then the two-phase mixture passed through the heated test section where additional air was injected through the walls of the heated porous tube. The two-phase mixture coming out of the test section was observed in the transparent plexiglass section and then returned to the storage tank. The storage tank was vented to allow the incoming air to escape.

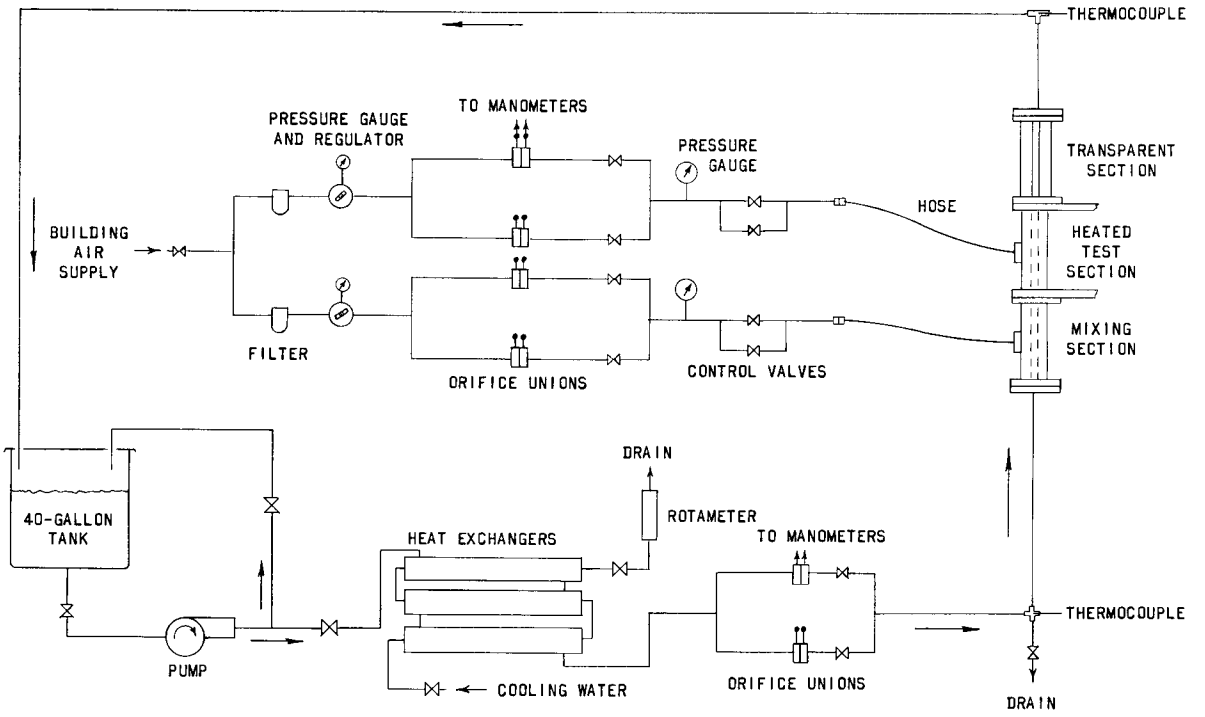

Fig. 1. Flow System Schematic Diagram

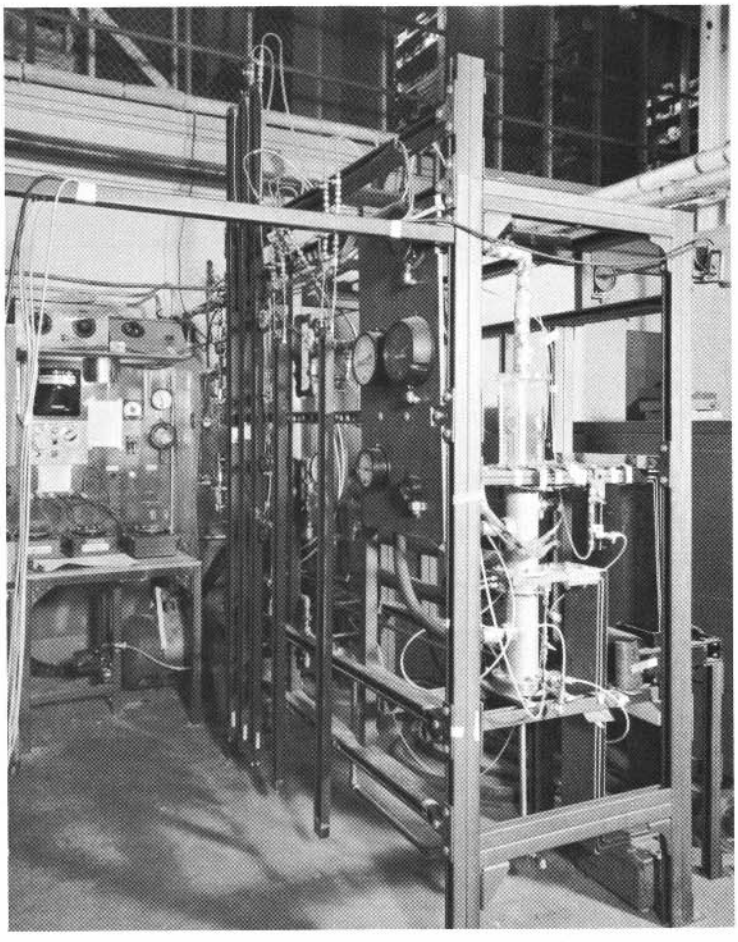

Fig. 2

General View of Forced-circulation Loop

112-2828

The circulation pump was an Aurora JZ4 S.S. type, with stainless steel working parts and a Teflon shaft seal. It was powered by a General Electric variable-speed A.C. motor of 7.5 horsepower. A bypass line from the pump to the storage tank made flow control more versatile. It was found, however, that the variable-speed motor, together with the control valves, provided sufficient liquid-flow control for all test conditions.

Three single-pass, counter-flow heat exchangers made of copper tubing (fourteen $\frac{1}{2}$-in.-O.D. inner tubes and 3.0-in.-O.D., 51-in.-long outer shell) were connected in series so that liquid going into the test section would be cooled to a desired temperature. The test liquid passed through the shell side of the heat exchangers, and cooling water (laboratory well supply coming in at about 55°F) passed through the tube side. A rotameter was used to help set the cooling-water flow rates.

Stainless steel (ASA Schedule No. 40, $\frac{1}{2}$-in.) pipe and stainless steel valves were used throughout the liquid-flow system.

Liquid-flow Measurement

Liquid flow to the test section was measured with a system of two orifices connected in parallel, but only one of the orifices was used for a given test. Both orifice meter branches were built identically, except for the orifice diameter. Fourteen inches of straight $\frac{1}{2}$-in. pipe (ASA Schedule No. 40) was provided upstream of the orifice unions, and ten inches after them to the needle control valves, so that flow disturbances would be minimized. The knife-edge orifices were installed and sealed with O-rings into $\frac{1}{2}$-in. orifice unions provided with throat-pressure taps (one pipe I.D. upstream, one-half pipe I.D. downstream). Orifice diameters of 0.062 in. and 0.300 in., machined to near knife edge, were used. The orifices were calibrated in place by weighing the water discharge. (The results of this calibration are presented in Appendix A.)

Two U-tube manometers (Meriam Instrument Co.) were used to measure the orifice differential pressure. One manometer was 100 in. long and contained mercury, the other one was 60 in. long and contained a manometer fluid of 1.75 specific gravity. The manometer connections were made so that either manometer could be used with either orifice to measure test-liquid flow rates.

Air-flow Measurement

The building air supply provided air at 100 psig for the mixing and the heated test sections. Since the air-flow measurement and control systems for both sections were built identically (see Fig. 1), except for the exact orifice diameters, only one is described in detail.

Stainless steel (ASA Schedule No. 40, $\frac{3}{4}$-in.) piping was used in the air-supply system throughout. The air coming in from the building line was first filtered through a sintered metal filter. A pressure regulator was used to set the air pressure supplied to the two parallel orifice lines. Only one orifice was used for a given test, and the air flow was controlled by a $\frac{3}{4}$-in. globe valve and a $\frac{1}{2}$-in. needle valve in parallel. The air-metering lines were connected to the test section with flexible pressure hose.

Eighteen inches of straight pipe upstream of the orifice unions, and twelve inches downstream to the gate shut-off valves minimized flow disturbances. The knife-edge orifices were installed and sealed with O-rings into $\frac{3}{4}$-in. orifice unions provided with throat pressure taps. Orifice diameters in the heated test section line were 0.0634 and 0.170 in., and the ones in the mixer section line were 0.0623 and 0.170 in. All orifices were calibrated in place with the water-weighing method. (The results of this calibration appear in Appendix A.)

Two, U-tube, 100-in.-long manometers (Meriam Instrument Co.), filled with manometer fluid of 2.95 specific gravity, were used to measure the orifice differential pressure. Four, Bourdon-type, 0- to 100-psig pressure gauges (Ashcroft Co.), which were checked with a dead-weight tester (Crosby Co., Style CC-110), served as air-line pressure indicators.

Test Section Design

The principal components of the test section were the gas-liquid mixing section, the heated test section, and the transparent observation section. A cross-sectional sketch of these components is shown in Fig. 3.

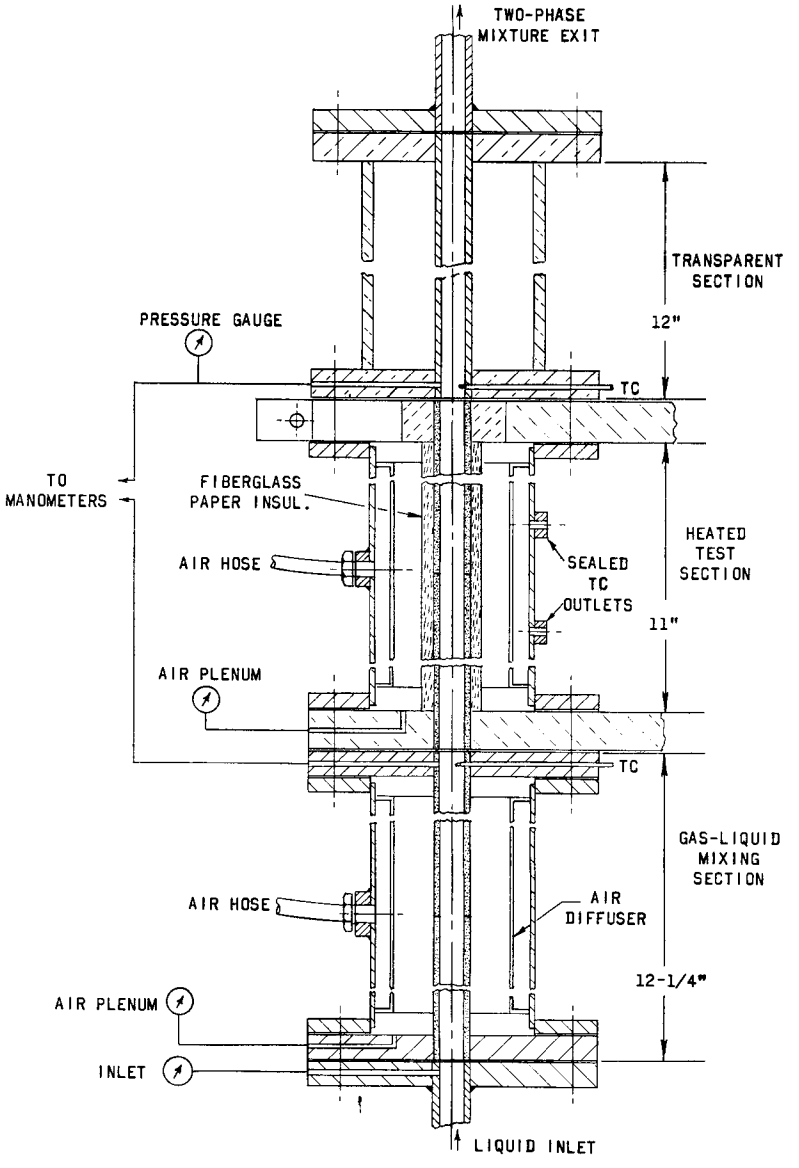

Fig. 3
Forced-circulation Test Section

The gas-liquid mixing section provided a given inlet quality into the heated section, the gas phase being introduced continuously along the length of the section in a manner similar to a boiling system. Thirty-two inches of

straight $\frac{5}{8}$-in.-I.D. piping was provided to stabilize the flow into the mixing section. The active air injection in the mixer section was 11 in. long. Air, entering the mixer plenum (made of aluminum) from the orifice metering system, was diffused by a perforated plate screen and then passed through the porous bronze tube ($\frac{5}{8}$ in. I.D., $\frac{7}{8}$ in. O.D.) into the flowing liquid.

The air plenum in the heated test section was the same as the one in the mixing section, except that in the former, two Conax multiple thermocouple glands with neoprene pressure sealants were provided for thermocouple leads. In the heated test section, the porous bronze tube itself ($\frac{5}{8}$-in. I.D., $\frac{7}{8}$-in. O.D.) served as a resistance heater to provide the heat flux for the two-phase mixture. Therefore, it was insulated with a $\frac{3}{16}$-in. wrap of Fiberglas paper insulation (Mine Safety Appliances Co., Type 1106 B), and the air had to pass through the porous insulation before going through the porous tube and into the two-phase stream.

The porous tubes used in the mixing and heated sections were machined from Oilite bronze-cored bar stock (Chrysler Corp., Amplex Div.). Machining was done according to manufacturer's specifications to maintain maximum porosity. Nevertheless, after the machined tubes were pressure-flushed with trichloroethylene to remove all traces of oil, they were etched in a dilute solution of nitric acid to improve the porosity. Since the maximum length of porous stock available was 6.5 in., two tube lengths were joined together to form a test section of satisfactory length. Four individual tubes were tested for total air-flow rates through the walls at various wall-pressure drops, and the two tubes having flow uniformity within 2% were chosen for the heated test section. The other two tubes were joined to form the porous mixing section.

The porous tubes were silver-soldered together to form the required lengths and then were silver-soldered to the flanges. Sections to be silver-soldered were first copper-plated to prevent the solder from being drawn into the pores through capillary action. The 1-in.-thick, 6-in.-wide copper power-supply bars for the porous tube also served as flanges for the heated test section. "Durabla" gaskets were used to insulate the electrically heated section and to form pressure seals between flanges.

The transparent section was made from Plexiglas for observation of two-phase flow patterns emerging from the porous test section. The $\frac{5}{8}$-in.-I.D. flow tube was supported between the flanges by four rectangular sides forming a waterproof box. This outer box could be filled with water to improve visual and photographic observations.

Pressure in the air plenums was measured with 0- to 100-psig, high-precision Marsh (Type 220-C) pressure gauges, which were calibrated with a dead-weight tester. Pressure taps were provided to determine the

fluid-stream pressure and pressure drop. Static pressures at the inlet to the mixing section, and at the exit of the heated section, were measured with 0-to 30 psig Ashcroft pressure gauges, which were checked with a dead-weight tester. A 60-in. U-tube manometer (Merriam Instrument Co.), filled with manometer fluid of 2.95 specific gravity, was connected to pressure taps at the inlet and exit of the heated section to measure the static two-phase pressure drop across it.

Fluid-temperature Measurement

A bare-junction thermocouple probe was installed into a standard $\frac{1}{2}$-in. cross fitting to measure liquid-inlet temperatures, which were approximately the same as room temperature. The fitting was located at the bottom of the liquid flow stabilizing section (Fig. 1), and also served as a mixing chamber. The outlet bulk temperatures of the two-phase fluid were measured in an insulated $\frac{1}{2}$-in. tee fitting at the end of a 12-in. insulated exit pipe section (Fig. 1) with a bare-junction thermocouple probe. Similar probes were also used to check the fluid temperature at the inlet to the heated section and close to the wall at the exit of the heated section. The probes were made of B & S gauge No. 30, premium-grade, copper-constantan thermocouple wire insulated with Teflon, with error limits specified by the manufacturer to be within $\pm \frac{3}{4}$ °F for the range -75 to 200°F.

Each pair of leads from the probes was wired to a common ice junction through an insulated switchbox. The selector switch was a Leeds and Northrup Type 8240. The thermocouple ice junction was placed in a glass tube and immersed in a distilled water-ice mixture. A Leeds and Northrup portable precision potentiometer was used to read the thermal electromotive force of the thermocouples. The probe assemblies were calibrated at the ice and the water boiling points at one atmosphere. Readings were within ±0.3°F of the National Bureau of Standards Reference Table values.

Wall-temperature Measurement

Temperatures in the heated test section were measured on the outer surface of the porous tube and inside the porous tube wall. Thermocouple installations in the wall were made so that inside surface temperatures of the tube could be determined accurately, and the outer surface thermocouples were added mainly to check these measurements. The thermocouple locations are shown in Fig. 4. The thermocouple junctions inside the wall were spaced every $1\frac{3}{8}$ in., except where noted.

The inside-wall thermocouples were installed in holes drilled in the wall as shown in detail in Fig. 5. The installation method was similar to those used by Bartle for transpiration cooling experiments[46] from porous surfaces. Premium grade, B & S gauge No. 36 (0.005-in. diameter), copper-constantan thermocouple wire with inner Teflon insulation was used. The

wire was passed through two-hole ceramic tubing (Du-Co Ceramics Co.) of 0.032-in. outside diameter, and the bead then formed with a mercury pool welder. The bead and the ceramic, together with a backup ceramic two-hole tube, were cemented into the 0.035-in. diameter hole with technical copper cement (W. V. B. Ames Co., Type G) to prevent air leakage around the assembly and the junction. Since the copper cement had an oxide base, it was an electric insulator, but only junctions Nos. 2, 3, 4, 7, and 8 were successfully insulated from the porous tube.

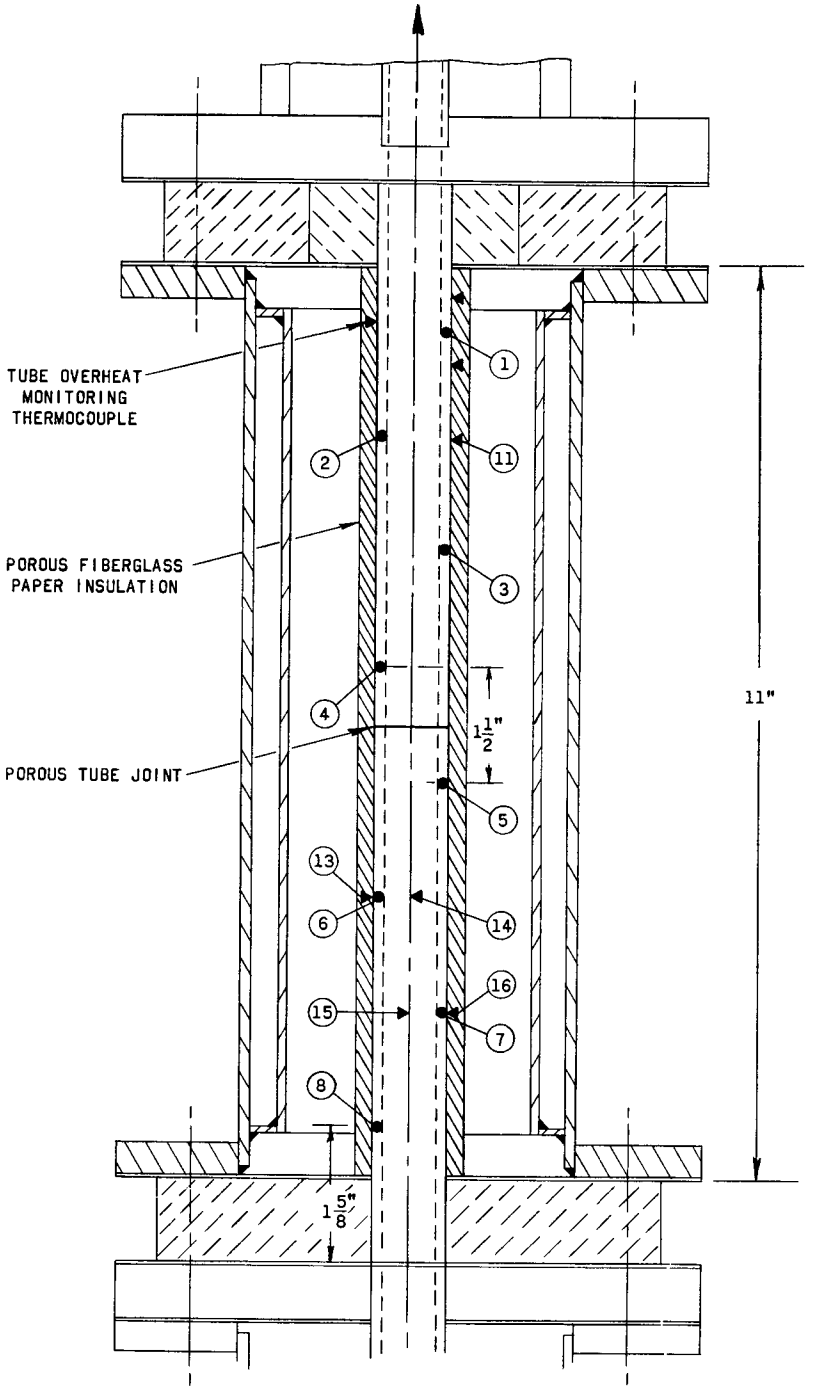

Fig. 4

Thermocouple Locations in Heated Tube

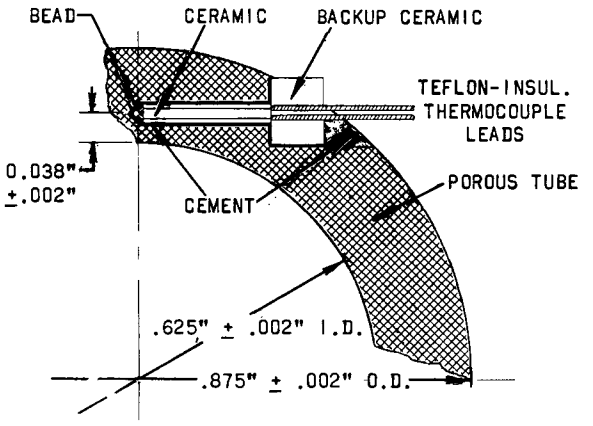

Fig. 5. Wall Thermocouple Installation

The outside-wall thermocouple junctions were formed by tacking the wires to the outside of the porous tube with a condenser discharge-type welder. The thermocouple wires were premium grade copper-constantan of B & S gauge No. 28.

All the thermocouple leads were wrapped around part of the porous-tube diameter and led to the outside of the air plenum through two pressure-sealing, multiple Conax thermocouple glands. The leads were wired through the same type insulated switchbox, selector switch, and common ice junction arrangement as the fluid thermocouples, and were read by the same potentiometer. In this case, however, the thermocouple used for indicating tube overheating and Nos. 2, 3, 6, and 7 were electrostatically shielded and equipped with individual ice junctions and switches, so they could be monitored continuously, if desired, on a four-channel, self-balancing, potentiometric, recording millivoltmeter (Texas Instruments, Inc., "Servo/riter" Recorder) which had a $\frac{1}{4}$-sec full-scale response.

The premium-grade thermocouple wire accuracy was guaranteed by the manufacturer (Thermo Electric Co.) to be within $\pm \frac{3}{4}$ °F for the temperature range of present operations. Readings of sample junctions of the Nos. 28 and 36 gauge wires and all No. 36 gauge junctions used were also checked at the ice and water boiling points at atmospheric pressure and were within $\pm \frac{1}{3}$ °F of reference table values. After the thermocouples were installed in the heated section, emf readings were checked by running water at 76°F (with room temperature at 78°F) through the section when no power was supplied to it. The readings were consistent within $\pm \frac{1}{5}$ °F of the water temperature.

Power Supply and Measurement

Power to the heated porous tube was supplied through copper bus bars from a Sciaky Co. portable transformer unit using a 440-Volt, 350-Ampere service line. The unit consisted of two independent sections, each capable of supplying 35 kW A.C. at 6.7 Volts. In each section, an Ignitron tube controlled the power output with a fluctuation of $\pm \frac{1}{3}$ %. Only one section was required to supply the power for the present tests.

The following interlocks were incorporated into the power supply control system to prevent overheating or failure of the porous test section:

1. A relay was provided to shut off the power if the electric supply to the pump motor failed.
2. A mercoid pressure switch was connected to the pump output line and wired to shut off the power if the pump output pressure went below a certain minimum level.
3. The porous tube temperature near the exit of the test section was monitored continuously with the potentiometric recorder. A relay was incorporated into the recorder to shut off the power if this temperature went above a certain set level.

Weston high-frequency electrodynamometers measured power input into the porous tube. Power was measured with a Model 310 wattmeter (accuracy of $\pm \frac{1}{4}$ % of full scale) and checked with a Model 341 voltmeter and a Model 370 ammeter (accuracy of $\pm \frac{1}{4}$ % of full scale). A current transformer (Electran Mfg. Co., accuracy of $\pm 0.3\%$), placed around one of the bus-bar lines, with a stepdown ratio of 500:1 was used to reduce the current level to measurable values. Voltage taps were taken from the test section copper flanges, and a potential transformer (Electran Mfg. Co., accuracy of $\pm 0.3\%$) with a step-up ratio of 10:1 was used to increase the voltage input into the wattmeter.

The test section and porous tube electrical resistances at room temperature were measured with a Rubicon Kelvin Bridge (Honeywell, Model 1622). The resistance between voltage taps was 0.525×10^{-3} ohms, the overall porous tube resistance was 0.515×10^{-3} ohms, and the resistances in the individual upper and lower porous tube sections (see Fig. 4) were 52.5 and 47.5 micro-ohms/inch, respectively.

Equipment for Void-fraction Measurement

Void fractions in the heated test section were measured with equipment designed and developed at Argonne National Laboratory. The measurement method is based on the different attenuation rates of a gamma-ray beam passing through two-phase mixtures of various densities. The principles, operation, and design of the equipment used in the present tests were described in detail by Hooker and Popper,[47] and by Petrick and Swanson.[48] A view of the gamma-attenuation equipment and instrumentation as used in the current experiments is shown in Fig. 6.

Briefly, the measurement equipment consisted of a radioactive thulium-170 source with a half-life of 129 days, a photomultiplier tube with a thallium-activated NaI scintillation crystal, a high-voltage supply, a linear current amplifier, and a Brown recording potentiometer. A schematic diagram of this equipment is presented in Fig. 7. The gamma rays from the thulium source (initially 9 roentgens per hour at a distance of 6 in. in air)

were directed through the test section to the NaI crystal-photomultiplier tube assembly, where the unattenuated part of the beam produced a signal. The signal was amplified and transmitted to the recorder.

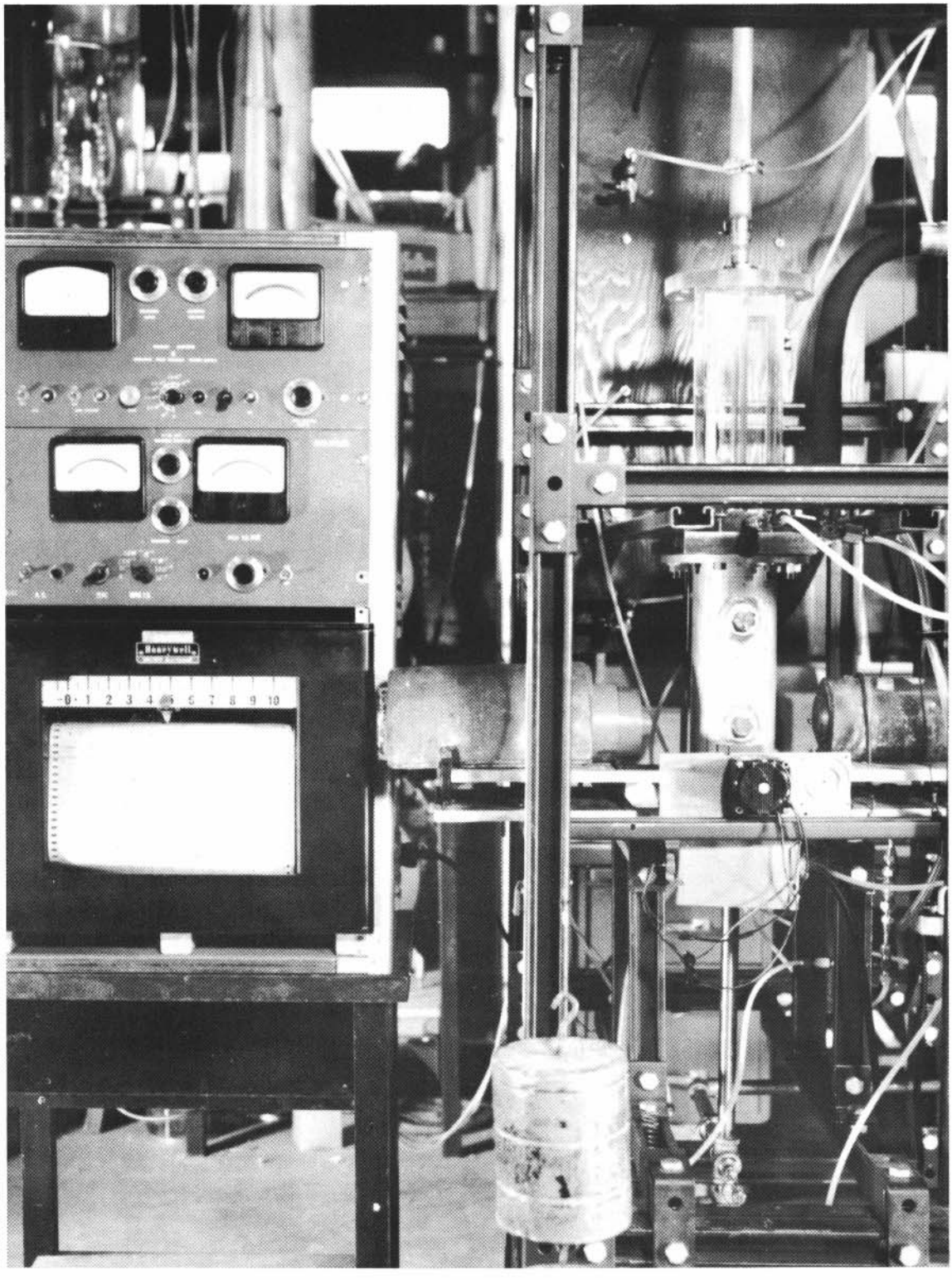

112-3457

Fig. 6. Void-fraction Measuring Equipment

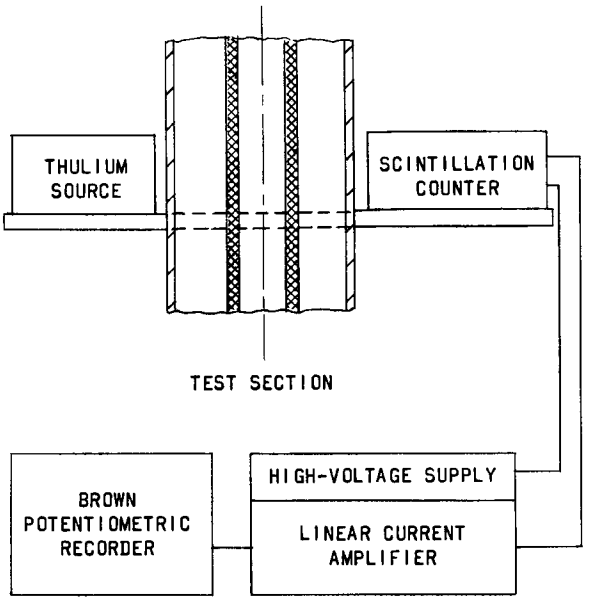

Fig. 7. Schematic Diagram of Void-measuring Equipment

The thulium source was shielded with lead for protection. A steel plate 0.25 in. thick was placed in front of the source to obtain a monoenergetic beam. The plate absorbed all lower-energy radiation except the 0.084-MeV peak gamma radiation. The scintillation crystal and photomultiplier tube assembly was cooled to ensure stable operation, and shielded with lead from stray radiation. Radiation to the scintillation counter was collimated by a 3-in.-thick lead shield with a $\frac{1}{16}$-in.-wide and $\frac{1}{2}$-in.-high window in front of the NaI crystal.

The source and the scintillation counter were mounted on a rigid carriage assembly which could traverse the test section horizontally and be adjusted vertically. Horizontal movement was controlled by a constant-speed motor, and vertical positioning was by means of a pulley arrangement.

Pool-gas-bubbling Equipment

The pool-bubbling experiments were performed in an open-top glass tank (13 in. x 24 in. x 12 in. high) filled with liquid about 4 in. above the top of the porous tube. The porous tube was held between two brass blocks fitted with neoprene gaskets, as shown in Fig. 8. The air system of the forced-circulation loop was used to provide metered air for the porous tube.

A 5-in.-long porous bronze tube (Oilite, $\frac{7}{8}$-in. O.D., $\frac{5}{8}$-in. I.D.), flushed and etched in the same way as the porous tubes used in forced-circulation tests, served for the demineralized water and ethylene glycol air-bubbling tests. For bubbling of air into "Freon-11," a 6.5-in.-long porous bronze tube (Oilite, 1-in. O.D., $\frac{7}{8}$-in. I.D.) was used. The Freon-11 (CCl_3F) used in these tests was supplied by E. I. du Pont de Nemours and Company. Pore density on the

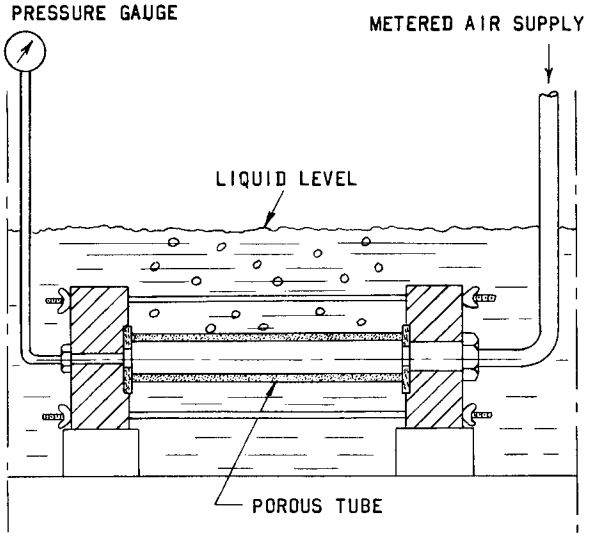

Fig. 8. Pool-bubbling Setup in Glass Tank

surface of both tubes, after being etched with dilute nitric acid, was determined by using a magnifying glass to count the pores in several $\frac{1}{4}$-in. x $\frac{1}{4}$-in. surface-area sections. The average density was found to be about 700 pores per square inch.

Pool-boiling Equipment

The Freon-11 pool-boiling experiments were performed in the same glass tank as the air-injection tests. A 6.5-in.-long porous bronze tube (Oilite, 1-in. O.D., $\frac{7}{8}$-in. I.D.), with its inside surface machined to close the inner pores, was used as a resistance heater to provide the heat flux for boiling. The outside surfaces of the Freon-11 boiling and air-bubbling tubes were machined and etched in an identical manner. The heated-tube arrangement used for the photographic studies is shown in Fig. 9, together with its insulated copper power cables. Power to the porous tube was provided through the forced-circulation loop power supply and measurement system.

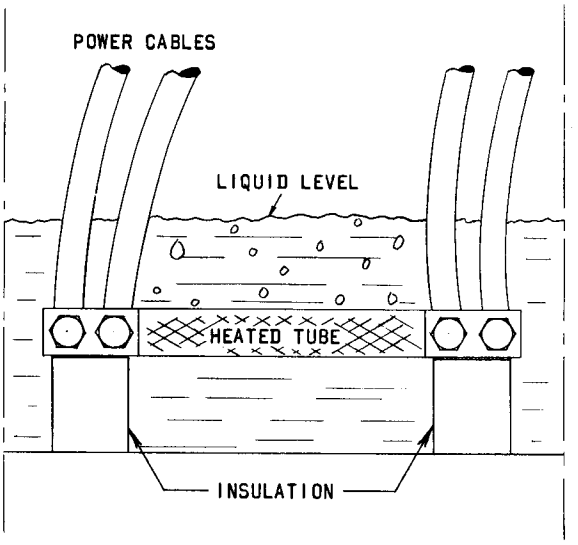

Fig. 9

Pool-boiling Setup in Glass Tank

Some of the equipment described was rather complex and involved. To ensure accuracy of results and safety of operation, specific procedures were outlined for operating the equipment and for taking data.

PROCEDURE

Test Procedure

This section describes the procedures followed in performing heat-transfer and void-fraction experiments with the forced-circulation loop.

In general, the loop operation in heat-transfer experiments was straightforward, since proper precautions had been taken to protect the

safety of the heated test section. The loop operation was usually stable, and equilibrium conditions were reached shortly after flow or power adjustments were made. Liquid-inlet temperatures were the only settings that required longer times to reach equilibrium operation at stable values.

Since the void-fraction measurements were made when the test section was neither insulated nor provided with power, loop-operation procedures were somewhat simpler. Thus, the loop-operation and void-measurement procedures for the void fraction tests are discussed separately in this section.

Procedure for Heat-transfer Experiments

Preparation for Tests. Before experiments were performed with the forced-circulation loop, all equipment operation was checked. The air supply, measurement, plenum systems, and liquid system were checked for leaks. The power supply and the heated test section were checked with a resistance meter for power leaks and shorts.

Demineralized water was used to wash the liquid lines before they were filled with the test water. For ethylene glycol tests, the lines were flushed with ethylene glycol after they were emptied of water, and then filled with the ethylene glycol used in tests. Surface tension of the test liquids was measured with a du Nouy tensiometer before and after the tests. Viscosity of ethylene glycol at room temperature was also measured with a calibrated Ostwald type Cannon-Fenske viscometer at the start and after completion of the tests. In all cases, measured properties changed less than 3% during the tests, and the values were within 2 to 4% of published values for water and ethylene glycol.[49]

Startup and Shutdown Procedure. Initially, the test sections in the forced-circulation loop had been drained of liquid. The air-flow rates to both porous sections were set at nominal values, and liquid line valves were opened to let the liquid into the test-section tubes. The liquid pump was started, and circulation continued until all the liquid in the tank was circulated through, so that any solution of air into liquid could take place.

All liquid manometer lines were bled to purge them of air. To bleed the test-section manometer and pressure-gauge transparent lines, liquid lines connected directly from the pump were used to purge them of air. This was possible because the pump lines were at higher pressure, and the liquid flow from the pump lines displaced any two-phase mixture in the manometer and pressure-gauge lines.

The desired liquid- and air-flow rates were then set. Control valves could be used to throttle the liquid flow, if necessary, to stabilize the pump supply.

All four channels of the temperature recorder were placed on monitoring positions, so that the temperatures in the tube could be observed continuously. Power to the test section was then turned on with the power control setting at zero input value, and power input was slowly increased to the desired value.

The loop was shut down by first turning off the power supply, then securing the manometers, and shutting off the liquid pump. The liquid from the test sections was then drained, the air lines to the test sections being left partly open to help drain the liquid and dry the tubes. Finally, the heat exchanger cooling-water supply was turned off, and all power supply-line circuit breakers were opened.

Taking of Data. The desired liquid-flow rate was set by adjusting the control valves and the pump motor speed. Air-flow rates were set by adjusting the control valves and pressure regulators.

The power setting was usually made so that fluid-film temperature drops for a given series of tests would be in the range of 30 ± 10°F. For a given series of tests at constant liquid-flow rate and changing air-flow rates, and even for specific series with varying liquid-flow rates, the power input was usually kept constant to eliminate the errors of power setting and power reading.

The desired liquid-inlet temperature to the test section was set by adjusting the cooling-water flow through the heat exchangers. Once stable operation was reached at a given liquid-flow rate, further adjustments were usually unnecessary if the power input was kept constant. Changing power, however, meant that a new equilibrium operating condition had to be reached, which sometimes took over an hour. Thus, there was an additional time-saving benefit from keeping power adjustments to a minimum.

After the desired air- and liquid-flow rates were set and the power input fixed, liquid inlet-temperature readings were taken every few minutes, and adjustments in cooling-water flow rate were made until the inlet temperature reached and maintained the desired value. During this time, wall thermocouples Nos. 2, 3, and 6 were monitored on the Texas Instruments recorder to determine when steady conditions in the heated test section were established.

After equilibrium conditions were established, all thermocouples were read on the potentiometer and recorded. Then all manometer, pressure-gauge, flow-pattern, and power-input readings were recorded. The inlet and exit fluid thermocouples, and also inside-wall thermocouples were then read again, and if the inlet liquid temperature (or any other temperature) deviated more than $\pm \frac{1}{2}$°F, the test was repeated. Sometimes,

when the load requirements of the laboratory were changing, significant (~2%) input-power fluctuations were caused by changes in the supply-line voltage. Therefore, tests were discontinued when these fluctuations occurred.

The procedure used for the tests with gas injection had to be modified somewhat for the all-liquid and zero-injection tests to prevent liquid from seeping through the porous heated tube. Although seepage was slow, only a limited time was available for taking readings. Therefore, for these tests, air injection to the heated section was set at a very small value, and shut off completely after equilibrium conditions were reached. Inside-wall thermocouples Nos. 2, 3, and 6 were monitored on the recorder, and Nos. 2 and 3 were also read on the potentiometer after the recorder traces indicated that they had reached a steady value. The air flow to the heated section was then set again at a nominal injection rate. The flow and pressure recordings, which were not visibly affected by the small changes in air injection, together with the temperature recordings described, provided the data for these tests.

The potentiometer (which picked up only D.C. output) was used to record thermocouple readings because it was more accurate than the Texas Instruments recorder. Although the input to the recorder was well-shielded and several input connections were tried, it could not be depended upon for greater than ±1°F accuracy. Nevertheless, the recorder was useful because it enabled continuous monitoring of wall temperatures.

Use of the recorder made the all-liquid and zero-injection tests possible because temperature traces could be followed visually and the reaching of steady-temperature conditions could be observed. This meant that equilibrium condition readings could be made and depended upon during the short times available for these tests. In tests with injection, heat-transfer effects could be observed when air- and liquid-flow conditions were varied slowly, or in small steps. The ability to observe continuous changes made it possible to select test conditions which were representative of local as well as overall heat-transfer trends. Thus, the recorder was useful in selecting test conditions and test points to be recorded.

Procedure for Void-fraction Measurements

Air-water void-fraction experiments were performed while there were still no insulation or wall thermocouples on the porous tube, and no power was supplied to the tube. This arrangement was necessary because void-fraction tests required frequent measurements taking several minutes when the tube was filled with liquid. The resulting seepage of liquid through the wall could damage the insulation or instrumentation, and this risk was not taken.

The preparation, startup, and shutdown procedures for the loop were the same as for the heat-transfer tests, except that no power or

wall-temperature measurements were involved. The amplifier and the photomultiplier tube system were warmed up for at least 24 hours before data were taken. Usually, the amplifier and photomultiplier tube, including the photomultiplier tube cooling, were kept on continuously during the months that tests were being performed.

The traversing technique described by Petrick and Swanson[48] was used to obtain void-fraction data. With this method, a continuous trace of the density variation across the tube was obtained on the Brown recorder while the source-scintillation counter (with the narrow $\frac{1}{16}$-in. window) table assembly traversed the tube cross section horizontally.

Calibration traverses were first made to obtain attenuation characteristics of the tube filled with liquid and with air. These empty and full recordings were made for each test position and repeated several times during the day to check amplifier drift. Full readings were taken with and without the tube wall filled with water, but no difference in the recordings could be detected. Actual two-phase void-fraction traverses were then made for the desired air- and water-flow conditions at given positions. These positions were usually at No. 2 and No. 6 thermocouple locations. A few traverses were also made in the transparent section.

Design of Experiments

The heat-transfer and void-fraction tests covered the area between equipment limits with approximately even spacing of test points for a given test series that examined a particular aspect of the program. General criteria for acceptable experiment design were also set to ensure that results would be accurate and valid. Sample runs were selected to be repeated to check the reproducibility of results.

In heat-transfer experiments, test-section temperatures were monitored continuously with changing conditions on the potentiometric recorder to check how well the chosen test points represented local and overall heat-transfer trends. Test points were adjusted, if necessary, to get a better representation of these trends.

Liquid test temperatures were kept in the same range as room temperatures (usually 70 to 80°F) so that liquid-vapor pressures would be low, and, thus, the effects of heat of vaporization on heat transfer would be minimized. The narrow range of test temperatures around room temperature also helped to keep liquid property changes to a minimum, and made heat losses in the lines negligible. In design of air-water heat-transfer experiments, a criterion was set to limit the transport of heat through heat of vaporization to 5% of the total heat flux input. The heat-of-vaporization effect and its influence on heat-transfer results are examined in detail in

Appendix C, where calculations are also outlined. The accuracy of air-water heat-transfer results could be optimized for latent heat transport by choosing fluid-film temperature drops in the range of 30 ± 10°F.

Criteria for air-heating losses, caused when air heats up in passing through the porous tube, were set at 2 and 5% of total heat flux for air-water and air-ethylene glycol experiments, respectively. A higher percentage could be used for air-ethylene glycol experiments because the heat of vaporization effects were negligible in air-ethylene glycol tests. Air-heating losses and their calculation are discussed in detail in Appendix C.

Restrictions were also placed on the degree of nonuniformity of gas-injection rate along the length of the heated tube caused by two-phase static-pressure drop along the tube. This limited the allowable two-phase pressure drop in the test section, consequently also limiting the mass-flow rates. The maximum variation of local gas-injection rates allowed at the ends of the porous tube from the average rate was limited to 50%. The variation of local gas-injection rates with static-pressure drop, and the calculation of local gas injection rates, are discussed in greater detail in Appendix C.

Although the design criteria discussed restricted the range of gas-injection rates and mass-flow rates that could be used in the present experiments, they provided uniform requirements for acceptable test points, and ensured that the accuracy of none of the results would be compromised by the extraneous effects listed.

Analysis of Data

Data of Heat-transfer Experiments

Heat-transfer data were analyzed to study the general behavior of two-phase heat transfer for various hydrodynamic conditions. The calculations that were required to process the data (tabulated in Appendix E) into final results are outlined in Appendix C. Accuracy and precision of the heat-transfer tests are analyzed in Appendix D.

After initial heat-transfer tests were completed to check out the operation of loop equipment and instrumentation, thermocouples Nos. 1, 4, 5, and 8 were recording lower than expected for all the tests. Since these inside-wall thermocouples were the ones closest to the silver-soldered flange and center joints of the porous tube (Fig. 4), the low readings could have been caused by lower heating rates at those points. The lower heating rates were probably caused by heat losses to the flanges and the center joint, because tube connections were made at the flanges and the center by first copper-plating and then silver-soldering these joints. These processes naturally reduced the resistance of the tube in the joined

areas, lowering the heating rates and the temperatures there proportionately. Since the actual heat fluxes could not be determined in these areas, only inside-wall thermocouples Nos. 2, 3, 6, and 7 remained useful for studying heat-transfer rates.

When the quality from position No. 7 to No. 2 (Fig. 4) did not change much for a given test, the flow type and conditions between these two positions did not vary much either, and parallel heat-transfer-coefficient curves typical of Fig. 10 were found at thermocouple positions Nos. 2, 3, 6, and 7 for each test series. The differences in the heat-transfer-coefficient values at the four positions were mainly due to deviations of the actual thermocouple junctions from their expected locations in the wall of the tube (see Appendix B), and in a small extent to different thermal entrance effects. The small variation of quality and flow conditions along the tube also had some effect. The influence of pressure drop on injection rate along the tube (which was minor for a majority of tests) should be included also, as discussed in Appendix C, when heat transfer at various positions is considered.

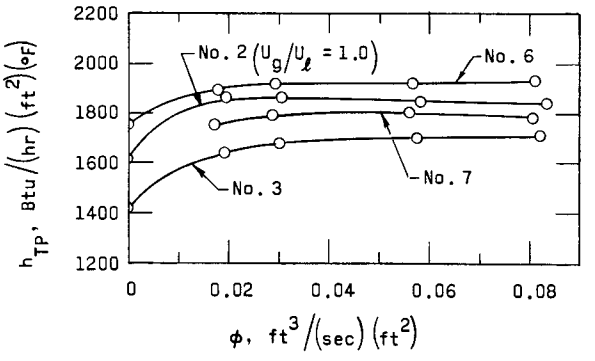

Fig. 10. Air Water h_{TP}'s at Four Thermocouple Positions (U_ℓ = 2.25 ft/sec)

Since the primary purpose of the experiments was to investigate the behavior of two-phase heat transfer for different conditions rather than to obtain average values of heat-transfer coefficients, a single-thermocouple rather than multi-thermocouple presentation was chosen for the results. This type presentation was feasible because the equipment was designed so that hydrodynamic conditions for a given position could be varied. When the experimental results were presented for a single thermocouple location, the heat-transfer trends under varying hydrodynamic conditions could be observed more clearly because they were not obscured by errors due to thermocouple junction location. Thus, in essence, the single-thermocouple presentation replaced the multiple graphs of Fig. 10 by a single graph of higher precision (see Appendix D), where relative heat-transfer behavior could be observed with greater accuracy.

Thermocouple position No. 2 was chosen for the single-graph presentation of all results because it was closest to the transparent section and because any entrance effects would be a minimum there. Since this location was close to the transparent section, it was fairly certain that the short extrapolation of the flow patterns observed from the transparent section into the heated section would not alter their basic character.

Data of Void-fraction Experiments

The data of void-fraction tests are tabulated in Appendix F. Air- and water-flow conditions in these tests were calculated in the same manner as for the heat-transfer tests. Void-traverse measurements were analyzed using a technique described in detail by Petrick.[42] The radial void fractions were expressed as a function of the polynomial

$$\alpha = d + a\left(\frac{r}{R}\right)^2 + b\left(\frac{r}{R}\right)^4 + c\left(\frac{r}{R}\right)^6, \tag{1}$$

and the average void fractions were obtained by integrating Eq. (1). In Eq. (1), $r = 0$ at the tube centerline and a, b, c, and d are constants characteristic of a particular void distribution. The $\bar{\alpha}$ values obtained by this method were checked for various selected void distributions using numerical integration of the void traverses as described in detail for tube geometry by Richardson.[50] The two methods were found to be consistent within 6%.

Accuracy of the gamma-attenuation technique has been analyzed in previous reports.[43,47,48,50] Its application in the present study is estimated to give average void fraction values within ±10%, the estimate being based on the previous analyses.

The data that were obtained and analyzed according to the procedures outlined in this chapter are discussed next.

PRESENTATION AND DISCUSSION OF RESULTS

Similarity between Boiling and Gas Bubbling

A purpose of this study was to investigate how well and for what conditions gas injection simulated the hydrodynamic aspects of boiling. N. Zuber and G. B. Wallis studied the similarities between nucleate boiling and gas bubbling from porous surfaces. Zuber[4] showed that the types of bubbles and bubble formations in nucleate boiling and in gas bubbling were hydrodynamically similar. More extensive analytical and experimental investigations by Wallis[2,11] have shown that both air and vapor bubbles in a liquid are formed, grow, and depart from the solid surface in essentially the same manner, resulting in similar initial and boundary conditions in both systems.

The porous tubes used in this experiment had a dense population of pores (counted to be about 700 per square inch) that were all potential bubbling sites. Since nucleate boiling is strongly dependent on surface conditions, it was felt that the same type of surface should be used for studying hydrodynamic similarity between boiling and bubbling. The outer surfaces of two, 1-in.-O.D. porous tubes were etched identically to study pool boiling and bubbling processes in Freon-11 (CCl_3F), which boils at 74.8°F at atmospheric pressure. Figs. 11 and 12 show that saturated Freon-11 boiling and air bubbling into Freon-11 at about 40 to 60°F are qualitatively similar, and that bubble diameters and flow formations are alike.

A quantitative comparison based on the similarity of photographs for these complex flow patterns is difficult since pictures of flow patterns appeared similar for a range of conditions. In addition, the air-injection rate does not reflect the actual gas phase seen in the bubbling pictures. Since, unavoidably, the vapor pressure of Freon-11 was significant at the temperatures of the air-bubbling tests, Freon-11 vaporized into the air, sometimes producing substantial additional gas volume and further obscuring quantitative comparison.

Bubbling of air from a porous, $\frac{7}{8}$-in.-O.D. tube into both water and ethylene glycol (Fig. 13) also produces bubbles and flow types similar to Freon 11 pool boiling. The air-bubbling pictures in Fig. 13 are similar to the same type of gas-injection pictures presented by Wallis[11] in his simulated boiling study, where bubbling flow patterns were investigated up to very high gas-injection rates. By correlating the pool-bubbling flow patterns to equivalent boiling patterns, Wallis further demonstrated the existence of hydrodynamic similarity between gas bubbling from porous surfaces and nucleate boiling.

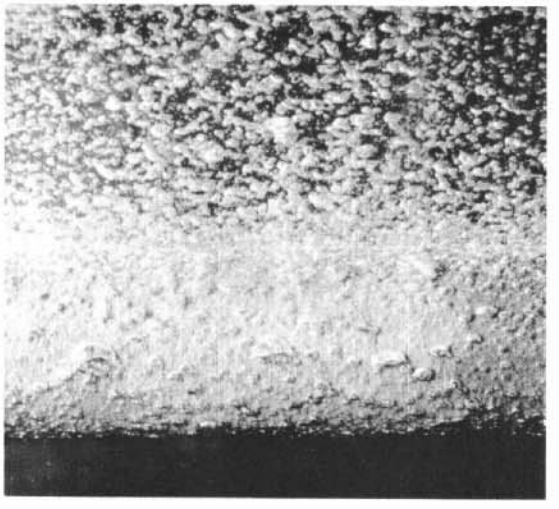

(A) BOILING
$q'' = 5{,}000$ Btu/(hr)(ft^2)

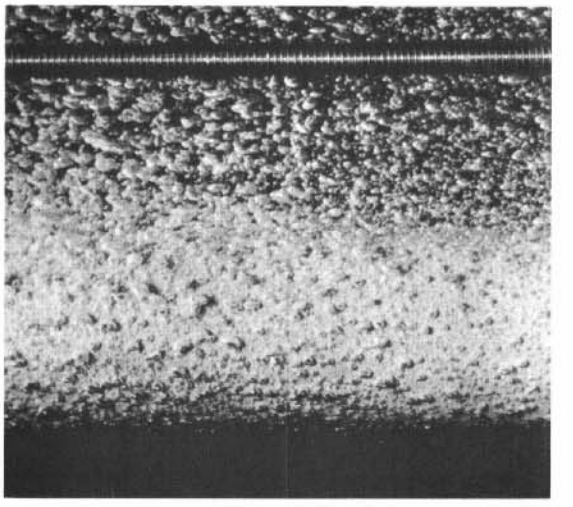

(B) BUBBLING
$\phi = 0.005$ ft^3/(sec)(ft^2)

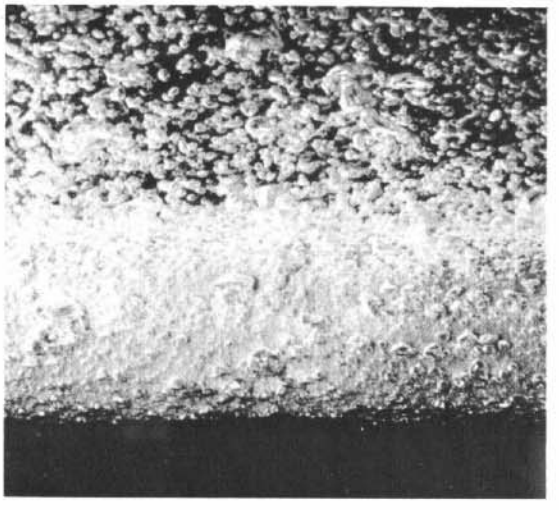

(C) BOILING
$q'' = 10{,}000$ Btu/(hr)(ft^2)

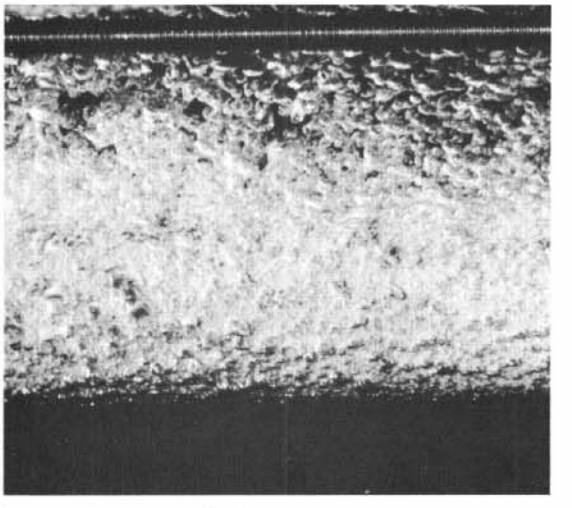

(D) BUBBLING
$\phi = 0.010$ ft^3/(sec)(ft^2)

112-3657

Fig. 11. Saturated Boiling and Gas Bubbling in Freon-11, Low Rates

(A) BOILING
$q'' = 28{,}500$ Btu/(hr)(ft^2)

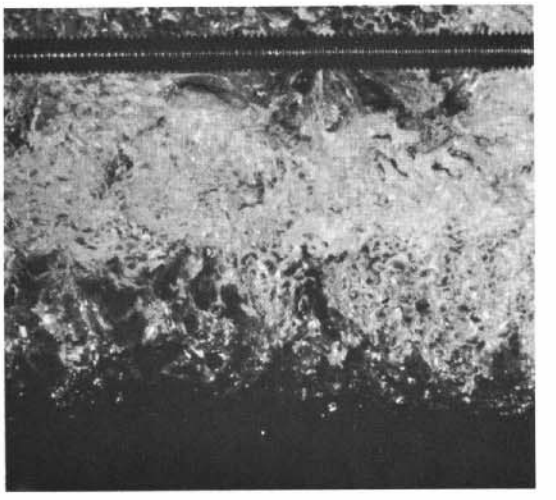

(B) BUBBLING
$\phi = 0.090$ ft^3/(sec)(ft^2)

(C) BOILING
$q'' = 70{,}000$ Btu/(hr)(ft^2)

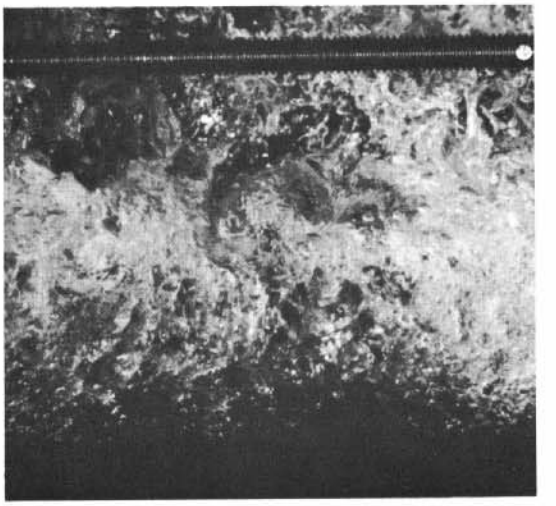

(D) BUBBLING
$\phi = 0.380$ ft^3/(sec)(ft^2)

112-3574

Fig. 12. Saturated Boiling and Gas Bubbling in Freon-11, High Rates

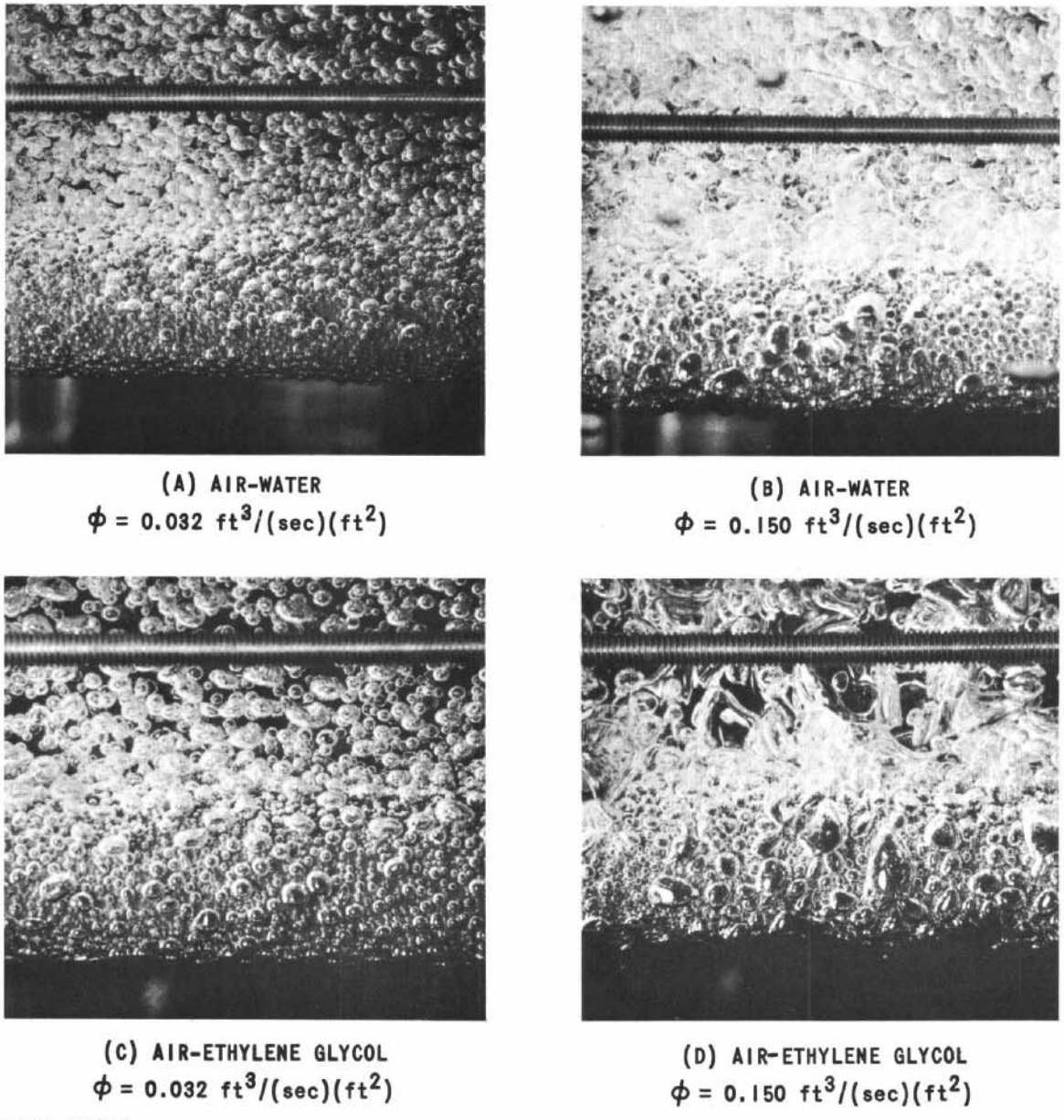

(A) AIR-WATER
ϕ = 0.032 $ft^3/(sec)(ft^2)$

(B) AIR-WATER
ϕ = 0.150 $ft^3/(sec)(ft^2)$

(C) AIR-ETHYLENE GLYCOL
ϕ = 0.032 $ft^3/(sec)(ft^2)$

(D) AIR-ETHYLENE GLYCOL
ϕ = 0.150 $ft^3/(sec)(ft^2)$

112-3573

Fig. 13. Gas Bubbling into Liquid from a $\frac{7}{8}$-in.-diameter Porous Tube

The gas-bubbling analogy can be extended to forced-circulation boiling, because growth and departure of bubbles from the wall are controlled by equivalent hydrodynamic forces and flow conditions in both gas-injection and boiling systems.

Although the effect of subcooling as such cannot be simulated by the gas-injection system, the hydrodynamic heat-transfer mechanisms in subcooled boiling should be represented as well for subcooled as for

saturated boiling by gas injection. In addition, the analogy is limited to two-phase flow types where nucleation (i.e., vapor-bubble generation) occurs on the heated wall. Hosler,[18] in his visual study of forced circulation boiling of water, observed nucleation in the bubble and slug-flow regions at lower qualities, but could not observe any at high qualities in the annular flow regime. Hewitt et al.,[51] however, did observe nucleation in annular film flow at lower mass-flow rates in their study of steam-water flow and heat transfer. Thus, although the gas-bubbling analogy is generally limited to lower qualities and corresponding flow patterns, it can be useful for studying the effect of nucleation in annular flow where such nucleation exists.

Two-phase Flow Patterns

Since flow patterns influence heat transfer in two-phase systems, they were observed and reported for every air-water and air-ethylene glycol test. The primary purpose of flow-pattern observations in the present experiments was not to study two-phase flow patterns as such, but rather to provide information so that heat-transfer results could be discussed in terms of flow patterns.

Because of the multitude of flow patterns and the various interpretations accorded to them by different observers, no uniform procedure exists at present for describing and classifying two-phase flow types. Thus, the flow patterns observed at the exit of the porous heated test section were classified into four basic types, and described according to the interpretation of this observer, as follows:

1. Bubble Flow. Liquid flows with gas bubbles more or less uniformly dispersed in it. As the liquid-flow rate is increased, the size of the gas bubbles decreases.

2. Slug Flow. Centrally located slugs of gas, surrounded by an annular core of liquid with some entrained gas bubbles, flow between plugs of liquid populated with gas bubbles. The flow progresses with oscillations or slugging, the liquid film falling back into the central gas core to form new liquid plugs and being pushed up again by the oncoming gas slugs. As the liquid flow rate is increased, gas slugs become smaller with more gas bubbles appearing in the liquid phase. Another variation of slug flow occurs when gas-flow rate is increased at lower Froude numbers, and froth flow develops a discontinuous gas core which appears to be progressing with impulse type motion.

3. Froth Flow. The gas-liquid mixture flows in a highly dispersed or emulsion type form, with turbulence and continuous interaction occurring between the phases.

4. Annular Flow. Gas flows in the central core, and liquid flows in an annular film on the tube walls. As the liquid-flow rate is increased, more gas bubbles become entrained in the liquid film, and the flow takes on an appearance of froth flow with a central air core.

The representative flow-pattern pictures in Fig. 14 illustrate the two-phase flow types discussed. These photographs are for the air-water system, but the flow patterns shown were also observed in the air-ethylene glycol experiments.

Although the flow patterns discussed and illustrated were observed at the exit of the porous section, the basic character of the flow pattern should remain the same for several tube diameters after gas injection ceases. Therefore, except for local gas-bubble effects at the solid-liquid boundary, the observations made should accurately represent flow patterns occurring in the porous tube.

The air-water flow patterns observed were plotted on superficial-gas-velocity versus superficial-liquid-velocity coordinates (Fig. 15) to show under what flow conditions they occurred in the present porous-tube system. The flow-pattern data in Fig. 15 were taken for conditions of equal gas-injection rates for a given test in both the heated and the unheated porous test sections in the range of $0.03 < \phi < 0.50$, but the flow-pattern regions shown in Fig. 15 were found, in general, to represent other conditions found in the tests just as well. Correlation of the data in Fig. 15 on the basis of gas-injection rate versus ratio of volumetric flow rates (ϕ versus U_g/U_ℓ) was tried also, but was not successful.

Since the transitions between flow patterns were not abrupt, but rather quite gradual under changing flow conditions, the flow-pattern regions shown in Fig. 15 present only general areas (without rigid boundaries) where the flow patterns occurred. Transitions between flow patterns for the air-ethylene glycol system occurred at somewhat lower air-superficial velocities than for the air-water experiments shown.

The outline of the annular region in Fig. 15 appears to be ambiguous because two different boundaries represent the transition to annular flow. This ambiguity is due to the nature of the flow and of the observation technique. It is also partly due to the way flow patterns are described and defined.

As the liquid-inlet velocity was increased in the tests, the slugging frequency increased and it became difficult to separate slugging flow from annular flow, especially since the flow was frothy. Therefore, the flow defined as slug flow for the sake of simplicity at $U_\ell = 2.25$ ft/sec was actually slugging-froth flow. At liquid-inlet velocities of 4.5 and 9.0 ft/sec, the two-phase flow mixture moved with high speed, and it was difficult to see whether the air core was continuous or had high-velocity slugs of

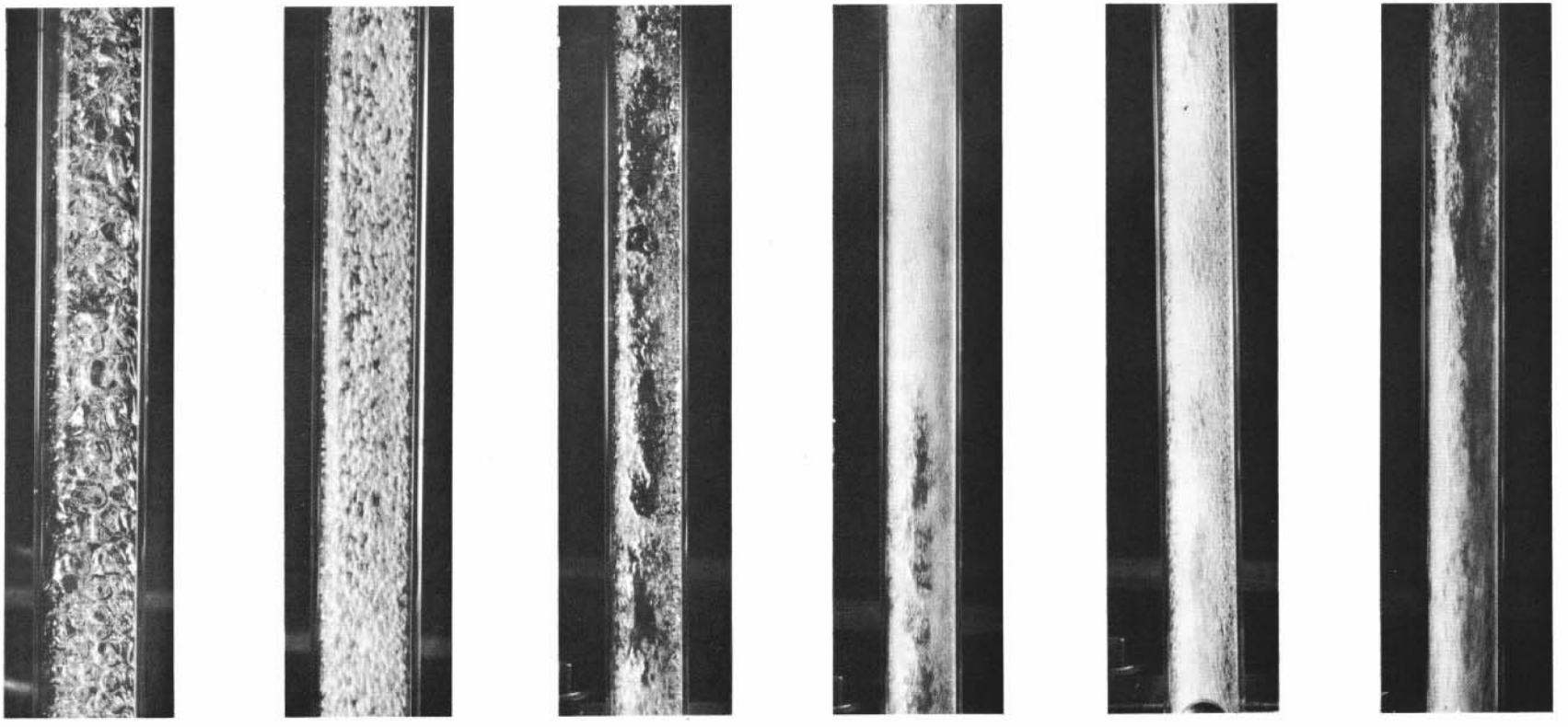

Fig. 14. Representative Two-phase Flow Patterns (Tube I.D. is $\frac{5}{8}$ in.)

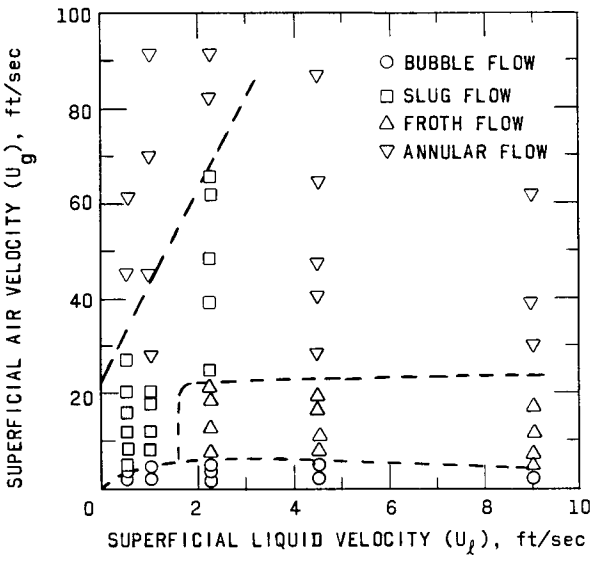

Fig. 15. Two-phase Flow-pattern Regions

water entrained in it. Therefore, what was defined as annular flow using the visual observation technique, could, quite possibly, have been defined as slug flow according to the electric probe technique developed recently for flow-pattern measurement.

Therefore, the visual technique could create some difficulties in observing the flow patterns and also in interpreting the observations. These difficulties would, in turn, affect the classification of two-phase flow patterns presented in Fig. 15. Apart from the uncertainties of the visual technique, the descriptions and illustrations of the flow patterns observed in this study correspond satisfactorily to flow types summarized by Vohr,[16] and in similar porous-wall gas-generation[11,19] or boiling[17,18] systems.

Void Fractions and Phase Distributions

It is generally accepted that gas and liquid phases do not flow with the same velocity in two-phase systems. Since relative velocity, or "slip," exists between the phases, neither average phase velocity nor void fraction (fractional area of pipe cross section occupied by the gas phase) can be determined from mass-flow rates alone. Because it was felt that actual liquid-phase velocity and phase distribution may be important in heat-transfer and bubble dynamics, void-fraction measurements at selected porous tube cross sections were made using the gamma-ray attenuation technique discussed previously.

Since it was not feasible to measure void fractions during heat-transfer tests, it was attempted to cover a wide range of conditions for the air-water void-fraction tests made before the heated section was instrumented and insulated. Nevertheless, the test conditions did not always reflect the most interesting conditions found later in heat-transfer tests.

Average phase velocities determined from void-fraction measurements are presented here in terms of phase velocity ratio (slip ratio), defined as

$$\frac{V_g}{V_\ell} = \frac{W_g}{W_\ell} \frac{\rho_\ell}{\rho_g} \left(\frac{1 - \bar{\alpha}}{\bar{\alpha}} \right). \qquad (2)$$

Equation (2) is derived from the conservation-of-mass relationship for each phase, i.e.,

$$W_g = \rho_\ell V_g A_g = \rho_g V_g A_T \bar{\alpha},$$

and

$$W_\ell = \rho_\ell V_\ell A_\ell = \rho_\ell V_\ell A_T (1 - \bar{\alpha}).$$

Slip ratios determined for several water-flow rates at tube cross sections $4\frac{1}{4}$ and $9\frac{7}{8}$ in. from the entrance of the heated test section (the No. 6 and No. 2 thermocouple positions, respectively) are presented in Fig. 16. Considering the accuracy of void-fraction measurements, the slip-ratio versus volumetric-air/water-ratio plots (Fig. 16) correlate the results fairly well for each position.

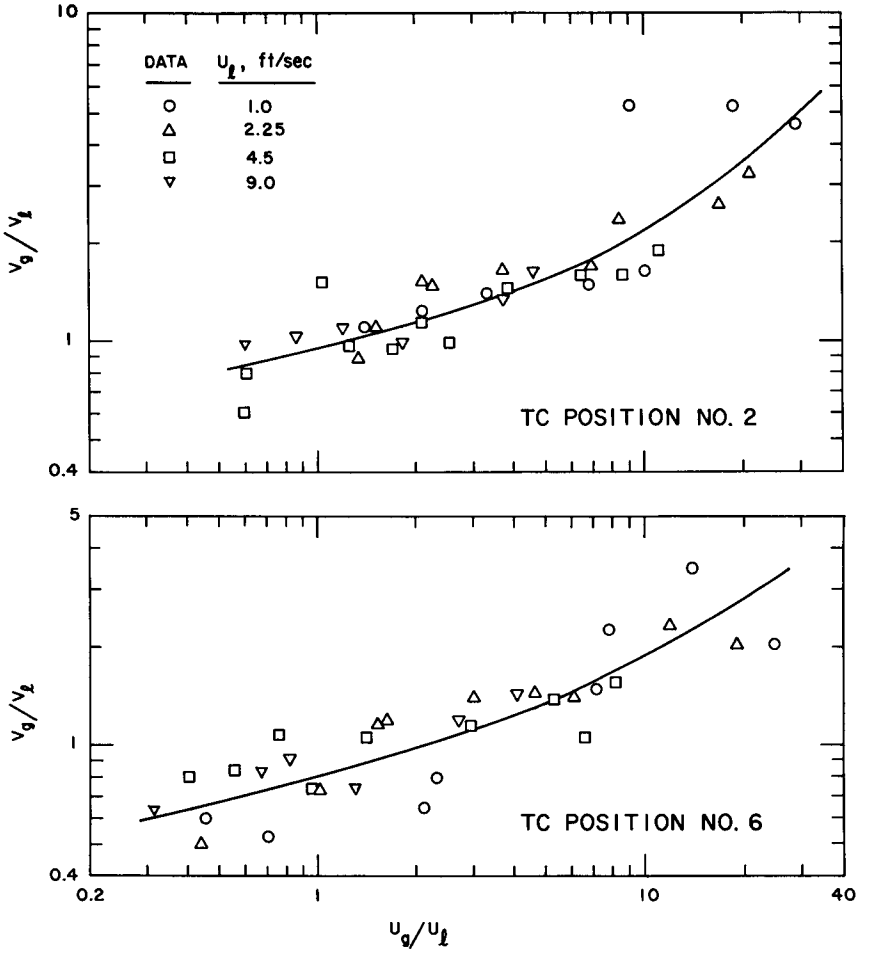

Fig. 16. Correlation of Slip Ratios

Although Marchaterre and Hoglund[41] found in their correlation that slip ratios decreased with increasing mass velocity, this effect could not be discerned to any extent from results in Fig. 16.

The influence of gas bubbling on slip ratio in this system is evidenced by the different slip ratios for the two positions (Fig. 16) at a given U_g/U_ℓ. The different slip ratios at the two positions illustrate that gas generation on the heated wall influences flow development and phase distribution in a tube. Another interesting point in Fig. 16 is that slip ratios become less than one at low U_g/U_ℓ values (or qualities), which at first glance would appear to be unusual for upward gas-liquid flow.

The low slip ratios, together with flow- and phase-distribution development, can be best discussed and explained in terms of radial-phase distributions found in the tube. Fortunately, the method of void-fraction analysis used in this study enabled radial-phase distributions to be obtained in addition to average void-fraction values. Typical phase distributions found for air-water tests are presented in Figs. 17 and 18 to facilitate this discussion. Since accuracy of the measurements decreased as the tube walls were approached, the curves near the wall are shown as dashed lines.

To simplify references to position, the positions at which void-fraction measurements were made are designated as follows:

No. 1 — $4\frac{1}{4}$ in. from entrance to heated section (No. 6 thermocouple position)

No. 2 — $9\frac{7}{8}$ in. from entrance to heated section (No. 2 thermocouple position)

No. 3 — 9 in. after exit from heated section (in the observation section)

The phase distributions for various conditions presented in Figs. 17 and 18 illustrate that two-phase flow development is influenced significantly by gas generation at the tube walls. Although phase-distribution data in literature are scarce, the results presented by Petrick[42] for upward flow of air-water in Plexiglass sections (non-porous) show a power-law type distribution of phases similar to that shown for position No. 3 in Fig. 17, A-1. Bankoff[44] also assumed a power-law distribution in the development of his variable-density model which was used for prediction of void fractions.

The present results show, however, that the distribution of phases when gas is generated at the walls is not very close to a power-law type, especially at low qualities in the bubble-flow region (Figs. 17B and 18B). The present phase distributions are more similar in their shape at low- and higher-void fractions to the phase distributions presented in an illustrative plot by Christensen[43] for upward flow of boiling water in a heated channel.

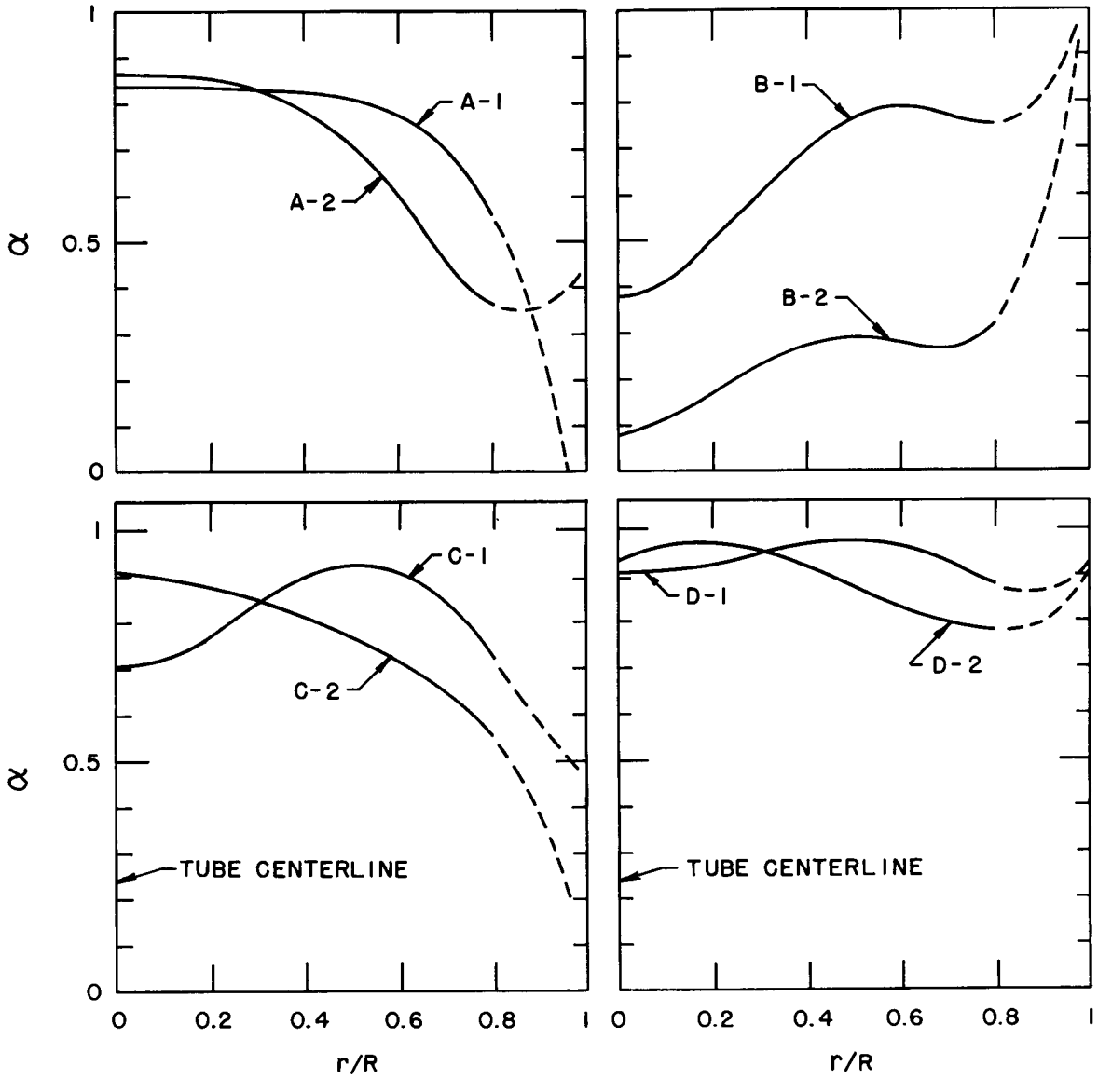

CURVE	TC POS.	V_g/V_ℓ	U_g/U_ℓ	ϕ
A-1	3	1.68	2.3	0
A-2	2	1.23	2.1	0.035
C-1	1	2.20	7.8	0.035
C-2	2	5.45	9.0	0.035

CURVE	TC POS.	V_g/V_ℓ	U_g/U_ℓ	ϕ
B-1	1	0.62	2.15	0.11
B-2	1	0.6	0.44	0.025
D-1	2	4.6	29.0	0.10
D-2	1	2.0	25.0	0.10

Fig. 17. Phase Distributions for Air-Water, with U_ℓ = 1.0 ft/sec

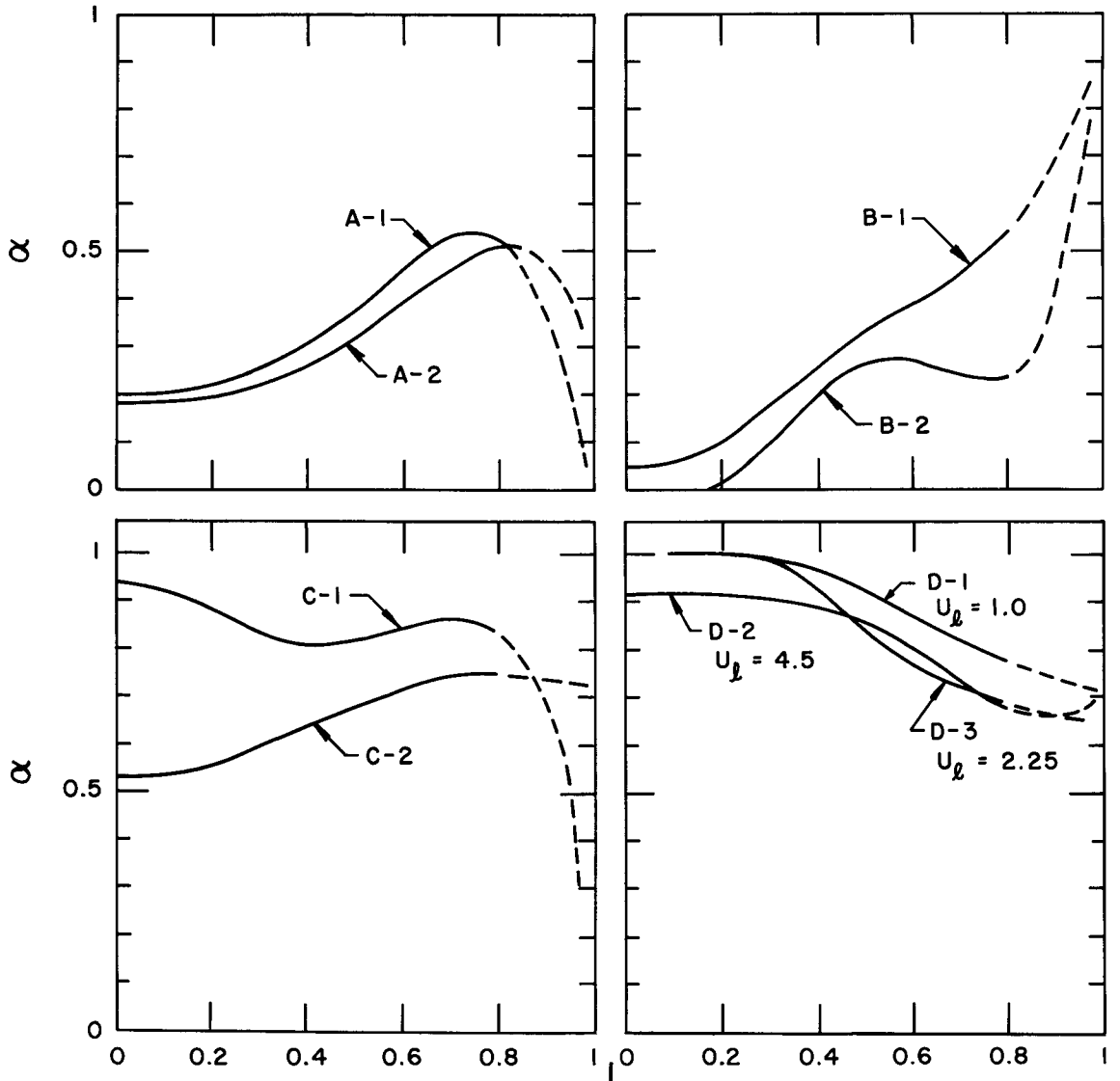

CURVE	TC POS.	V_g/V_ℓ	U_g/U_ℓ	ϕ
A-1	3	1.05	0.63	0
A-2	1	1.08	0.75	0.035
C-1	2	1.4	3.8	0.10
C-2	1	1.15	2.9	0.10

CURVE	TC POS.	V_g/V_ℓ	U_g/U_ℓ	ϕ
B-1	2	0.6	0.61	0.045
B-2	1	0.35	0.19	0.045
D-1	2	1.5	6.35	0.110
D-2	2	1.64	6.65	0.110
D-3	2	1.70	6.37	0.135

Fig. 18. Phase Distributions for Air-Water, with U_ℓ = 4.5 ft/sec (except as noted)

Since flow velocity can be expected to be higher in the center of the tube than near the wall, slip ratios of less than one are not surprising for the phase distributions shown here at low values of U_g/U_ℓ. Quantitatively, this can be examined by calculating the slip ratio obtained by using the phase distributions shown in Figs. 17 and 18. To perform the calculations, two assumptions made by Bankoff[44] are used here. It is assumed that there is no local slip between the phases:

$$V_g(r) = V_\ell(r) = V(r).$$

Furthermore, it is assumed that the local velocity can be represented by the following power-law distribution, as for single-phase flow:

$$V(r) = V_{r=0}\left(1 - \frac{r}{R}\right)^m,$$

where $r = 0$ at the tube centerline, and m is a positive constant.

The liquid and gas mass-flow rates are given by

$$W_\ell = \rho_\ell \int_0^R V_{r=0}\left(1 - \frac{r}{R}\right)^m \left[1 - \alpha(r)\right] 2\pi r dr,$$

and

$$W_g = \rho_g \int_0^R V_{r=0}\left(1 - \frac{r}{R}\right)^m \alpha(r) 2\pi r dr.$$

Since the local void fractions in this study were calculated (see PROCEDURE chapter) from the polynomial

$$\alpha = d + a\left(\frac{r}{R}\right)^2 + b\left(\frac{r}{R}\right)^4 + c\left(\frac{r}{R}\right)^6, \tag{1}$$

it can be used to integrate out the mass-flow rate expressions. Then the slip ratio can be calculated from

$$\frac{V_g}{V_\ell} = \left(\frac{1 - \bar{\alpha}}{\bar{\alpha}}\right)\left(\frac{W_g}{\rho_g}\right)\left(\frac{\rho_\ell}{W_\ell}\right), \tag{2}$$

resulting in

$$\frac{V_g}{V_\ell} = \left(\frac{1 - \bar{\alpha}}{\bar{\alpha}}\right)\left[\frac{\dfrac{d}{(m+1)(m+2)} + \dfrac{3!a}{(m+1)(m+2)\ldots(m+4)} + \dfrac{5!b}{(m+1)(m+2)\ldots(m+6)} + \dfrac{7!c}{(m+1)(m+2)\ldots(m+8)}}{\dfrac{1-d}{(m+1)(m+2)} - \dfrac{3!a}{(m+1)(m+2)\ldots(m+4)} - \dfrac{5!b}{(m+1)(m+2)\ldots(m+6)} - \dfrac{7!c}{(m+1)(m+2)\ldots(m+8)}}\right]. \tag{3}$$

Table I compares the slip ratios found using Eq. (3) to the actual slip ratios determined from Eq. (2) using experimental U_g/U_ℓ values.

Table I

COMPARISON OF SLIP RATIOS

Test	Slip Ratio		
		Eq. (3)	
	Eq. (2)	m=1/7	m=1/3
Fig. 17, B-1, No. 1	0.62	0.95	0.78
Fig. 17, B-2, No. 1	0.60	0.785	0.65
Fig. 18, B-1, No. 2	0.60	0.885	0.74
Fig. 18, B-2, No. 1	0.35	0.835	0.67
Fig. 18, A-2, No. 1	1.08	1.02	0.98
Fig. 17, A-1, No. 3	1.68	1.18	1.42
Fig. 17, C-2, No. 2	5.45	1.75	1.30

Although this analysis was a simplification (since local slip most likely does exist, and since the velocity distribution was approximated by a power-law distribution), it does predict the correct trends in slip ratios for different phase distributions. In addition, it shows that slip of less than one is reasonable at low-void fractions where bubble flow is developing, because most of the gas phase is concentrated near the walls of the tube (Figs. 17B and 18B).

The previous analysis (where the power-law distribution for local velocity was used) also showed why the slip ratios are somewhat higher for position No. 2 than for position No. 1 at a given U_g/U_ℓ, and why they increase with increasing U_g/U_ℓ. Phase distributions for any run, such as in Figs. 17C, D, and 18B, C, whether at low or high average-void fraction, show that the gas phase in position No. 2 is developed more towards the center of the tube when the velocity is higher. Consequently, the slip ratios are also higher for position No. 2. The phase distributions presented also show how the gas phase develops towards the center of the tube with increasing U_g/U_ℓ values, resulting in higher mean gas-phase velocities, and, therefore, higher slip ratios. Similar development of the gas phase toward the center of the channel with increasing void fraction was also observed in Christensen's[43] results for boiling water.

If it is assumed that the bubble-flow distribution in Fig. 18A-1 for position No. 3 will eventually assume the same type of distribution as in Fig. 17A-1 for position No. 3, it can be observed that flow development at higher mass velocities is slower because the higher momentum of the liquid

phase tends to reduce the effect of the transverse velocity of the bubble departing from the wall. At higher void fractions, however, this difference in flow development becomes less pronounced. Thus, although Fig. 18D shows that gas phase is more developed towards the center of the tube for lower mass velocities, the difference in phase distributions is not significant. In this connection, it may also be mentioned that the similar phase distributions of Fig. 18D also have similar slip ratios, illustrating again the dependence of slip on phase distribution.

Two-phase Heat Transfer without Gas Injection

Some two-phase heat-transfer results were obtained in this study when air flow was shut off in the heated test section during the regular test series with gas injection. These experiments with no gas bubbling, or zero injection, are substantially equivalent to two-phase, two-component heat transfer in a heated tube with solid walls and are treated as such in this presentation.

The zero-injection results are presented and discussed first, so that the phenomena involved in two-phase heat transfer without boiling or evaporation can be examined before trying to explain gas bubbling and other effects in the more complicated two-phase flow system with injection. The procedure of investigating various hydrodynamic effects separately, to which the present experimental system is well suited, is followed in this study because it is hoped to reach a better understanding more easily of the overall processes involved in the complicated heat-transfer system by examining individually all the effects that are involved.

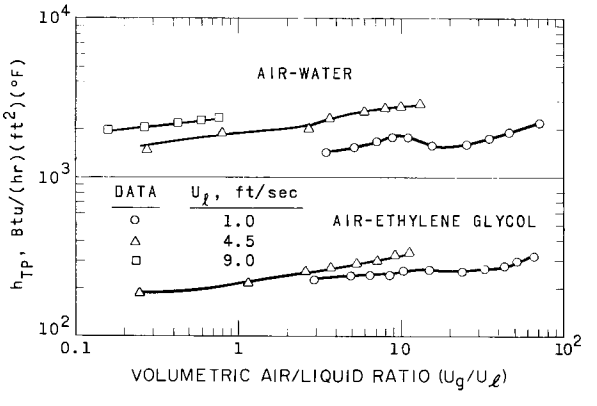

Fig. 19. Zero-injection Heat-transfer Results

Air-water zero-injection results are presented in Fig. 19. Heat-transfer coefficients increase slowly in the bubble, froth, and annular flow regimes with increasing air/water ratios for the three liquid flow rates tested. Heat transfer in the slug-flow regime at a low mass-flow rate appears to become rather uncertain, as the loop in the plot for U_ℓ = 1.0 ft/sec illustrates. This behavior is possible in the slug regime because of the nature of slug-type flow. Slugs of vapor rising between plugs of liquid carry the liquid downstream, and the liquid film on the heated walls can be accelerated or slowed down by this action. Even actual downflow of liquid at the wall can occur, since the net liquid flow can be propagated by the liquid plugs interspersed between vapor slugs.

At higher liquid mass-flow rates, froth flow replaced slug flow in the present system, resulting in monotonic behavior of h_{TP} with increasing air flow. Air-ethylene glycol results are also presented in Fig. 19. The heat-transfer coefficients for air-ethylene glycol are much lower than for air-water because the viscosity of ethylene glycol is about 17 times that of water for test conditions. Otherwise, the trends in heat-transfer rates with increasing U_g/U_ℓ values are seen to be about the same as for air-water. The results presented in Fig. 19 are primarily for lower qualities, because study of heat transfer for annular flow was not the main purpose of this program, and equipment was designed accordingly.

The results presented in Fig. 19 were correlated within ±20%, as shown in Fig. 20, by the following relationship:

$$Nu = \frac{h_{TP}D}{k_\ell} = 125\left(\frac{U_g}{U_\ell}\right)^{0.125}\left(\frac{\mu_g}{\mu_\ell}\right)^{0.6}(Re_L)^{1/4}(Pr)^{1/3}\left(\frac{\mu_b}{\mu_w}\right)^{0.14}. \qquad (4)$$

The physical properties used for Pr and bulk-to-wall viscosity corrections are those of the liquid.

Figure 20 shows the small dependence of heat-transfer rate on volumetric flow ratio. In single-component two-phase flow, heat transfer in the region of low qualities is usually considered to be controlled mainly by heat flux,[40] thus being independent of quality. The results of the present investigation have shown here, however, that small dependence on quality is characteristic of the low-quality range and the flow patterns associated with it. Therefore, it would appear that, while heat flux in boiling-heat transfer adds to the heat-transfer rate, it may not determine heat-transfer characteristics as far as dependence on quality is concerned.

The present correlation for low qualities also shows that the dependence of h_{TP} on mass velocity (presented in terms of $Re_L^{0.25}$) is significantly lower than for single-phase heat transfer. The same low dependence can be observed in Verschoor's and Stemerding's[20] results at low qualities, where $h_{TP} \alpha U_\ell^{0.23}$ at $U_g/U_\ell = 1.0$. The exponent of U_ℓ in their study changes at higher qualities, however, and becomes approximately $h_{TP} \alpha U_\ell^{0.8}$ at $U_g/U_\ell = 100$, where annular flow would be likely to occur. This contrasting change with U_g/U_ℓ ratio shows why correlations of the type[39,40]

$$\frac{h_{TP}}{h_L} = C_1\left(\frac{1}{X_{TT}}\right)^{C_2}, \qquad (5)$$

where C_1 and C_2 are constants for a given system, are successful in correlating two-phase heat-transfer coefficients within ±20% at high U_g/U_ℓ ratios associated with the annular flow region.

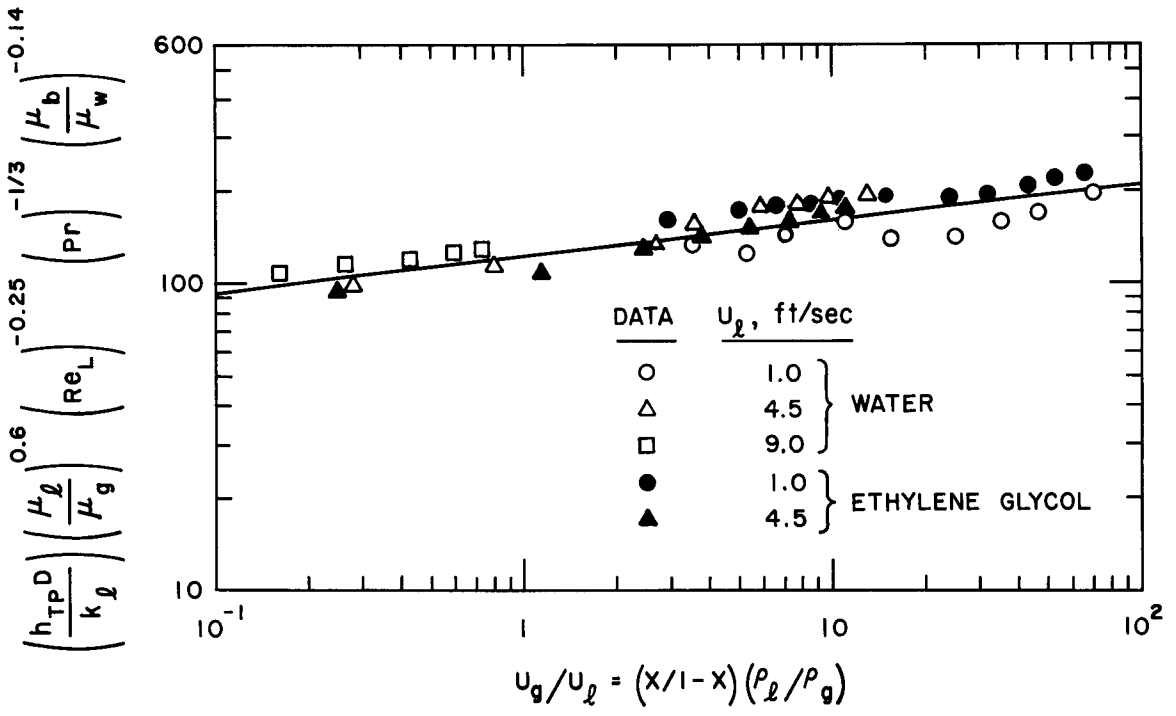

Fig. 20. Correlation of Zero-injection Results

Since Eq. (5) and the proportionality of h_{TP} to $Re_L^{0.8}$ necessarily associated with it are usually connected with annular flow, the low dependence of h_{TP} on mass velocity found for the entire range of U_g/U_ℓ's in the present results could mean that annular heat transfer did not really develop even at the higher U_g/U_ℓ ratios tested. This conclusion is also supported by the fact that dependence of heat-transfer rate on U_g/U_ℓ for the region where a relationship of the type of Eq. (5) applies usually ranges between the $\frac{1}{3}$ and $\frac{2}{3}$ powers of U_g/U_ℓ.[40] However, it was only to the $\frac{1}{8}$ power for present experiments, and this low power is characteristic at low qualities.

Single-component and two-component, two-phase heat-transfer results have been presented and compared in the literature in terms of h_{TP}/h_L ratios for high and low qualities.[20,22,23]. The authors who used this type of presentation at low qualities encountered difficulties in correlating and comparing results that could not be satisfactorily accounted for. One difficulty in correlating results at low qualities in terms of h_{TP}/h_L or $1/X_{TT}$ is the mass-velocity effect discussed previously. Other factors that have to be considered when comparing various two-phase heat-transfer results were brought out in part by the results of this study, and will be discussed now.

Graphs in terms of h_{TP}/h_L for air-water and air-ethylene glycol results are presented in Figs. 21 and 22, respectively. The h_{TP}/h_L values are ratios of two-phase to single-phase heat-transfer coefficients for the

same liquid-mass velocity, adjusted to the same bulk/wall liquid-viscosity ratio (where necessary) according to the Sieder and Tate[52] correction. Liquid heat-transfer coefficients for water were obtained from the Sieder and Tate equation, and corrected for entrance effects as discussed in Appendix D. Actual h_L values obtained in the tests were used for ethylene glycol comparisons.

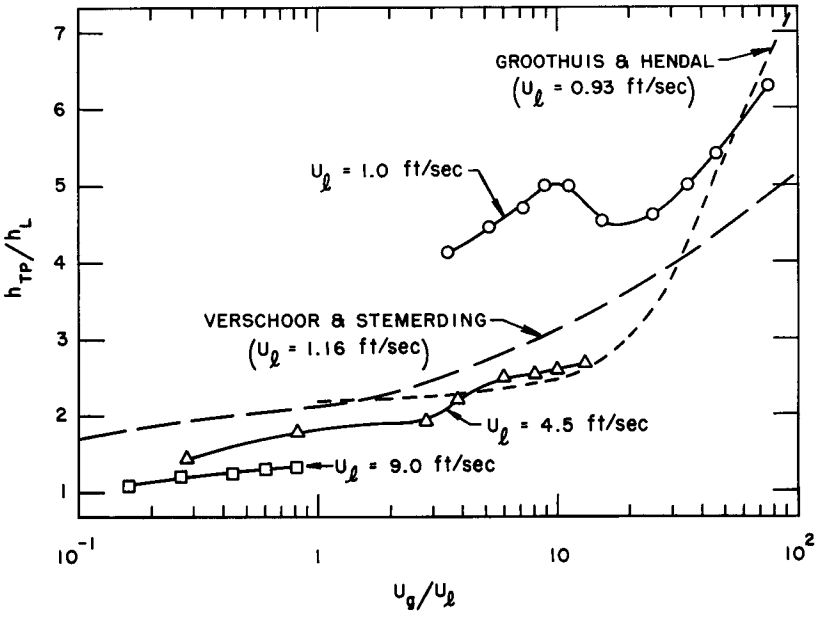

Fig. 21. Comparison of Zero-injection Air-Water Results

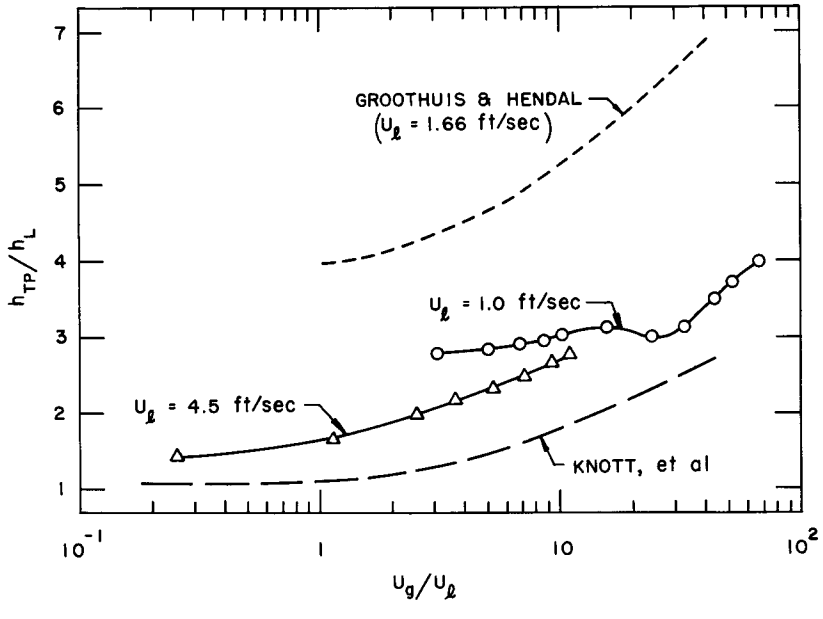

Fig. 22. Comparison of Zero-injection Air-Ethylene Glycol Results

Presentation of results in terms of h_{TP}/h_L illustrates effectively the increases in heat-transfer rates caused by adding a gas phase to liquid flow. The reasons for these increases can be best discussed in terms of possible mechanisms enhancing heat transfer in two-phase, two-component flow. When air is added at a given liquid-flow rate, the increase in the heat-transfer coefficient can be caused by the following mechanisms:

1. Liquid and mixture velocity increase caused by addition of the gas phase.

2. Increased turbulence and mixing action in the main stream caused by continuous interaction of the two phases.

3. Increased turbulence near the heated wall caused by gas bubbles, resulting in disturbance and decrease in the effective thickness of the laminar boundary sublayer.

The increases in heat-transfer rates attributed to the mechanisms listed must be examined in terms of initial liquid-flow and heat-transfer rates because values of h_{TP}/h_L ratios depend on them.

The increase in heat-transfer rate caused by addition of gas phase should be more pronounced when the initial turbulence intensity of liquid flow is relatively low. Mechanisms 2 and 3 can then be expected to be effective in enhancing heat transfer. This point is illustrated by the high increase in heat-transfer rates found (Fig. 21) when air was added to liquid flow at U_ℓ = 1.0 ft/sec, where the initial liquid flow was semi-turbulent[25] at $Re_L \approx 5500$.

On the other hand, when initial turbulence intensity is high, such as for U_ℓ of 4.5 and 9.0 ft/sec (Fig. 21), mechanisms 2 and 3 cannot be expected to contribute effectively to the already high turbulence intensity present in liquid flow, and the resulting h_{TP}/h_L ratios are therefore lower.

The same dependence of h_{TP}/h_L ratios on h_L values, which are determined by liquid-flow conditions, can be observed in Verschoor's and Stemerding's[20] air-water experiments, and also appears for horizontal air-water tests,[23] although it received no comment from any of these authors. In their results, dependence of h_{TP}/h_L on initial liquid-flow conditions was significant for low initial-turbulence intensities, and decreased as the initial liquid-turbulence intensity developed.

Although void-fraction data could not be obtained for zero-injection tests with the present equipment, a void correlation[45] of the type

$$\frac{h_{TP}}{h_L} = \left(\frac{1}{1-\bar{\alpha}}\right)^{0.8} = \left(1 + \frac{U_g}{U_\ell} \cdot \frac{V_\ell}{V_g}\right)^{0.8} \qquad (6)$$

was tried for air-water results, using the void results of Fig. 16. The correlation of Eq. (6) accounts for the velocity increase of the liquid caused by the gas phase when mass velocity and viscosity dependence is the same for both two-phase and liquid-heat transfer. A satisfactory correlation of results could not be obtained using Eq. (6), perhaps primarily because the mass-velocity effect was not the same for two-phase and single-phase heat transfer in the range of low qualities investigated. In addition, turbulence effects caused by mechanisms other than increase in liquid velocity were significant, especially at U_ℓ = 1.0 ft/sec, and added more to the heat-transfer rate increase than would be expected from velocity increase alone. Correlation of Eq. (6) would give an effect of slip on heat-transfer rate opposite to the one observed here, if slip decreased with mass velocity at a given U_g/U_ℓ, as is sometimes found.[41]

Some of the air-water results obtained by Groothuis and Hendal,[21] and by Verschoor and Stemerding[20] for similar conditions, are shown in Fig. 22 for comparison. The same type heat-transfer behavior, and similar trends with increasing air/water ratios as in the present experiments, can be observed. Part of the discrepancy may be due to the way the gas phase is injected in the different studies, and this may influence the development and formation of flow patterns. In addition, average h_{TP}'s are reported in the previous studies, while local h_{TP}'s at L/D of about 14 are plotted for the present study.

Groothuis and Hendal[21] correlated their results in the annular-flow region (for the steep part of the curve shown as an example in Fig. 22) by interrelating Nusselt number with Reynolds and Prandtl numbers. Their Reynolds number was correlated to the 0.87 power, suggesting the same relationship as for single-phase turbulent-heat transfer. Their correlation cannot be applied at lower U_g/U_ℓ ratios examined in the present experiments.

Figure 22 compares air-ethylene glycol zero-injection results on the h_{TP}/h_L basis to the results of two previous air-oil investigations.[21,22] The apparent discrepancies between results of the three studies are more pronounced here than for air-water results because the liquids compared here cover a wide range of viscosities. Previous investigators[20,22,23] were not able to attribute these discrepancies to specific reason. Groothuis and Hendal[21] mentioned, in comparing their own air-oil and air-water results, that the influence of air on heat transfer was most pronounced at the lowest Re numbers because air would be more effective in promoting turbulence there.

Expanding this reasoning to cover a wide spectrum of viscosities, some of the apparent discrepancies encountered in an h_{TP}/h_L type presentation can be explained logically in terms of initial liquid and final two-phase flow types. These types include laminar and turbulent single-phase flow, as well as various two-phase flow types as defined by Lockhart and Martinelli.[53]

Liquid viscosities for nitrogen-oil experiments by Knott et al.[22] were high, giving initial liquid Reynolds numbers from 6.7 to 162 for liquid velocities from 0.11 to 5.65 ft/sec tested. All their nitrogen-oil results for a vertical tube were correlated fairly well by the single plot shown in Fig. 22.

The authors compared their results to

$$\frac{h_{TP}}{h_L} = \left(1 + \frac{U_g}{U_\ell}\right)^{1/3}, \tag{7}$$

derived from the laminar Sieder-Tate heat-transfer relationship (see Ref. 22) by assuming that the heat-transfer increase is due to the velocity increase, and that the slip ratio is unity. Knott et al. found that Eq. (7) predicted h_{TP}/h_L values somewhat larger than the experimental ones. The low liquid Reynolds numbers and the success of Eq. (7) in predicting results indicate that addition of the gas phase, while increasing flow velocity, still keeps the flow in the viscous-viscous range. Therefore, the turbulence intensity remains low, resulting in a low heat-transfer enhancement of a viscous type by the gas phase.

The liquid Reynolds number for Groothuis' and Hendal's[21] U_ℓ = 1.66-ft/sec air-oil results plotted in Fig. 22 was 3400. Addition of a small amount of gas changed the flow from semiturbulent[25] to turbulent-turbulent, with the attendant large increase in turbulence intensity and, consequently, heat-transfer rate. This effect was also observed for the present U_ℓ = 1.0-ft/sec air-water results (Fig. 21), where $Re_L \approx 5500$. Since Re_L for the present air-ethylene glycol tests was 380 for U_ℓ = 1.0 ft/sec, and 1700 for U_ℓ = 4.5 ft/sec, addition of the gas phase changed the flow from viscous to viscous-turbulent, and the increases in turbulence intensity and heat-transfer rates were moderate.

Thus, the type of liquid flow for which h_L is determined must be considered when comparing results on an h_{TP}/h_L basis, in addition to any mass-velocity effects. Correlations of this type that have been used successfully at high qualities were usually for conditions of initially turbulent liquid flow. While the general effects of h_L in the viscous and semiturbulent range on h_{TP}/h_L values were described here qualitatively, two-phase heat transfer in the region of viscous-turbulent flows needs to be investigated more thoroughly for a wide range of viscosities and mass velocities to attempt a quantitative correlation on the basis of h_{TP}/h_L.

In summary, the following points have been brought out about two-phase heat-transfer behavior in this presentation and discussion of zero-injection results:

1. The dependence of h_{TP} on G at low qualities was much smaller than at high qualities associated with annular flow.

2. Liquid viscosity was important in determining two-phase heat-transfer rate, the dependence being inverse between h_{TP} and viscosity.

3. The dependence of h_{TP} on U_g/U_ℓ at low qualities was small, and not unlike that of boiling-heat transfer in forced circulation, but was considerably higher at qualities associated with annular type of flow.

4. The differences in h_{TP} behavior at low and high qualities require that different heat-transfer correlations be used in the two ranges.

5. If liquid-heat transfer for which h_L is determined is not in the fully developed turbulent range ($Re_L > 10,000$), important influences of h_L (which vary with Re_L) on h_{TP}/h_L values must be considered when the results are compared on this basis.

Two-phase Heat Transfer with Gas Injection

This study investigated the various hydrodynamic aspects of two-phase heat transfer in a forced circulation system. Since the overall processes are very complicated, different aspects were studied individually, and the gas-bubbling equipment was designed with this purpose in mind. Thus, being able to vary parameters independently was one of the advantages of the present system in studying two-phase heat transfer. Since the analogy between the gas-bubbling and -boiling systems could be established with confidence only for lower gas/liquid flow ratios, the investigation was conducted mainly in this range.

Two-phase heat-transfer results without gas bubbling on the heated walls were presented first to lay the groundwork for examining the influence of gas bubbling itself on heat-transfer rates. In this section, results for two-phase heat transfer with gas bubbling on the heated walls are presented and evaluated, and boiling heat-transfer phenomena are discussed and interpreted in terms of these results. Both air-water and air-ethylene glycol results are presented and compared to observe any property effects.

First, the influence of gas bubbling on variation of heat-transfer rate with mass velocity change is examined. Then the influence of gas injection on heat-transfer rates for various flow patterns and volumetric gas/liquid flow ratios is observed. Finally, the influence of gas-bubbling rate, or "heat flux" on heat-transfer rate for various flow patterns and gas/liquid ratios is examined, and the significance of these results is discussed.

Effect of Mass Velocity on Heat Transfer

In the correlation of zero-injection results, mass velocity affected heat transfer, but it is desirable to examine these effects more specifically at a low quality, and to see how gas bubbling from the walls influences them. Results showing effects of mass velocity on heat transfer at U_g/U_ℓ = 1.0 for a low air-injection rate are presented in Fig. 23. These results are for a low volumetric gas/liquid flow ratio, corresponding to bubble flow (or froth flow at higher mass velocities). The mass-velocity effect in Fig. 23 can be represented approximately as h_{TP} being proportional to $U_\ell^{0.22}$ and $U_\ell^{0.30}$, respectively, even though the exponent increases with increasing mass velocity. This dependence is about the same as was found in the correlation of zero-injection results, i.e., $U_\ell^{0.25}$, indicating that, although gas bubbling may enhance heat transfer, it does not influence the effect of mass velocity on heat transfer to a great extent.

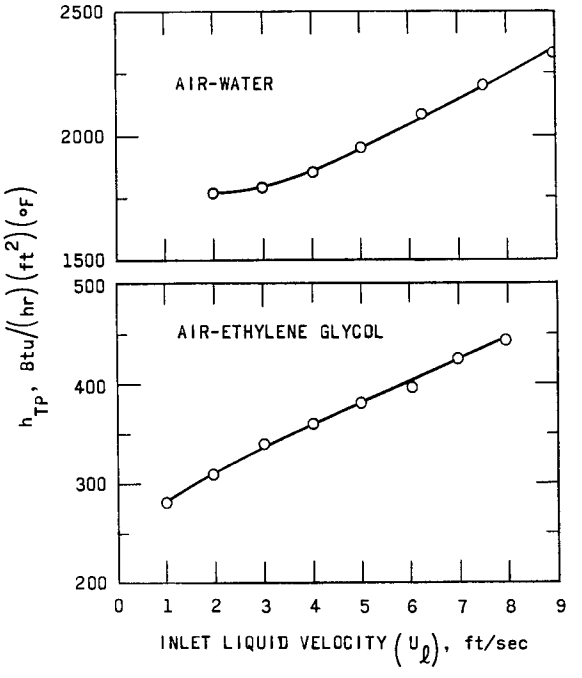

Fig. 23. Effect of Mass Velocity on Heat Transfer (Conditions are at U_g/U_ℓ = 1.0 and ϕ = 0.030)

Mumm[34] found that the mass-velocity effect in his boiling-water experiments was effectively represented to the 0.344 power for liquid-inlet velocities from 1.5 to 6.0 ft/sec at 50% quality. The effect of liquid-inlet velocity on heat-transfer rates was also studied by Bogdanov[35] and Sterman.[37] Their data were correlated with the effect of velocity presented as $G_T^{0.1}$. Thus, the comparison with boiling-heat transfer shows the same type of dependence on mass velocity as was found in the present results.

Air-water results of Fig. 23 are presented in terms of two-phase to single-phase heat-transfer coefficient ratios in Fig. 24. Water h_L's were calculated using the Sieder-Tate relationship and including entrance effects, as is presented in detail in Appendix D. The range of ethylene glycol liquid velocities tested was in the transition region from laminar to turbulent liquid flow. Because of this transition, meaningful presentation of air-ethylene glycol results of Fig. 23 using h_L as a reference basis could not be made.

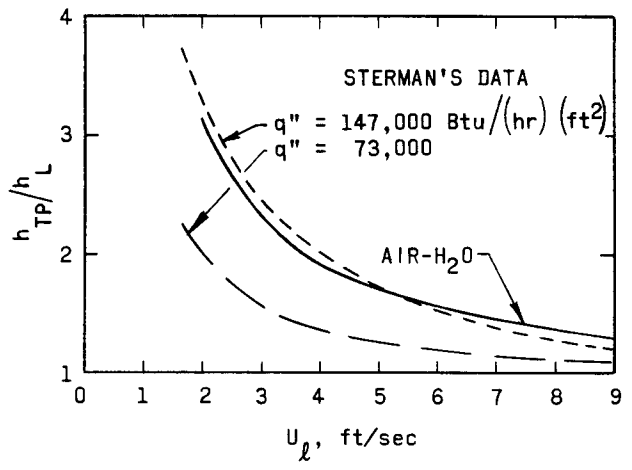

Fig. 24. Comparison of Two-phase Heat Transfer at Constant U_g/U_ℓ

Sterman[36] studied the effect of mass velocity for boiling water at 2 atmospheres in a vertical tube. The results for inlet velocities from 1.5 to 20.0 ft/sec, as reported by Collier (Fig. 19, Ref. 5), were presented for the regions where volumetric steam quality had little effect on h_{TP}, i.e., at U_g/U_ℓ = 0.3 to 1.5. The Dittus-Boelter equation for liquid-heat transfer at the same temperatures was plotted alongside for comparison. The h_{TP}/h_L values determined from this plot are shown in Fig. 24 for comparison with the results of the present investigation, and the agreement in the mass velocity trends is excellent. Sterman[37] also obtained results at 7 atmospheres, where the effect of mass velocity on h_{TP} was less, but h_{TP} still approached the Dittus-Boelter equation value at high mass velocities.

The downward trend of the h_{TP}/h_L ratio with increasing mass velocity was also observed in the zero-injection results of the present study (Fig. 21), and was seen to be present in Verschoor's and Stemerding's[20] air-water results.

This downward trend of h_{TP}/h_L ratio with increasing mass velocity (Fig. 24) can be discussed again in terms of turbulence intensity of the reference liquid-flow rate. When the initial turbulence intensity is low, as indicated by low Re_L, the additional turbulence caused by the gas phase is most effective in promoting heat transfer. On the other hand, at high mass velocities, where the turbulence intensity of liquid flow is already high (producing high convective heat-transfer rates), additional turbulence caused by the gas phase cannot be expected to be as effective in enhancing heat-transfer rates. In addition, Fig. 24 shows that the h_{TP}/h_L ratio approaches a constant value at high mass velocities, indicating that mass-velocity effect in two-phase heat transfer becomes similar to that of single-phase heat transfer when the convective heat-transfer rates in liquid flow become high enough. The void correlation of Eq. (6) was applied to Fig. 24, but it failed to predict any mass velocity effect, and it predicted an asymptotic value of h_{TP}/h_L that was about 30% too high.

Effect of Volumetric Gas/Liquid Ratio and Flow Pattern

Several experiments were performed at constant gas-bubbling rates of approximately 0.035 and 0.200 $ft^3/(sec)(ft^2)$, including zero-gas

injection, while the volumetric gas/liquid ratio was varied over the widest range that could be obtained with the equipment by varying the gas input into the mixer section. These tests were for 1.0- and 4.5-ft/sec liquid-inlet velocities for both ethylene glycol and water. The results are presented in Figs. 25 and 26; the zero injection results are also shown for comparison.

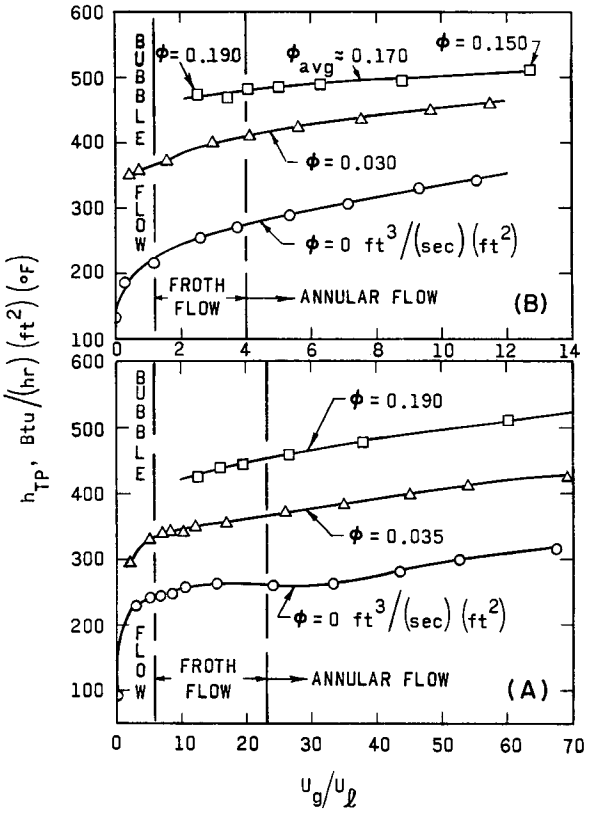

Fig. 25. Air-Ethylene Glycol Heat-transfer Characteristics (A is at U_ℓ = 1.0 ft/sec, B is at 4.5 ft/sec)

The approximate flow-pattern ranges marked on the figures indicate that heat-transfer rates in the air-water system are more sensitive to flow pattern changes than air-ethylene glycol heat-transfer rates, since the higher viscosity of ethylene glycol dampens the interaction between phases in the fluid stream. Flow patterns also influence heat transfer more readily in the slug-flow region at U_ℓ = 1.0 ft/sec (Fig. 26), where the Froude number is 0.6. Therefore gravity effects are important in determining the development of a given flow regime.

In slug flow, the nature of the flow itself is affected by gas injection. This influence is in turn reflected in the heat-transfer results, as can be seen for the slug-flow region of Fig. 26. Apparently, gas injection reduces the slugging and back-flow tendencies, stabilizing the flow pattern near the heated wall, thus influencing heat transfer in this way. Furthermore, gas injection appears as an important influence for the air-water system in the bubbly and slug- or froth-flow regimes because heat-transfer coefficients at ϕ = 0.035 ft^3/(sec)(ft^2) in Figs. 25 and 26 are little affected by U_g/U_ℓ changes in these regimes.

The transition to the annular flow regime, as defined for this study, is also accompanied by a noticeable change in heat-transfer rate for air-water results. This change is evident both with and without gas bubbling, and may be due to reorientation of the phases in the fluid stream.

Similar influence of flow patterns on heat-transfer rate for increasing U_g/U_ℓ ratios at low qualities is also present for steam-water flow

as Anderson et al.[38] have observed and noted. In Anderson's study, this influence was especially evident at low mass velocities.

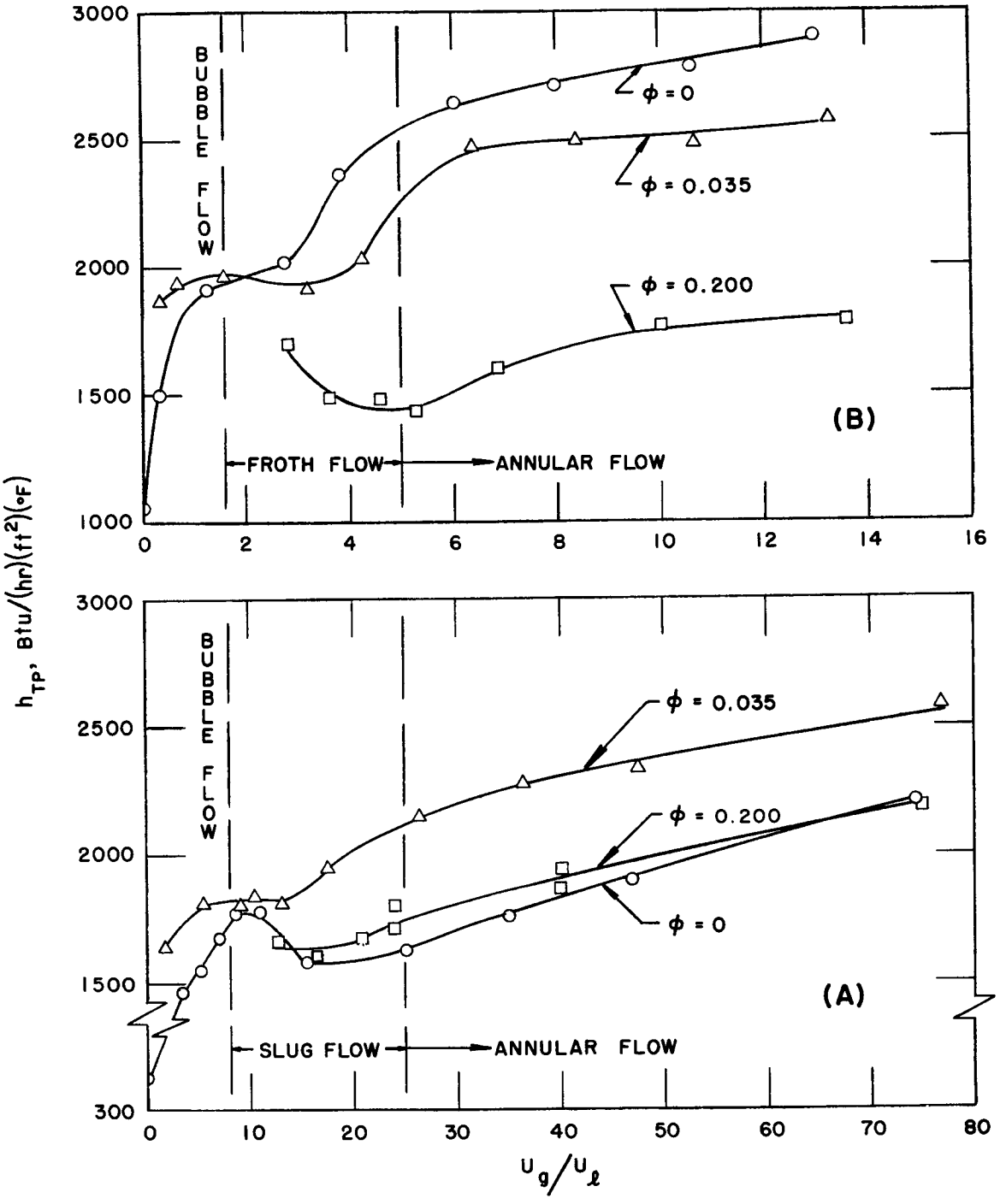

Fig. 26. Air-Water Heat-transfer Characteristics (A is at U_ℓ = 1.0 ft/sec, B is at U_ℓ = 4.5 ft/sec)

When gas bubbling does not change the nature of flow patterns, its effect appears to be additive (Figs. 25 and 26). It is algebraically additive, not linearly additive as Gose[13] has claimed.

The next section discusses, in detail, what determines the nature of this addition process, and the effects of gas injection rate on heat transfer accompanying the presentation of results in Figs. 25 and 26. It may be briefly noted here, though, that the much higher viscosity of ethylene glycol is the main difference between the properties of the two liquids. Therefore, the difference in the injection heat-transfer results should be investigated in terms of the effects of viscosity. When mass-velocity effects at low U_g/U_ℓ ratios were examined previously, the largest increases in heat-transfer rates due to gas addition occurred when the initial liquid heat-transfer rates were low, but only small increases occurred when initial liquid heat-transfer rates were high. Trends in the same direction can be also observed when injection effects are compared for ethylene glycol and water results in Figs. 25 and 26.

Effect of Gas Bubbling or Injection

Effects of air injection on the heat-transfer coefficient were investigated by varying the injection rate for several liquid flow rates at a set volumetric gas/liquid flow ratio. The constant U_g/U_ℓ for a given test series was maintained by adjusting the air input into the mixer section. The heat-transfer coefficients in zero-injection tests were influenced by the U_g/U_ℓ values. Therefore, the fact that injection heat-transfer coefficients reflect the zero-injection values must be considered when examining these results.

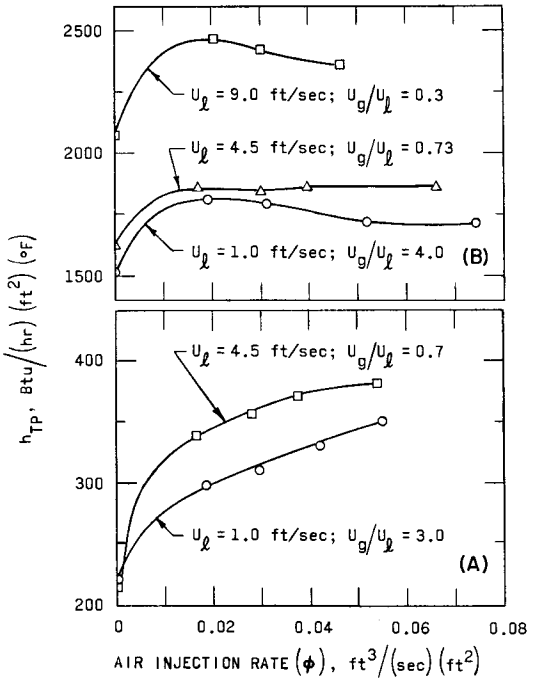

Fig. 27. Effect of Low-injection Rates on Heat Transfer (A - Ethylene Glycol, B - Water)

Results for low injection rates are presented in Fig. 27. The difference in the influence of air injection on heat-transfer coefficients for water and for ethylene glycol is quite apparent. While an initially low air-injection rate increases the heat-transfer coefficient significantly for both liquids, further injection increases keep improving h_{TP} for ethylene glycol, but appear to interfere with water-heat transfer.

The opposite effect of injection on h_{TP} for the two liquids is more

apparent at high volumetric gas/liquid flow ratios, shown in Figs. 28 and 29. The zero-injection h_{TP} at U_g/U_ℓ = 26 in Fig. 29 was determined by interpolation of data presented in Fig. 19. The increase in h_{TP} with increasing injection rate for ethylene glycol in Fig. 28 is certainly expected, but interference of gas bubbling with heat transfer for water in Fig. 29 is not expected from previous two-phase heat-transfer experience, except perhaps from the results of Anderson et al.(38)

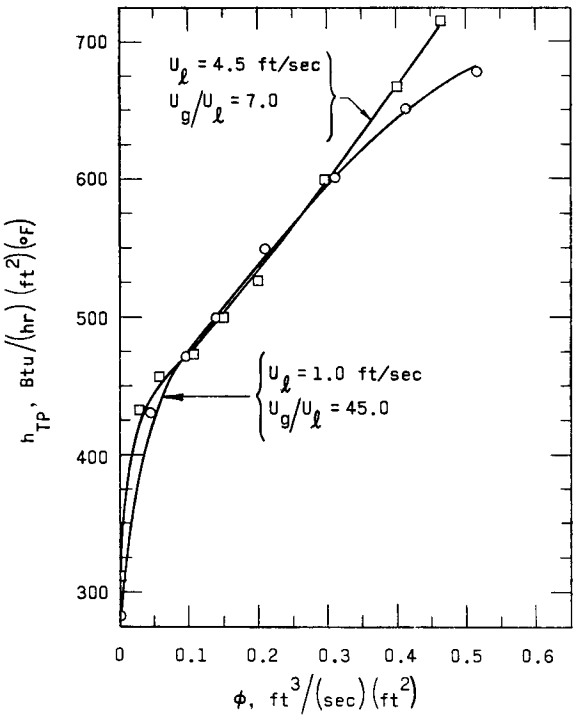

Fig. 28. Effect of Moderate-injection Rates on Heat Transfer in Ethylene Glycol

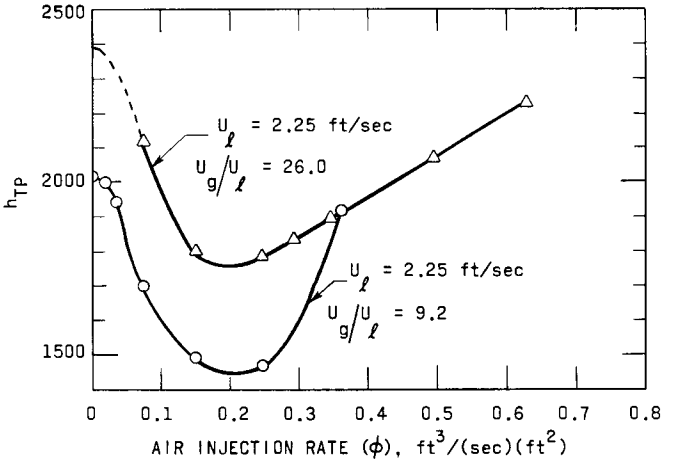

112-3701

Fig. 29. Effect of Moderate-injection Rates on Heat Transfer in Water

The phase distributions found in this study (Figs. 17 and 18) do not satisfactorily explain this interference. Even if it is postulated that air presence near the wall interferes with heat transfer, results presented in Fig. 26 for U_ℓ = 4.5 ft/sec contradict this explanation because they show that gas bubbling enhances heat transfer at low U_g/U_ℓ and interferes with it at higher U_g/U_ℓ ratios. The phase distributions for U_ℓ = 4.5 ft/sec presented in Figs. 18B and C show, however, that gas concentration near the wall is greater at low, than at high, U_g/U_ℓ ratios. In addition, phase distributions for ethylene glycol would show even higher gas concentration near the walls than for water at similar conditions because the drag on air bubbles in ethylene glycol is greater, making their propagation towards the center of the tube (initiated by their transverse departure velocity) slower.

Since the overall phase distributions do not help much in the explanation, attention is turned to local conditions at the heated wall. Most of the unexpected and expected results can be explained when they are examined in terms of the hydrodynamic heat-transfer mechanisms involved in boiling-circulation heat transfer.

Model for Heat-transfer Processes. It is postulated that the air bubbles generated on the heated tube wall in the present system enhance heat transfer by

1. Increasing turbulence in the boundary layer (microconvection mechanism).

2. Displacing the hot liquid from the wall into the main liquid stream with cold liquid coming in after the bubble departs (vapor-liquid exchange mechanism).

The air bubbles on the heated wall also reduce the area available for convection, decreasing the convective heat-transfer rate.

The heat-transfer processes, based on the physical model briefly outlined above, will now be examined in detail.

It was first proposed by Jakob,[25] and later by others,[26,27] that the high heat-transfer rates in boiling are due to the agitation of liquid by vapor bubbles. In addition, several proposed models[28,29] explained the high heat-transfer coefficients for pool boiling as being caused by the convective currents that bubbles set up when they grow and depart, creating a source and a wake type of flow, respectively. The heat-transfer coefficients were then calculated by assuming an analogy between natural convection and boiling processes, using the much larger density variations created by the gas bubbles near the heated surface to explain the increase in heat-transfer rates. It is difficult to extrapolate this model to forced-circulation heat transfer, but growing and departing bubbles act as turbulence promoters, increasing eddy diffusivity near the heated wall, and therefore enhancing heat transfer. The turbulence created by the bubbles was illustrated well by Gunther's[54] shadowgraph pictures of boiling on a heated metal strip in laminar stream flow. While a bubble is growing, it may thus act as a surface roughness in promoting heat transfer, and when it departs, it leaves a wake behind, increasing turbulence in the boundary layer.

Although it is difficult to estimate the magnitude of microconvection on heat-transfer rate (no general correlation even exists for pipe-roughness effects on heat transfer), the relative effect of the mechanism may be examined. The turbulence created by gas bubbles growing and departing in the neighborhood of the boundary layer can be expected to be

more effective in promoting heat transfer when gas bubbling is superimposed on laminar-boundary sublayers that are initially thicker. For laminar-boundary sublayers that are initially thin, so that turbulent mixing is already high, additional turbulence created by the gas bubbles can be expected to be less effective in enhancing heat transfer. These trends are confirmed by comparing the average increase in h_{TP} due to $\phi = 0.020$ ft^3/(sec)(ft^2) for ethylene glycol and for water (Fig. 27), as follows:

	Increase in h_{TP} (percent)	
U_ℓ (ft/sec)	Air-Ethylene glycol	Air-Water
1.0	40	20
4.5	75	15
9.0		18

The vapor-liquid exchange mechanism, discussed in detail next, also predicts the same trend in h_{TP} for different thermal-boundary-layer thicknesses (δ_t's) when D_b is greater than δ_t. However, for a given δ_t/D_b ratio, the vapor-liquid exchange mechanism predicts a linear increase in h_{TP} with increasing air-injection rate. Therefore, most of the initially high increase in h_{TP} when air injection is started, such as shown in Figs. 27 and 28, is assumed to be due to the turbulence created by the bubbles. Further increases in injection rate, however, do not appear to increase turbulence effectively in the neighborhood of the boundary layer because h_{TP} variation with injection becomes fairly linear. Therefore, when the information is available, the influence of microconvection on h_{TP} may be estimated by extrapolating the linear portion of the h_{TP}-versus-ϕ curve to zero-injection rate. The difference between the extrapolated and the actual $\phi = 0$ is then taken to be due to microconvection.

The vapor-liquid exchange mechanism proposed by Engelberg-Forster and Greif[30] states essentially that most of the heat during boiling is transferred by a vapor-liquid exchange action, where the growing bubbles pump the hot liquid mechanically from the heated wall into the bulk, and the cold liquid from the bulk to the heated wall. The heat-transfer coefficients are high because this bubble activity is much more efficient than eddy diffusion as a mode of heat transfer.

The heat taken away by the bubble-pumping action in forced-circulation heat transfer depends on the gas-bubble diameters and on the thermal boundary layer thickness. Using

$$\delta_t = \frac{k_\ell}{h_{TP}} \tag{8}$$

to represent the thermal boundary layer, the range of δ_t values was 0.5×10^{-3} to 1.0×10^{-3} ft for air-ethylene glycol experiments, and 0.1×10^{-3} to 0.25×10^{-3} ft for air-water experiments. The h_{TP} values in Eq. (8) are for two-phase heat transfer without gas bubbling at the walls.

It is difficult to determine the exact gas-bubble-departure diameters for the forced circulation experiments because bubble diameters may be influenced by injection rate, mass velocity, U_g/U_ℓ ratio, and properties of the liquid. Departing gas bubbles also could not be observed in the forced circulation system (as they were in the pool system) but had to be estimated from available information. From pool-bubbling photographs, such as in Fig. 13, the average bubble diameter was found to be about $\frac{1}{16}$ in. for moderate bubbling rates. This value agrees reasonably with results by Siemes and Borchers[55] for gas bubbles generated from porous plates.

Air bubbles observed in flow-pattern photographs (such as Fig. 14) were also found to be about $\frac{1}{16}$-in. diameter for bubble type flow when they did not coalesce.

Hirata[56] studied diameters of air bubbles injected from a hole in a channel wall into water flowing in a horizontal channel with velocities of 0.8 to 2.6 ft/sec. Since he also did not observe any effect of velocity on bubble diameter, a bubble-departure diameter of $\frac{1}{16}$ in. is used as a representative value in the calculations.

Comparison of departing gas-bubble radii with the thermal-layer thicknesses indicated that bubble radii are larger than δ_t for most of the test results. Gaertner[57] found that even for pool boiling of saturated water, bubble radii are larger than the thermal-layer thickness.

Therefore, when $D_b > 2\delta_t$ and the temperature distribution in the thermal boundary layer is assumed to be linear, the heat removed by the vapor-liquid exchange action of a gas bubble can be calculated (see Fig. 30) as follows:

$$dq = \Delta t c_p \rho_\ell A dx,$$

where

$$\Delta t = (t_w - t_b)\left(1 - \frac{x}{\delta_t}\right),$$

and

$$A = \pi\left[R_b^2 - (R_b - x)^2\right];$$

thus

$$q = \int_0^{\delta_t} (t_w - t_b) c_p \rho_\ell \left(1 - \frac{x}{\delta_t}\right) \pi \left[R_b^2 - (R_b - x)^2\right] dx,$$

and

$$q = (t_w - t_b) c_p \rho_\ell \frac{\pi}{6} (\delta_t)^2 \left(D_b - \frac{\delta_t}{2}\right).$$

Since

$$\phi = \frac{\pi}{6} D_b^3 nf \text{ ft}^3/\text{hr}/\text{ft}^2,$$

and the heat flux removed by the gas-liquid exchange action is

$$q'' = nfq,$$

the heat-transfer coefficient due to the vapor-liquid exchange mechanism is

$$h = \frac{q''}{(t_w - t_b)} = c_p \rho_\ell \phi \left(\frac{\delta_t}{D_b}\right)^2 \left(1 - \frac{\delta_t}{2D_b}\right). \tag{9}$$

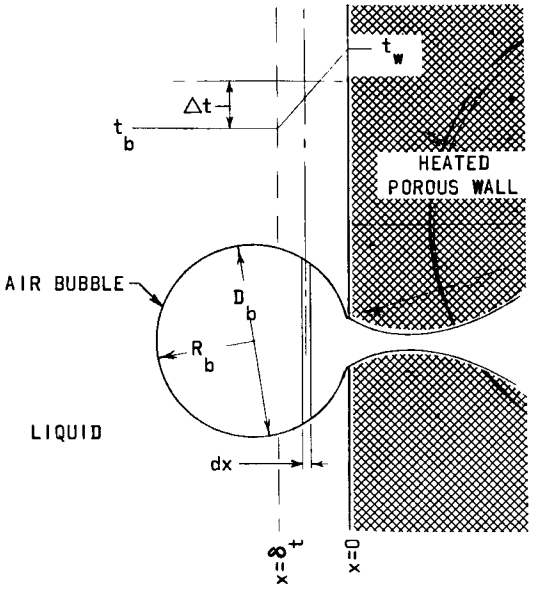

Fig. 30
Relationship of D_b to δ_t

The microconvection and the vapor-liquid exchange mechanisms both predict that gas injection should increase heat-transfer coefficients. The air-water graphs of Fig. 29 show, however, that gas injection can also interfere with heat transfer. Anderson et al.[38] in the discussion of their

forced-circulation boiling-heat-transfer results stated that: "the residual nucleation, whilst insufficient to give good agitation is sufficient to hinder true film flow, and so results in lower values of h." While it can thus be postulated that nucleation slows the annular liquid film down, the present results indicated that nucleation enhances heat transfer in the annular flow regime for U_ℓ = 1.0 ft/sec (Fig. 26A). On the other hand, h_{TP} was reduced by gas bubbling in the froth flow regime for tests at U_ℓ = 4.5 ft/sec (Fig. 26B).

Therefore, a more tenable explanation would be that the gas bubbles formed on the heated surface reduce the area available for convection. When convection heat transfer is high, and consequently the thermal boundary layer is thin, gas bubbles add very little to heat-transfer rate. As the time-averaged area of the heated surface covered by bubbles increases, the decrease in h_{TP} due to convection-area reduction overcomes the beneficial effects of gas bubbles, and h_{TP} goes down.

The time-averaged area taken up by the gas bubbles on the heated surface can be expressed as a surface-void fraction, α_w. Zuber[28] took it to be equal to the mean void fraction for a nonflow system where there is no growth of bubbles in the liquid. While the extrapolation of α_w from a nonflow system to the present system may be questioned, because α_w values depend on the terminal velocity of bubble rise, there is no other way of obtaining surface-void fractions. Therefore, this method is used as an approximation so that the heat-transfer trends due to convection area reduction can be predicted.

Wallis[11] studied the bubbling of air from a porous horizontal plate into a column of water, and from a porous tube into a tank of water. He measured the mean void fraction for various air-injection rates for distilled, tap, and soapy water in the porous-plate experiments. Wallis found that there was a transition from bubbly to slug type flow at a certain air-injection rate, the rate depending on the coalescence tendencies of the bubbles. The bubbly regime could be prolonged by adding surface active agents (such as soap) to reduce coalescence. Wallis related the transition from bubbly to slug-flow regime in the porous-plate experiment, to the transition from bubbly to patchy flow in the porous-pipe pool-bubbling experiment. The transition region extended from ϕ = 0.16 to 0.24 $ft^3/(sec)(ft^2)$ for bubbling of air into water. This transition region agrees well with the change in heat transfer observed in Fig. 29. Zuber and Hench[58] also studied void fractions and flow patterns for bubbling of air from a flat plate into a column of water and found that $\bar{\alpha}$ was fairly constant in the "transition," or slug region.

Figure 31 presents void-fraction values found by Wallis and by Zuber and Hench. Since $\bar{\alpha}$ values for demineralized water used in the present experiments were not available, an approximate plot was drawn

to represent these values. Comparison of pool-bubbling pictures at the same injection rate (Fig. 13) shows that bubble coalescence is somewhat higher in ethylene glycol than in water. Because this analysis is made to predict only trends in heat-transfer rates, however, the same void-fraction plot is used for both liquids.

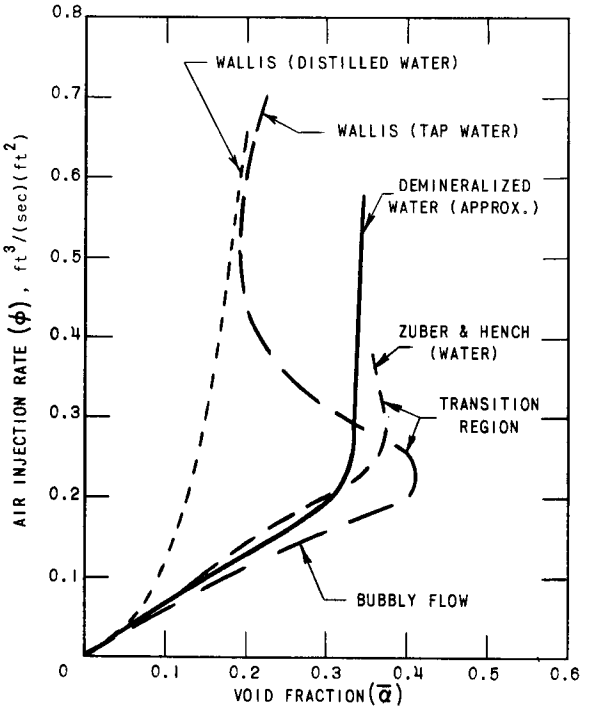

112-3698

Fig. 31

Void Fractions for Bubbling of Air into Water Columns

The effect of convection-area reduction on the heat-transfer coefficient can be presented quantitatively in terms of surface-void fraction up to the transition region shown in Fig. 31. After the transition, this presentation becomes questionable, although α_w may actually remain constant if gas columns replace bubbles emanating from the porous wall.

Noting that

$$h_{TP} = \frac{q''}{\Delta t} = \frac{q}{\Delta t A} = \frac{q}{\left(\frac{\Delta t}{C}\right) CA},$$

where

$$C = \frac{A'}{A},$$

A = total area available for convection when injection is zero,

and

A' = area available for convection when injection is present,

the effective heat-transfer coefficient for the reduced area becomes

$$(h_{TP})_{effective} = \frac{q''}{\Delta t/C}.$$

Therefore, the decrease in heat-transfer rate due to convection area reduction can be represented as

$$h = \frac{q''}{\Delta t} - \frac{q''}{\Delta t/C} = \frac{q''}{\Delta t}\left(1 - \frac{A'}{A}\right),$$

or

$$h = \alpha_w h_{TP}. \tag{10}$$

The heat-transfer coefficient values used in Eq. (10) are for two-phase heat transfer without injection.

The effects of microconvection, vapor-liquid exchange, and convection-area reduction can be combined using the superposition method to predict the total effect of gas bubbling on two-phase heat-transfer coefficient in the present forced-circulation system. The superposition method consists of subdividing a complex heat-transfer problem into subproblems. The solutions to subproblems are added algebraically to obtain a representation of the entire process. Although this method is approximate, because it neglects the interaction of the constituent solutions upon one another, it may be used to predict the correct trends. For this study, when individual solutions for the effects described are combined, the result is

$$h_{TP} = (1 - \alpha_w)(h_{TP})_{zero\ inject} + c_p \rho_\ell \phi \left(\frac{\delta_t}{D_b}\right)^2 \left(1 - \frac{\delta_t}{2D_b}\right) + h_{microconv}. \tag{11}$$

Because of the necessarily approximate analysis used to calculate the individual effects of gas injection, Eq. (11) is only intended for predicting the overall trends of injection on heat transfer. To predict these trends, experimental h_{TP} zero-injection values were used, and the microconvection effect was estimated by graphical extrapolation as described in detail previously. Typical results, shown in Figs. 32 and 33, illustrate that Eq. (11) does predict the trends reasonably well, indicating that the previously formulated mechanisms to explain the effects of gas bubbling are not only logically reasonable, but also quantitatively fairly accurate.

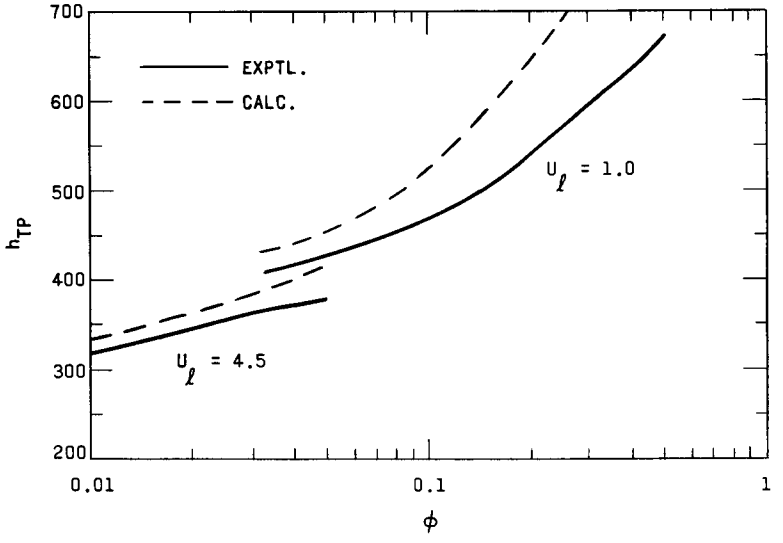

Fig. 32. Comparison of Heat-transfer Trends for Air-Ethylene Glycol

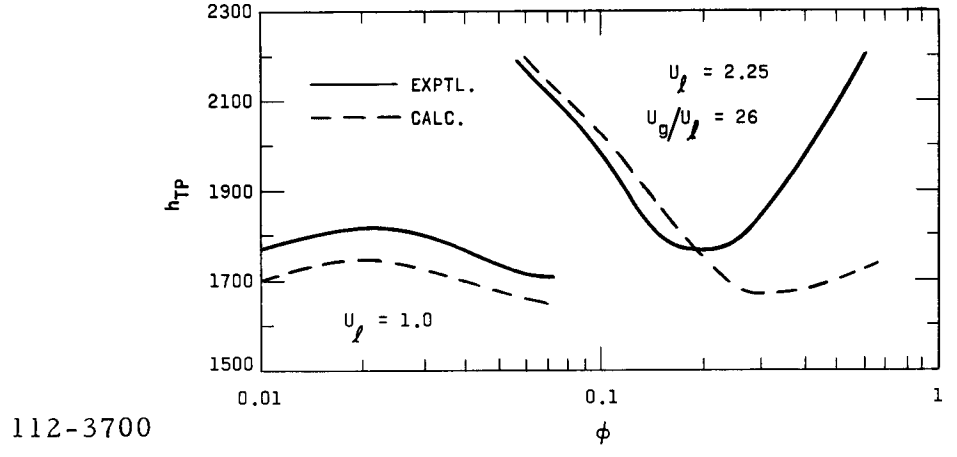

Fig. 33. Comparison of Heat-transfer Trends for Air-Water

The reason that prediction of Eq. (11) for air-water h_{TP}'s at high gas-injection rates in Fig. 33 does not follow the experimental trend very well is probably due to the considerable heat of vaporization losses (in addition to the air heating) encountered at high air-injection rates, making the experimental results in this extreme case not very accurate. Although a method (see Appendix C) that was satisfactory for limits specified for experiment design accounted for these losses, in this case for air-water, the limits were exceeded for $\phi > 0.300$ ft^3/(sec)(ft^2). At $\phi = 0.60$ ft^3/(sec)(ft^2), the losses (based on calculations for thermal equilibrium conditions) amounted to 18% of heat flux input, influencing the accuracy of results to a similar extent.

If the microconvection effect is neglected, Eq. (11) can be represented as

$$h_{TP} = (1 - \alpha_w)(h_{TP})_{\phi=0} + c_p \rho_\ell \phi \left(\frac{k_\ell}{D_b}\right)^2 \left[1 - \frac{k_\ell}{2D_b(h_{TP})_{\phi=0}}\right] \left(\frac{1}{h_{TP}}\right)^2_{\phi=0} \qquad (12)$$

by substituting $\delta_t = k_\ell/(h_{TP})_{\phi=0}$. The heat-transfer coefficients for zero injection, designated as $(h_{TP})_{\phi=0}$ here, can then be calculated from Eq. (4) for any specific condition. The results presented in Figs. 25 through 29 for air-water and air-ethylene glycol were correlated within ±30% by Eq. (12) using Eq. (4) to obtain values for $(h_{TP})_{\phi=0}$. This agreement is quite good, considering that heat-transfer results without injection were correlated within ±20% by Eq. (4).

Since the mechanisms discussed explain the present gas-bubbling results quite well, these results will next be compared with other gas-bubbling and boiling investigations.

Comparison at Low Bubbling Rates. When test results by Mixon et al.(12) for natural convection with electrolytic gas generation were analyzed for comparison, it was observed that the electrolytic gas bubbles coming off the heated surface are much more effective in enhancing heat transfer for low natural-convection rates. Figure 34 shows how the effectiveness of bubbles decreases for higher natural-convection rates where turbulence intensity near the boundary layer is greater, and δ_t is smaller.

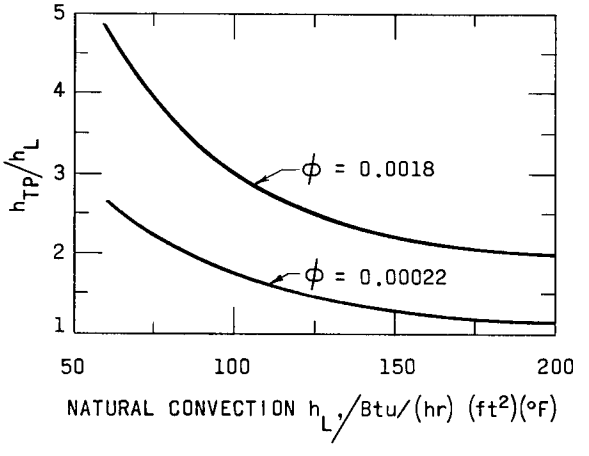

Fig. 34

Convection Effect in Results by Mixon et al.

Analysis of gas-injection effects in the current forced-circulation experiments has shown that microconvection and vapor-liquid exchange mechanisms are more effective in increasing h when δ_t is large and turbulence intensity is low, and that their effectiveness decreases considerably with decreasing δ_t values. This analogous trend in heat-transfer behavior for both systems indicates that the same microconvection and

vapor-liquid exchange mechanisms may be applied to explain natural-convection heat transfer under the influence of gas generation.

Although Mixon did not report what the electrolytic bubble sizes were, a useful comparison, based on the relationship between heat-transfer coefficient and gas-bubbling rate, could still be made. From Mixon's results, the net effect of electrolytic bubbles on heat-transfer rate was found to be $h_{TP} = \text{const.}\ (\phi)^{3/8}$ for a given $(t_w - t_b)$ at 80°F solution temperature.

For nucleate pool boiling, the data of many observers[59] can be represented as

$$q'' = c_1 (t_w - t_s)^m, \tag{13}$$

where m is a constant ranging from 3 to 4, and c_1 is a constant whose value depends on the properties of the liquid and the heated surface, and also on pressure. Therefore,

$$h_{TP} = \text{const}\,(q'')\left(1 - \frac{1}{m}\right), \tag{14}$$

resulting in q" to the power from $\frac{2}{3}$ to $\frac{3}{4}$.

The dependence between heat flux and vapor volume generated on the boiling surface cannot be determined accurately since bubbles grow as they rise through the somewhat superheated liquid in a saturated boiling system. However, a fair estimate can be made by using the results for pool boiling of water at atmospheric pressure reported by Nishikawa and by Gaertner and Westwater.

Nishikawa[29] expressed the growth of vapor bubbles for low boiling-heat fluxes (up to 8100 Btu/hr/ft^2) in terms of nucleation-site density as

$$\frac{Q_u}{Q_0} = \text{const}\,(n)^{-1/2}. \tag{15}$$

Gaertner and Westwater[60] expressed q", where natural convection contribution was small, in terms of nucleation-site density as

$$q'' = 1400(n)^{0.47}. \tag{16}$$

Determining Q_u from a heat balance,

$$q'' = \frac{\rho_g h_{fg} Q_u}{A}, \tag{17}$$

Eqs. (15), (16), and (17) may be combined to give

$$\frac{Q_0}{A} = \text{const}\ \frac{(q'')^{2.06}}{\rho_g\, h_{fg}}\ \text{ft}^3/(\text{hr})(\text{ft}^2), \tag{18}$$

where Q_0/A is the vapor-generation rate, or ϕ, for boiling.

Therefore, the resulting relationship for pool boiling is

$$\phi = \text{const}\,(q'')^{2.06}. \tag{19}$$

Combining Eqs. (14) and (19),

$$h_{TP} = \text{const}\,(\phi)^{\left(\frac{1-1/m}{2.06}\right)}, \tag{20}$$

with the exponent ranging from 0.325 to 0.365.

The relationship between air-bubbling rate and the net heat-transfer coefficient due to air bubbling at low rates was also determined for the ethylene glycol results of Fig. 27. This relationship could be expressed approximately as $h_{TP} = \text{const}\ (\phi)^a$. For the air-water results of Fig. 27, no such relationship could be established because forced convection heat transfer was dominant, and bubbling was not very effective in promoting heat transfer. This aspect will be discussed in further detail under the comparison with forced-circulation results.

The results discussed here are compared as follows to show their agreement:

	Value of exponent in $h_{TP} = \text{const}\ (\phi)^a$
Nucleate boiling	0.325 to 0.365
Mixon's results	0.375
Air-ethylene glycol:	
U_ℓ = 1.0 ft/sec	0.45
U_ℓ = 4.5 ft/sec	0.30

In this discussion of low bubbling rates, the same type of relationship was found between gas bubbling or generation rate and heat-transfer coefficient due to it. Good agreement between exponent values for low gas-bubbling rates and low nucleate-boiling heat fluxes was also observed. These findings indicate that the influence of gas generation on heat-transfer rate for both boiling and bubbling is similar when convective heat transfer is relatively low. This further suggests that the high heat-transfer rates at low boiling-heat fluxes are due to the turbulence and the vapor-liquid exchange action created by vapor bubbles.

Comparison at Moderate Bubbling Rates. At moderate and high nucleate-boiling-heat fluxes, growth of vapor bubbles in the bulk of the liquid can be expected to become less significant than at low boiling-heat fluxes. Hence, comparison with gas bubbling can be tried by assuming that all vapor is generated near the heated wall, where it influences the heat transferred from the wall to the liquid. The comparison can be based, then, on equal gas and vapor generation rates.

One of the more widely accepted heat-transfer correlations for pool boiling at saturated temperature is Kutateladze's[15] relationship,

$$\frac{h_{TP}}{k_\ell}\left(\frac{\sigma}{g\Delta\rho}\right)^{0.5} = C_1(Pr)^{0.35}\left[\frac{q''\rho_\ell}{\rho_g\, h_{fg}\, \mu_\ell}\left(\frac{\sigma}{g\Delta\rho}\right)^{0.5}\right]^{0.7} \times \left[\frac{144 \times 10^{-4}\, p}{\sqrt{\sigma\Delta\rho/g}}\right]^{0.7}, \qquad (21)$$

where the Pr number contains all liquid properties. Since the first and second groupings in Eq. (21) are in forms of Nu and Re numbers, respectively, the relationship may be written in abbreviated form as

$$Nu^* = C_1(Pr)^{0.35}(Re^*)^{0.7}\left[\frac{144 \times 10^{-4}\, p}{\sqrt{\sigma\Delta\rho/g}}\right]^{0.7}, \qquad (22)$$

where

$$Nu^* = \frac{h_{TP}}{k_\ell}\left(\frac{\sigma}{g\Delta\rho}\right)^{0.5},$$

and

$$Re^* = \frac{q''\rho_\ell}{\rho_g\, h_{fg}\, \mu_\ell}\left(\frac{\sigma}{g\Delta\rho}\right)^{0.5}.$$

Kutateladze used $C_1 = 0.44$, but Gambill and Bundy[61] found C_1 to be about 50% higher than 0.44 for their pool- and forced- circulation boiling studies with water and ethylene glycol. Gambill and Bundy used the boiling-heat flux (that is, total minus convection-heat flux) to correlate their forced-circulation results with Eq. (21).

Since group $q''/h_{fg}\rho_g$ is the volume rate of vapor production by boiling per unit time and per unit area of heating surface, gas bubbling and boiling can be compared on the basis of equal vapor and gas generation rates by substituting

$$\frac{q''}{h_{fg}\rho_g} = 3600\,\phi \qquad (23)$$

into Eq. (21). With this substitution, heat transfer with gas injection can be correlated in terms of Kutateladze's relationship, since gas-bubbling rates are known.

Air-ethylene glycol results of Figs. 27 and 28 at low and moderate gas-injection rates are plotted in Fig. 35 for comparison with Kutateladze's equation. Fluid properties were evaluated at the heated surface, and heat-transfer coefficients due to air bubbling alone were used. Agreement is quite good at moderate bubbling rates, although some deviation is seen at low bubbling rates. This deviation occurs because only a part of $q''/h_{fg}\rho_g$ is generated near the heated surface at low boiling-heat fluxes where it can enhance heat transfer. Therefore, ϕ in Eq. (23) should be divided by the fraction of vaporization occurring at the heated surface to keep the comparison on the same basis. The division would bring the points at lower Re* closer in line with Kutateladze's relationship. Unfortunately, the fraction of vaporization occurring near the surface at low boiling-heat fluxes is not available, making a more quantitative presentation impossible.

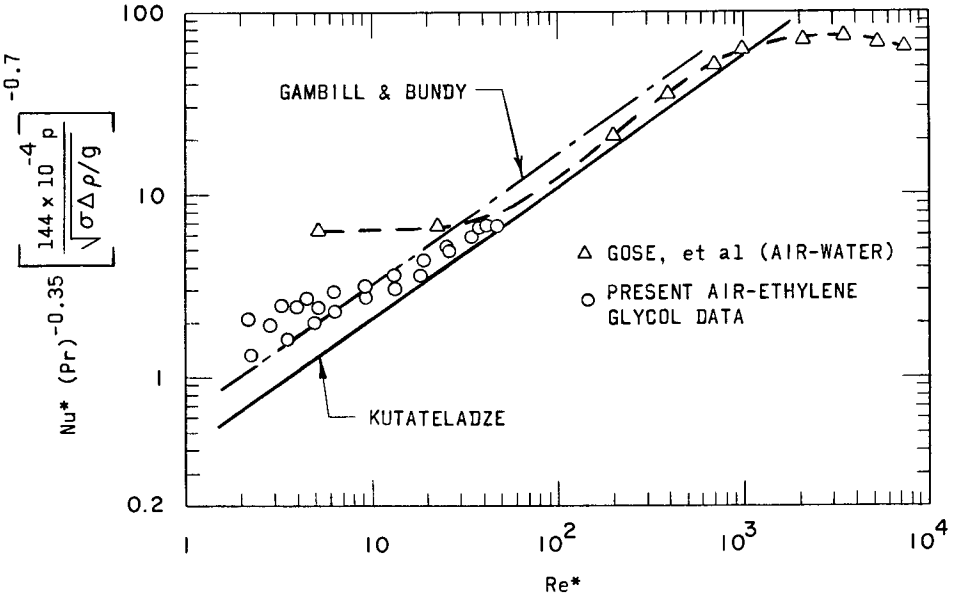

Fig. 35. Comparison with Saturated Pool Boiling

Gose's[13] heat-transfer results for bubbling of air from a horizontal porous plate into a pool of water are also shown in Fig. 35 to illustrate the agreement with Kutateladze's relationship at higher Re* numbers. It is seen, however, that gas-bubbling heat-transfer rates start dropping below pool-boiling rates at high gas-injection values ($\phi > 0.6$ ft^3/sec-ft^2). The magnitude of the deviation increases with increasing gas rates because heat of vaporization, perhaps, becomes an important heat-exchange mechanism at high boiling-heat fluxes. The heat of vaporization influence cannot, of course, be simulated by the gas-bubbling system.

A complete analysis of Gose's pool-bubbling data for water, ethylene glycol, and several oils was performed by Sims et al.[14] who correlated the results for horizontal and vertical porous plates of different porosities satisfactorily with Kutateladze's pool-boiling relationship.

The air-water results of the present tests could not be correlated with Eq. (21), and the reasons for this will be discussed under the comparison with forced-circulation results. They also do not compare well with Gose's pool air-water results because of the differences in convection heat-transfer rates. Natural convection was initially quite low in the pool system, and every increase in injection increased the microconvection and the gas-liquid exchange actions. Conversely, the initial convection without gas bubbling in the forced circulation experiments was high (Fig. 26), and gas bubbling removed valuable convection area while adding very little to turbulence or gas-liquid exchange action at the low δ_t/D_b ratios encountered. Since Gose did not report any bubble diameters for his tests, a comparison on the basis of heat-transfer mechanisms discussed in this study could not be made.

The good agreement between gas bubbling from porous surfaces and nucleate boiling, both in this study and by Sims et al.[14] shows that bubbling simulates boiling-heat transfer quite well at moderate boiling-heat fluxes. The simulation appears to be equally good for pool boiling and for circulation boiling when the convection rates without bubbling are relatively low in the gas-injection system. The ability to correlate boiling and gas bubbling on the basis of equal gas and vapor generation rates indicates that the high heat-transfer rates at moderate boiling-heat fluxes are caused mainly by microconvection and vapor-liquid exchange action of bubbles. Hence, the enhancement in heat transfer is hydrodynamic in nature.

Comparison with Two-phase Circulation Heat Transfer. The results of Gose's[13] forced-circulation tests under the influence of gas injection were reported in terms of injection effects on h_{TP} without taking volumetric gas/liquid flow ratios into account. It was found in the current experiments that the increase in heat-transfer coefficient caused by the liquid velocity increases (due to introduction of the gas phase) was just as important as that due to gas injection. Therefore, since the above two effects were not separately evaluated in Gose's experiments, comparison on an equal basis was impossible. Gose concluded from his two-phase forced-circulation results that the increase in h due to injection did not depend on the value of h without injection; that is, the effects of convection and injection were additive. It was shown in the present experiments, however, that this addition was not of an arithmetic but rather of an algebraic nature, since gas injection was found to reduce h when convection rates were high.

A paper on forced-circulation two-phase heat transfer by Collier and Pulling,[40] which made good use of the experience gained in previous investigations, was chosen as typical for comparison with the present results (Fig. 36) because it represented fairly well the type and nature of heat transfer encountered in two-phase systems. The authors grouped their results into two heat-transfer regions: nucleate-boiling type heat transfer, where heat flux effects were dominant; and convective type heat

transfer, where quality or volumetric steam/water ratio was the controlling parameter. Although their data indicated presence of a transition region between the two regions mentioned, this region was neglected because of its shortness.

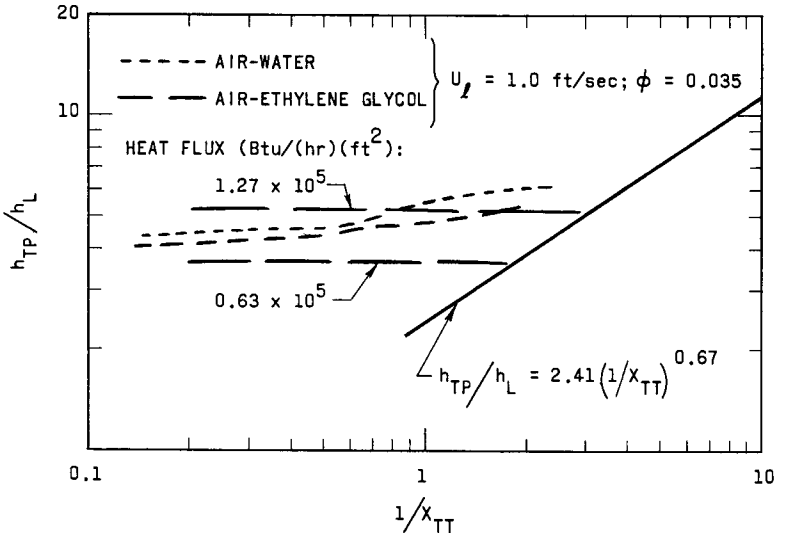

Fig. 36

Comparison with Steam-Water Forced Convection

In the low-quality range, representative air-water and air-ethylene glycol results for $U\ell$ = 1.0 ft/sec exhibit the same heat-transfer trends (Fig. 36) as Collier's and Pulling's steam-water results at 30 psia (0.625-in.-O.D. heater and 0.866-in.-I.D. flow tube) for liquid-inlet velocities of 0.85 to 0.95 ft/sec. Although the results of present experiments shown in Fig. 36 reached well into the annular-flow regime, comparison with steam-water results shows that they did not extend into the convective type heat-transfer region as defined by the strong dependence of h_{TP} on $1/X_{TT}$. This behavior was also observed in the present zero-injection results, indicating that transition to annular flow cannot be associated with transition to heat transfer of the type

$$\frac{h_{TP}}{h_L} = \text{const}_1 \left(\frac{1}{X_{TT}}\right)^{\text{const}_2}.$$

Furthermore, it may be noted that h_{TP} is almost independent of $1/X_{TT}$, as observed in Fig. 36 at low $1/X_{TT}$ values, but not because heat transfer is controlled by heat flux or by gas bubbling there. Rather, as results for two-phase heat transfer without gas bubbling have shown, the low dependence of h_{TP} on $1/X_{TT}$ is characteristic of the low-quality range and the flow patterns associated with it. Hence, as was pointed out in the discussion of zero-injection results, heat flux in boiling-heat transfer (while influencing heat-transfer rate) does not appear to determine heat-transfer characteristics as far as dependence on $1/X_{TT}$ is concerned.

The steam-water results of Collier and Pulling[40] in the nucleate-boiling region were effectively represented in terms of heat flux, and compared quite well with water-pool-boiling results on a similar surface when plotted on a heat-flux-versus-temperature basis. The effect of gas injection on heat transfer for most air-ethylene glycol forced-circulation results was also found to be approximately the same as the effect of vapor generation on heat transfer in pool boiling. For air-water gas-injection results, however, the effect of gas injection on heat transfer was not found to be the same as for air-ethylene glycol results, and therefore the air-water results could not be represented in terms of boiling-heat transfer.

Since convection heat-transfer rates were high and δ_t/D_b ratios were low in the air-water experiments, injection was found to have a small, or even a negative, effect on heat-transfer rates. Differences between the air-water, air-ethylene glycol, and steam-water systems have to be examined to determine why the gas generation effects in the air-water system are not the same as in the other two systems. The principal difference between water and ethylene glycol systems was the higher viscosity of ethylene glycol, producing lower convection rates and thicker thermal-boundary layers (consequently also higher δ_t/D_b ratios) in the air-ethylene glycol experiments. The heat-transfer coefficients for both air-water gas-injection and water-boiling results (presented in Fig. 36) are in the 2000-Btu/(hr)(ft^2)(°F) range, indicating that thermal boundary layers are approximately the same in both systems, and that the differences are not likely to be due to microconvection effects produced by bubbles. Since it was found that both air-water and air-ethylene glycol pool heat-transfer results compared favorably with pool-boiling results at low and moderate gas-generation rates, it is further unlikely that the difference in injection effects is due to latent heat transport in the steam-water system. The only mechanism remaining to explain the difference in results is the vapor-liquid exchange mechanism. It follows, therefore, that the δ_t/D_b ratio had to be smaller in the present air-water experiments than in either the air-ethylene glycol or steam-water tests discussed. Previous thermal boundary-layer calculations have shown that δ_t/D_b ratios for the present air-ethylene glycol experiments were several times larger than for air-water experiments. The δ_t/D_b values for Collier's and Pulling's[40] steam-water experiments, however, were difficult to estimate. The only saturated-boiling investigation that is known to have measured both bubble diameters and heat-transfer rates in a forced circulation system did not report them in the initial publication[18] on this study. Therefore, a meaningful comparison of steam-water δ_t/D_b ratios with the air-water ratios determined in the present tests could not be made.

It is hoped that the various influences and characteristics of two-phase heat transfer that were presented and discussed will shed new light on the complex problem of boiling-heat transfer. The important facts found in this investigation and the conclusions drawn from them are summarized in the next section.

SUMMARY AND CONCLUSIONS

During this study, similarity between boiling and gas bubbling from a porous surface, and various hydrodynamic aspects of two-phase circulation heat transfer were investigated.

Photographic comparison of pool boiling and air bubbling from tubes etched identically and placed in a tank of Freon-11 showed that qualitatively both processes were similar, and that bubble diameters and flow formations were alike. Bubbling of air from a porous tube into a tank of water and a tank of ethylene glycol also compared favorably with boiling.

Two-phase flow patterns for air-water observed in the forced-circulation system were described and mapped on the basis of superficial liquid and gas velocities for the low-quality range investigated in this study. This was done so that heat-transfer results could be discussed in terms of flow patterns.

Void-fractions and phase distributions in the tube were studied using the gamma-ray attenuation technique. Slip ratios for air-water were correlated on the basis of the volumetric gas/liquid flow ratio. No effect of mass velocity could be discerned, but gas bubbling influenced slip ratio by affecting distribution of gas and liquid phases in the tube. The increase in slip ratio with increasing quality was due to developing-phase distribution, the gas phase developing towards the center of the tube. Since distributions without gas injection differed from those with gas injection at the wall, it was concluded that phase distributions for adiabatic wall conditions cannot be considered the same as for heated-wall conditions with gas generation at the interface.

Two-phase heat-transfer results were obtained with zero injection in the heated tube to provide a basis for studying the influence of gas-injection rate on heat transfer, but were also found to be quite informative in their own right. Air-water and air-ethylene glycol results were correlated by the same equation, and it was observed that dependence of h_{TP} on G at low qualities was much smaller than is usually associated with higher qualities for annular flow. The dependence of h_{TP} on U_g/U_ℓ at low qualities was also found to be small, and not unlike that of boiling-heat transfer in forced circulation. Thus, while increase in heat flux in boiling-heat transfer at moderate heat fluxes adds to the heat-transfer rate, it may not really determine heat-transfer characteristics as far as dependence on quality is concerned.

Effects of mass velocity, flow pattern, void fraction, phase distribution, U_g/U_ℓ, and gas-bubbling rate on heat transfer were also examined for air-water and air-ethylene glycol mixtures at low qualities.

It was found that, although gas bubbling enhances heat transfer, it does not greatly influence the dependence of heat transfer on mass velocity. It was also found that for a given U_g/U_ℓ and ϕ, the h_{TP}/h_L ratio decreased with increasing mass velocity because the turbulence intensity of liquid flow increased with increasing mass velocity and the gas phase became less effective in promoting additional turbulence.

In the range of U_g/U_ℓ values tested, the influence of gas-bubbling rate on heat transfer was found to be algebraically additive, rather than linearly additive as was previously claimed. It was also found that in the slug-flow region the variation of h_{TP} with U_g/U_ℓ was influenced by gas bubbling at the wall. This was attributed to the stabilization of the flow produced by gas generation at the wall. Comparison of flow patterns and heat-transfer rates strongly indicated that transition to annular flow cannot be associated with transition to heat transfer of the type correlated by

$$\frac{h_{TP}}{h_L} = \text{const}_1 \left(\frac{1}{X_{TT}}\right)^{\text{const}_2},$$

as is usually assumed.

It was found that two-phase heat-transfer results could be correlated better in terms of volumetric gas/liquid ratios than in terms of experimental void fractions. Correlation of the void type was found to be unsatisfactory in explaining heat-transfer behavior. In addition, it was found that heat-transfer results could be explained in terms of local phase conditions at the wall, but not in terms of the overall phase distributions found in the void tests.

Study of the influence of gas-bubbling rate on circulation heat transfer revealed that h_{TP} always increased with increasing bubbling rate for air-ethylene glycol but sometimes decreased for air-water. A model based on microconvection, vapor-liquid exchange, and "convection area reduction" mechanisms was proposed to explain these results. This simplified model predicted the experimental trends of bubbling rate on heat transfer satisfactorily. Even when microconvection was neglected, the results of the present tests could be correlated within 30% using this model in conjunction with the correlation for zero-injection results.

Comparison of bubbling results at low bubbling rates with nucleate boiling showed that the relationship between gas-bubbling rate and heat-transfer coefficient due to it could be expressed in the same form as for nucleate boiling, when convective heat-transfer rates were relatively low. The relationship was $h_{TP} = \text{const}\ (\phi)^a$, where the exponent agreed favorably for both bubbling and nucleate boiling systems. This agreement

indicated that the high heat-transfer rates at low boiling-heat fluxes in circulation as well as pool systems are due to the turbulence and the vapor-liquid exchange action created by vapor bubbles.

Comparison of bubbling results at moderate bubbling rates with nucleate boiling also indicated that the high heat-transfer rates at moderate boiling-heat fluxes in circulation as well as pool systems were caused mainly by microconvection and vapor-liquid exchange action of bubbles. Hence, the enhancement in heat transfer could be taken as hydrodynamic in nature, making latent-heat transport unimportant as a heat-transfer mechanism. These conclusions were reached because the present air-ethylene glycol results and previous pool air-water results were correlated successfully with Kutateladze's Eq. (21) for saturated pool boiling at moderated boiling-heat fluxes.

For current forced-circulation air-water results with gas injection, convection was found to be dominant, and increases in heat-transfer rate with gas addition were found to be mainly due to increased convection rates. Since the influence of injection rate on heat transfer was not found to be the same as for ethylene glycol circulation, the air-water results could not be represented in terms of nucleate boiling-heat transfer. Since the turbulence intensity in the air-water system was already high without gas injection, additional turbulence created by bubbling at the wall was not found to be very effective in promoting heat transfer. From examination of differences between air-water, air-ethylene glycol, and steam-water forced-circulation systems, it was concluded that the diameter of air bubbles in the air-water system may be important in determining the influence of air-injection rate.

Hence, in future experiments of this type, porous metals of various pore sizes should be tried to detect the influence of bubble diameter on two-phase heat transfer, if any. It would also be quite interesting to know how air injection at the walls influences boiling-heat transfer in a forced-circulation system, and if there may be any advantage in having such a system. Possibilities such as improvement of heat transfer, or influence on burnout, could be investigated.

APPENDIX A

Calibration of Flow-Metering Orifices

The knife-edge orifices used to measure air and liquid flow rates in the experiments were calibrated by weighing a volume of water discharged during a period of 5 to 12 minutes. Calibrations were performed with the orifice assemblies and their piping systems placed on the loop. The results of these calibrations are presented in Fig. 37. Orifice-discharge coefficients were calculated from

$$K = \frac{W}{359.1 d^2 \sqrt{\rho h_w}}. \tag{24}$$

K includes the velocity of approach factor, and was plotted against Reynolds number in the orifice throat.

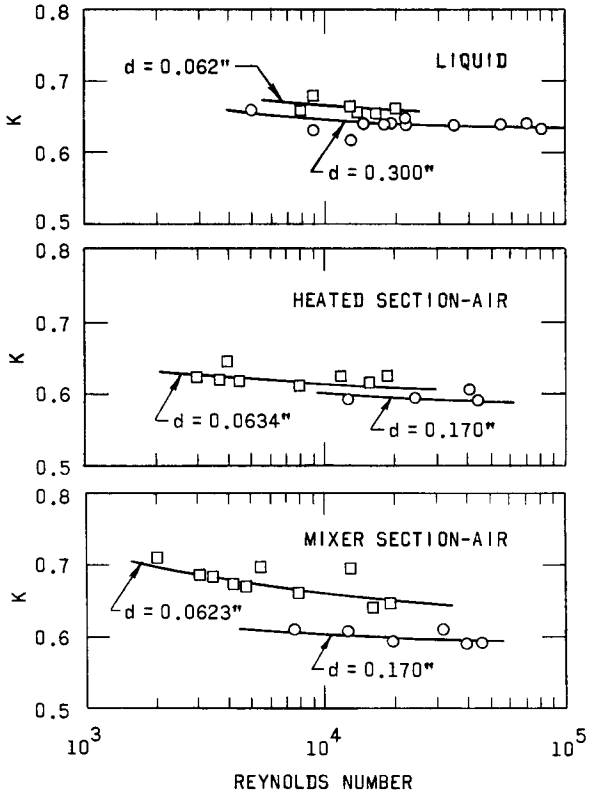

Fig. 37

Calibration of Flow Orifices

The liquid flow rates in experiments were computed using Eq. (24). For air-flow-rate computations, K was multiplied by the expansion factor Y_1 (determined from graphs in Ref. 62) to compensate for density change from the upstream to the downstream side of the orifice, and the upstream density of air was used in Eq. (24).

APPENDIX B

Analysis of Temperature Distribution in the Heated Wall of the Porous Tube

To help determine inside-surface temperatures of the wall more accurately from wall thermocouple measurements, the temperature drop and distribution across the tube wall were analyzed analytically and experimentally. The analyses included calculation of temperature distribution without any air flow, and the effects of air flow and thermocouple installation inside the wall on temperature distribution in the heated wall. The calculations and junction location of some inside-wall thermocouples were checked by a statistical analysis of the temperature differences between inside- and outside-wall thermocouples at various power inputs.

Temperature Distribution without Air Flow

The temperature distribution in the heated wall was calculated using the heat-conduction equation for a cylinder with uniform heat generation. Proceeding from

$$q''' = -k\nabla^2 t(r),$$

with the boundary conditions, as illustrated in Fig. 38, being

$$\frac{dt}{dr} = 0 \quad \text{at } r = b$$

and

$$t = t_a \quad \text{at } r = a$$

the expression for temperature distribution in the tube was

$$t - t_a = \frac{q'''}{4k}\left[2b^2 \ell n(r/a) - r^2 + a^2\right]. \tag{25}$$

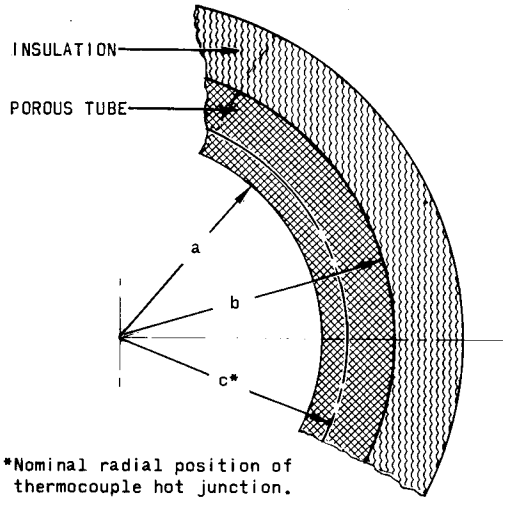

Fig. 38

Porous Tube Cross Section

Thermal conductivity of Oilite porous bronze was determined from the plot by Grootenhuis et al.,[63] of thermal conductivities for bronzes (11% Sn, 89% Cu) of various porosities, measured at 122°F. For nominal conditions of the Oilite bronze (10%, 90% Cu, minimum density 6.4 gms/cc, and a porosity of 18 to 23%), Grootenhuis' plot gave a k of 17.0 Btu/hr-ft-°F. Since the average tube wall temperatures in the present heat-transfer tests were 110 to 120°F, no temperature corrections were required for k.

The relationship between heat flux at the inside diameter of the tube and heat generation in the wall is

$$q''' = q'' \frac{2\pi a}{\pi(b^2 - a^2)}. \tag{26}$$

Using the nominal tube dimensions given in Fig. 5, Eqs. (25) and (26) were combined to give the temperature drop across the wall in terms of heat flux as

$$t_b - t_a = 0.282 \times 10^{-3} q''°F. \tag{27}$$

The temperature drop from the nominal thermocouple junction position (Fig. 38) to the inside diameter of the tube was

$$t_c - t_a = 0.15 \times 10^{-3} q''°F. \tag{28}$$

If the possible ±0.003-in. variation in junction position due to tube tolerances is taken into account, however, the $(t_c - t_a)$ value given in Eq. (28) can vary ±9%.

Effect of Air Flow on the Temperature Distribution in the Tube

To determine what effect air flow through the porous heated tube has on the temperature distribution in the tube, the problem was set up in one-dimensional slab-geometry form for an iterative numerical solution on a digital computer.

The equations for this type of heat transfer in a heated porous wall with cocurrent gas flow through it, as given by Grootenhuis,[64] are:

$$q''' + k \frac{d^2t}{dx} = (Gc_p)_g \frac{dT}{dx} = h'(t - T). \tag{29}$$

To set up the equations for numerical solution, the insulation and porous-bronze regions shown in Fig. 39 were divided into a number of

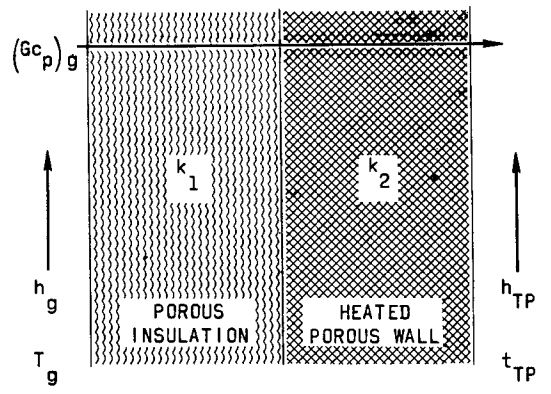

Fig. 39

Cross Section for Investigation of Air-cooling Effects

blocks of equal length Δx as shown below, and a heat balance was performed on each, to result in the following equation:

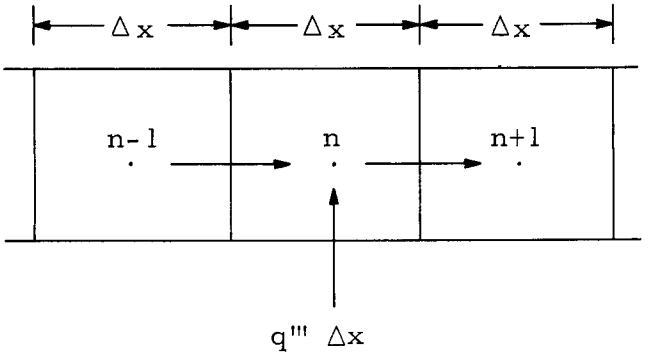

$$q''' \Delta x + \frac{t_{n-1} - t_n}{\Delta x} \cdot \frac{k_{n-1} + k_n}{2} + (Gc_p)_g T_{n-1}$$

$$= (Gc_p)_g T_n + \frac{t_n - t_{n+1}}{\Delta x} \cdot \frac{k_n + k_{n+1}}{2}. \qquad (30)$$

But

$$(Gc_p)_g (T_n - T_{n-1}) = h_n' \Delta x \, (t_n - T_{n-1}). \qquad (31)$$

Combining these equations and solving for t_n,

$$t_{n,i+1} = \frac{\left(q_k''' + T_{n-1,i+1} \, h_k'\right)(\Delta x)^2 + t_{n-1,i+1} \frac{k_{n-1} + k_n}{2} + t_{n+1,i} \frac{k_{n+1} + k_n}{2}}{h_k'(\Delta x)^2 + k_n + \frac{k_{n-1} + k_{n+1}}{2}}, \qquad (32)$$

where the subscripts are:

k = 1 for insulation,

k = 2 for heated wall,

and

i = number of iteration to which a value belongs.

From Eq. (31),

$$T_{n,i+1} = \frac{h'_k \Delta x}{(Gc_p)_g} t_{n,i+1} + T_{n-1,i+1} \left(1 - \frac{h'_k \Delta x}{(Gc_p)_g}\right). \tag{33}$$

Since fluids are encountered at both boundaries, the numerical boundary equations are different. For the air-insulation boundary,

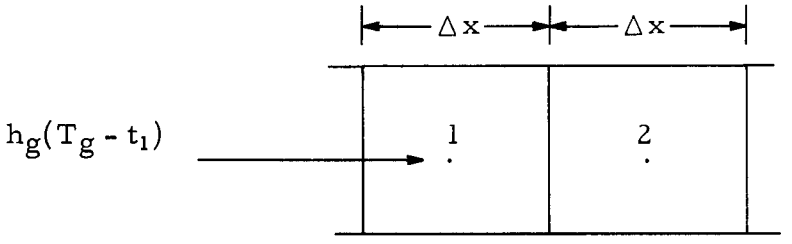

$$t_{1,i+1} = \frac{q''' \Delta x + (h'_1 \Delta x + h_g) T_g + (k_1/\Delta x) t_{2,i}}{h_g + h'_1 \Delta x + (k_1/\Delta x)},$$

and from Eq. (33),

$$T_{1,i+1} = \frac{h'_1 \Delta x}{(Gc_p)_g} t_{1,i+1} + T_g \left(1 - \frac{h'_1 \Delta x}{(Gc_p)_g}\right). \tag{34}$$

For the heated-wall, two-phase, fluid boundary,

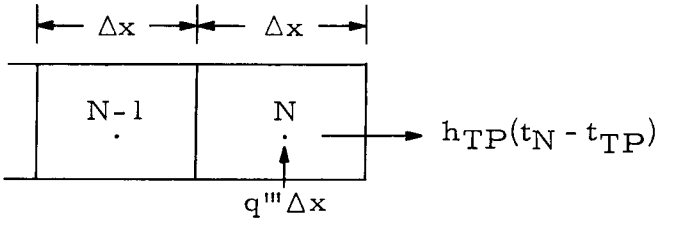

$$t_{N,i+1} = \frac{q'''_2 \Delta x + t_{N-1,i+1}\left(\frac{k_2}{\Delta x}\right) + h_{TP} t_{TP} + h'_2 \Delta x T_{N-1,i+1}}{h_{TP} + h'_2 \Delta x + \frac{k_2}{\Delta x}}, \tag{35}$$

and

$$T_{N,i+1} = \frac{h_2' \Delta x}{(Gc_p)_g} t_{N,i+1} - T_{N-1,i+1}\left(1 - \frac{h_2' \Delta x}{(Gc_p)_g}\right), \tag{36}$$

where

N = total number of blocks.

The system of equations presented was programmed using Fortran language for a digital computer. The program (1565/AMU-101) is available from Argonne National Laboratory. To start the interations, initial insulation and wall-temperature guesses (obtained from a solution for no air flow) were inserted as input. The only requirement for convergence of the system of numerical equations is that the $[h_k' \Delta x]/[(Gc_p)_g]$ term be less than unity. Although the convergence criterion was adjustable, the solutions checked well when heat balances were made, if the iteration was concluded when all temperature differences for each block between successive iterations were less than 0.01°F.

The temperature distributions in this porous-wall system for two air-injection rates, obtained from the numerical program described, are shown in Fig. 40. The heat generation of $q''' = 4.1 \times 10^6$ Btu/(hr)(ft^3) used in the solutions was typical of heating rates used in the experiments. Other property and heat-transfer values used in these solutions were

$k_1 = 0.1$ Btu/(hr)(ft)(°F),

$k_2 = 17.0$ Btu/(hr)(ft)(°F),

$h_g = 1.6$ Btu/(hr)(ft^2)(°F),

$h_{TP} = 2000$ Btu/(hr)(ft^2)(°F),

$h_1' = 500$ Btu/(hr)(ft^3)(°F),

and

$h_2' = 3000$ Btu/(hr)(ft^3)(°F).

The value of the volumetric heat-transfer coefficient for the heated tube was obtained from Grootenhuis'[64] empirical, internal heat-transfer correlation for porous bronze with transpiration air-cooling, and the value of h_1' was estimated from porous-bronze values.

The air and wall temperature distributions in Fig. 40A for a moderate air-injection rate of about $\phi = 0.10$ ft^3/(sec)(ft^2)(when $\rho_g = 0.08$) show that air leaves the porous wall at approximately the same temperature as

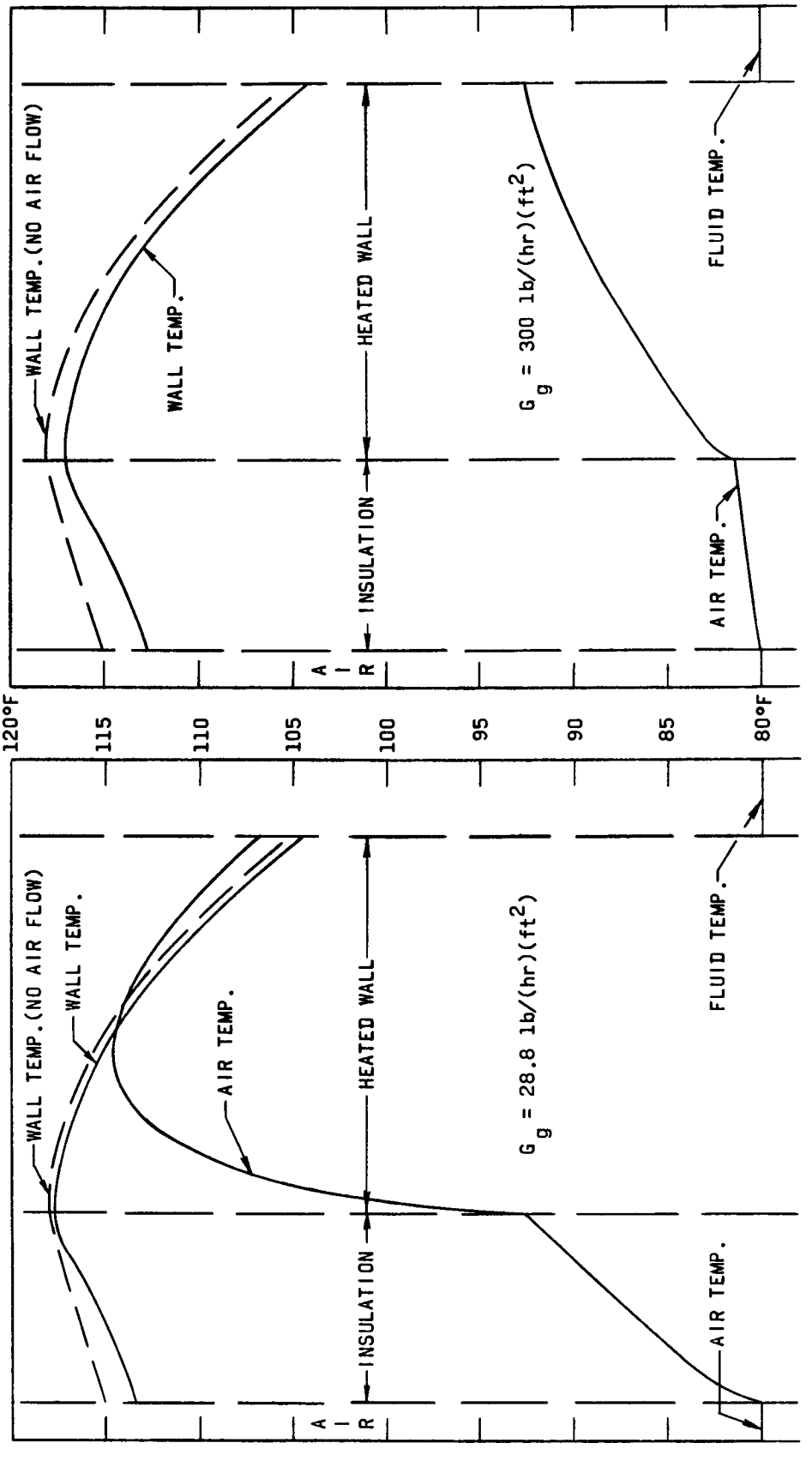

Fig. 40. Temperature Distribution with Air Flow through the Wall
(A - moderate flow, B - high flow)

that at the wall surface. Even for a high injection rate of about $\phi = 0.70$ ft^3/(sec)(ft^2) (when $\rho_g = 0.12$), the air temperature (Fig. 40B) comes fairly close to the heated-wall surface temperature. The temperature distributions in Figs. 40A and B show, however, that for the range of air-injection rates used in the present experiments, the temperature of the heated wall is depressed only slightly by the flow of air through it. This depression is small because heating of the air-to-wall surface temperature usually required less than 2% of the total power input.

Effect of Thermocouple Installation on Temperature and Heat-flux Distribution

Drilling of a hole for thermocouple installation into the electrically heated tube wall disturbed both the temperature distribution and the heat generation in that area. The magnitude of this disturbance had to be determined to arrive at more accurate wall-surface temperature and local heat-flux values.

The local heat-generation rates in the inhomogeneous area were determined by simplifying the heated-wall geometry as shown in Fig. 41. The round thermocouple hole was represented by a square insulator of the same area, i.e.,

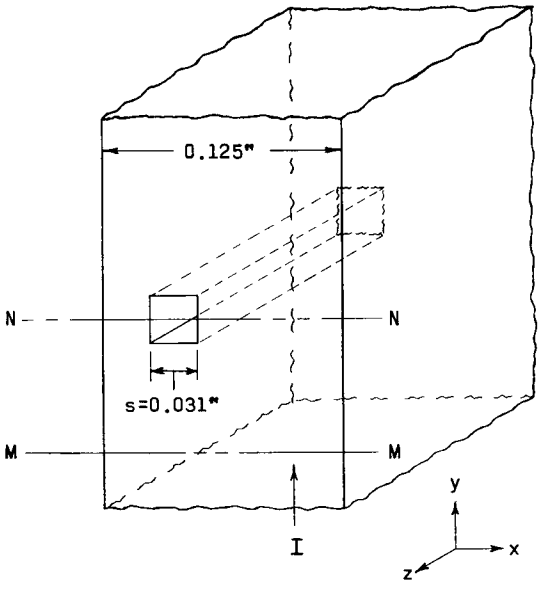

Fig. 41. Cross Section for Thermocouple Installation Analysis

$$s = \pi^{1/2} r = \pi^{1/2} \frac{0.035}{2} = 0.031 \text{ in.}$$

Since the total current I at cross sections M-M and N-N must be the same, the current density at the two sections is inversely proportional to their area. In addition, since heat generation is proportional to the square of current density for a material of given resistivity, the ratio of heat-generation rates at the two cross sections is

$$q'''_{N-N}(0.125 - 0.031)^2 = q'''_{M-M}(0.125)^2,$$

giving

$$q'''_{N-N} = 1.78 q'''_{M-M}. \qquad (37)$$

Thus, the heat generation rate at the thermocouple section may be about 80% higher than average. However, there is no heat generation in the low-thermal-conductivity ceramic occupying the hole.

To determine how the inhomogeneous heat generation and thermal conductivity affect local temperature and heat flux, the cross section shown in Fig. 41 was divided into 25 blocks as shown in Fig. 42, and a heat balance

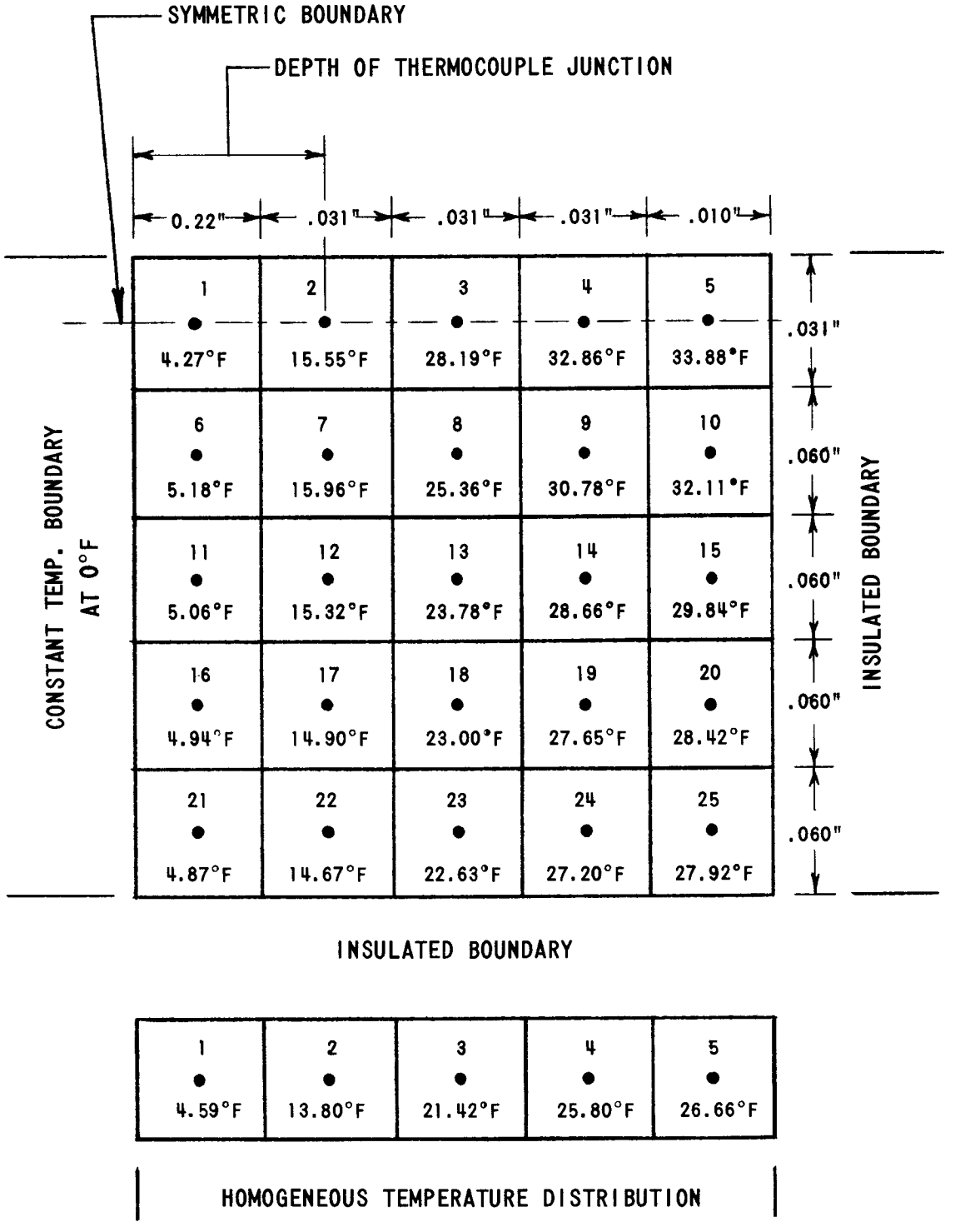

Fig. 42. Two-dimensional Temperature Distribution in the Thermocouple Region

was performed on each block using the following general finite-difference, heat-conduction equation:

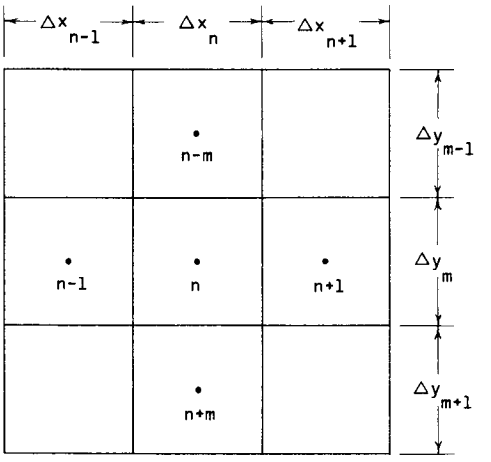

$$q'''_n \Delta x_n \Delta y_m = (t_n - t_{n-1}) \frac{\Delta y_m}{\left(\frac{\Delta x_n + \Delta x_{n-1}}{2}\right)} \cdot \frac{k_n + k_{n-1}}{2}$$

$$+ (t_n - t_{n+1}) \frac{\Delta y_m}{\left(\frac{\Delta x_n + \Delta x_{n+1}}{2}\right)} \cdot \frac{k_n + k_{n+1}}{2}$$

$$+ (t_n - t_{n-m}) \frac{\Delta x_n}{\left(\frac{\Delta y_m + \Delta y_{m-1}}{2}\right)} \cdot \frac{k_n + k_{n-m}}{2}$$

$$+ (t_n - t_{n+m}) \frac{\Delta x_n}{\left(\frac{\Delta y_m + \Delta y_{m+1}}{2}\right)} \cdot \frac{k_n + k_{n+m}}{2}. \qquad (38)$$

The 25 linear algebraic equations resulting from these heat balances contained the 25 temperatures as unknowns and were solved using a standard matrix-inversion subroutine (ANL-F-402) on a digital computer. The resulting temperature distribution, with boundary conditions as indicated, is presented in Fig. 42. The temperatures shown are for an average $q''' = 8.5 \times 10^6$ Btu/(hr)(ft^3) (15.1×10^6 for block Nos. 1, 3, 4, and 5), but the temperature distribution for any q''' would only differ by a constant multiplier, as can be seen from Eq. (38). Thus, the relative temperature distribution obtained for this inhomogeneous case applies to any power input, and the actual power inputs used in the air-water tests were lower (much lower for air-ethylene glycol tests) than in this example. Block No. 2 was represented as insulation with k = 1.0 Btu/(hr)(ft)(°F) and no heat

generation. A one-dimensional temperature distribution for a homogeneous part of the porous tube with the same slab geometry, boundary conditions, and average heat-generation rate is also shown in Fig. 42 below the two-dimensional mesh for comparison of values.

The two-dimensional temperature distribution shown in Fig. 42, however, is only an approximation to the three-dimensional problem. As can be seen in Fig. 5, no inhomogeniety exists in front of the thermocouple junction. Therefore, some distance away from it, the temperature distribution will be normal. The temperature measured at the junction would reflect the homogeneous and inhomogeneous distributions presented in Fig. 42, as illustrated in Fig. 43. Therefore, the final temperature at the thermocouple junction is 14.67°F, or about 6% higher than the temperature gotten from a homogeneous solution. The surface heat flux at the measuring point, as given by this type analysis, can be determined from the temperature at radial position No. 1. Since the temperature of 4.43°F at the measurement position is 3.5% lower than the homogeneous temperature at position No. 1, the heat flux would also be about 3.5% lower there.

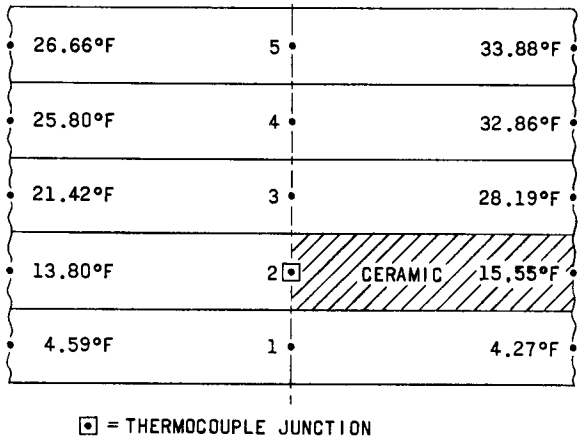

Fig. 43. Three-dimensional Approximation of Temperature Distribution

Comparison of Calculated and Experimental Temperature Drops

As was discussed in the chapter on DESCRIPTION OF APPARATUS, several thermocouples that were spot-welded to the outside of the heated tube were used to check inside-wall thermocouple measurements. The outside thermocouples, as shown in Fig. 4, were placed at the axial locations to be checked, and at several circumferential locations around the outside of the tube.

Temperature differences between the outside and corresponding inside locations were determined for the first 50 air-water experiments, and analyzed statistically. The results of this analysis are presented in Table II. The heat flux appearing in the presentation is a net q", with losses due to heating of air flowing through the tube already subtracted [see Eq. (43)].

Comparison of measured and calculated temperature drops in Table II indicates that both the homogeneous and nonhomogeneous temperature-distribution analyses can predict temperature drops in the heated wall reasonably well, considering that the thermal conductivity value used for the bronze tube may not be exact. However, the percentage deviations tend

to be greater than would be expected when the error due to junction location is given as ±9%. This suggests that the effective thermocouple-junction locations could be off more than was expected from a tolerance analysis allowing a ±0.003-in. deviation. It may also be observed that the standard deviations of Δt's vary from about $\frac{1}{2}$ to 1°F for the narrow range of q''' used in these tests. These standard deviation values are about what would be expected since the Δt's were calculated from individual temperature readings and the potentiometer reading error could be as great as $\pm\frac{1}{2}$°F.

Table II

COMPARISON OF EXPERIMENTAL AND ANALYTICAL TEMPERATURE DROPS

Δt between Thermocouples Indicated	Relative Circumferential Position of Thermocouples	Δt/q"	Standard Deviation of Δt/q"	Standard Deviation at a Representative q" of 6.0×10^4	Deviation from Homogeneous Analysis [Eq. (28)]	Deviation from Nonhomogeneous Analysis (Fig. 43)
	Degrees	$\frac{(hr)(ft^2)(°F)}{Btu}$	$\frac{(hr)(ft^2)(°F)}{Btu}$	°F	Per Cent	Per Cent
$t_{13}-t_6$	0	1.21×10^{-4}	0.085×10^{-4}	0.5	-9	-32
$t_{16}-t_7$	0	1.73×10^{-4}	0.076×10^{-4}	0.5	31	8
$t_{14}-t_6$	90	1.11×10^{-4}	0.19×10^{-4}	1.1	-19	-11
$t_{15}-t_7$	90	1.48×10^{-4}	0.094×10^{-4}	0.5	12	20
$t_{11}-t_2$	180	1.47×10^{-4}	0.20×10^{-4}	1.2	11	19

The temperature drop from the thermocouple junction location inside the wall to the inside surface of the tube could be calculated from Eq. (28) if uniform heating was assumed. However, it was found from the nonuniform heating analysis (Fig. 42) that the thermocouple installation disturbed the heating and the temperature distribution in the tube wall. The analysis presented in Fig. 43 showed that the effect of nonhomogeneity was to increase the temperature drop by 6%. Since both types of analyses predicted temperature differences presented in Table II with about the same overall accuracy, the average value of the temperature drop calculated by both methods was used in determining the temperature drop from the thermocouple junction inside the wall to the inside surface of the tube. The temperature-drop relationship resulting from this type of averaging was

$$\Delta t = t_c - t_a = 0.155 \times 10^{-3} q'' \ (°F), \tag{39}$$

where the value of q" was found from the average heat-generation rate in Eq. (44) from which the heat-generation rate required for heating of air passing through the porous wall had already been subtracted [see Eq. (43)].

APPENDIX C

Calculations for Heat-transfer Experiments

This appendix outlines the calculations performed to arrive at the results for heat-transfer experiments. Calculation of air and liquid mass-flow rates, and of surface temperature of the tube at its inside diameter, were discussed in Appendices A and B, respectively. Therefore, this appendix will cover only calculation of net heat flux, fluid bulk temperature, heat-transfer coefficient, and gas-bubbling rate and superficial gas velocity.

Net Heat Flux

Since the purpose of this study was to investigate the hydrodynamic effects of gas bubbling on heat-transfer rates, any thermal effects associated with bubbling of gas into the fluid stream had to be excluded when determining the effective heat-transfer rates in these tests. The air being bubbled into the two-phase stream was not saturated with liquid vapor, and the heat transferred from the wall to the fluid through evaporation of liquid into the gas (latent heat transport) had to be subtracted from the total heat flux. Air was also heated when it passed through the heated porous tube, and later cooled again in the two-phase fluid. The heat transferred in this way also had to be subtracted when calculating the net heat flux. As observed in Appendix B, the thermocouple installation produced nonuniform heat generation in the measurement area that affected the heat flux there, and this nonuniformity effect also had to be considered.

Although the heat-transfer effects discussed usually had only a minor influence on the local heat flux (because of the design of the experiments), they had to be accounted for to obtain more accurate net heat-flux values at measurement points. These effects had to be calculated for various conditions first so that experiments could be designed to minimize their magnitudes.

Effect of Heat of Vaporization. Heat of vaporization was significant as a heat-transport mechanism only for the air-water system. The vapor pressure of ethylene glycol at test temperatures, which were usually around room temperature, was low enough (0.002 to 0.005 psi) to make heat-of-vaporization effects insignificant.

For the air-water experiments, the percentage of total heat input transferred by the heat of vaporization process from the heated wall to the fluid involved a complex rate process and could not be calculated exactly. The time that effective vaporization into a particular air bubble could occur was limited by the time that the bubble remained on the surface. After the

bubble left the surface, additional vaporization into it did not affect the net heat flux at the wall. In addition, heat transfer occurred between the air bubble and the liquid, resulting in the lowering of air temperature, and hence equilibrium vapor pressure.

However, latent-heat transport could be estimated conservatively by calculating the equilibrium vaporization conditions and adjusting them according to the extent of nonequilibrium estimated. The rate of heat removal through latent-heat transport was the amount of water vaporized per unit time at the fluid-solid interface, times the heat of vaporization for water; i.e.,

$$q_{\text{heat of vaporization}} = h_{fg} W_v.$$

For equilibrium conditions, the mass ratio of water vapor to air in a unit volume at a given air temperature, as established using the ideal gas equation, is $0.622\,[p_v/(p_T - p_v)]$. If it is at first assumed that equilibrium vaporization occurs, the amount of water vaporized can be calculated from the amount of air passing through the walls, and the latent-heat transport then is

$$q_{\text{heat of vaporization}} = h_{fg} A_T \rho_g \cdot 3600\,\phi \cdot 0.622\left(\frac{p_v}{p_T - p_v}\right). \tag{40}$$

The heat flux corresponding to Eq. (40) is obtained by dividing it through by the total surface area; i.e.,

$$q''_{\text{heat of vaporization}} = 2240 h_{fg} \rho_g \phi \left(\frac{p_v}{p_T - p_v}\right)_{t_g}. \tag{41}$$

Equation (41) for equilibrium vaporization is unduly conservative, however, since the contact period of air bubbles with the heated surface during which time the only effective vaporization could occur was quite short. Even bubble-tray absorbers, which are designed to achieve maximum vaporization efficiency, only reach 85% of equilibrium vaporization at similar conditions. Therefore, to make the latent heat-transport effect more realistic, the right side of Eq. (41) was multiplied by a vaporization efficiency factor of 0.60, resulting in the following relationship for calculation of the latent heat-transport effect:

$$q''_{\text{heat of vaporization}} = 1400 h_{fg} \rho_g \phi \left(\frac{p_v}{p_T - p_v}\right)_{t_g}. \tag{42}$$

Effect of Air Heating. When the effect of air flow on temperature distribution in the heated wall of the tube was studied (as described in Appendix B), it was found that air coming in at room temperature was heated when passing through the porous tube. For most of the air-flow conditions in the tests, air left the heated wall at about the same temperature as the inside surface of that wall. When the air entered the fluid stream, it was cooled again to about its initial temperature.

Although heat transferred by the air in this way only formed a small part of the total heat input, it was subtracted when calculating the net heat flux because it was not part of the hydrodynamic aspects studied. The heat input required to heat the air was

$$q = 3600 A_T \phi \rho_g (c_p)_g (t_{exit} - t_{inlet})_g,$$

and the corresponding heat flux, using the fact that air-exit and tube-I.D. temperatures were about the same, was

$$q''_{\text{air heating}} = 3600 \phi \rho_g (c_p)_g (t_w - t_{inlet})_g. \tag{43}$$

Calculation of Net Heat Flux. The net heat flux at the points where temperature measurements were made was calculated by using current readings and resistance measurements of the test section and subtracting the latent-heat transport and air heating effects. Any nonhomogeneous heating effects were also accounted for. The total average heat flux was found from

$$q''_{\text{total}} = \frac{3.413}{\pi(0.625/12)} I^2 R_e = 20.9 I^2 R_e. \tag{44}$$

The resistance values reported in the Power Supply and Measurement section of the chapter on DESCRIPTION OF APPARATUS were used in Eq. (44). They were corrected for variation with temperature using the average temperature of the tube as follows:

$$R_e = (R_e)_{70°F} [1 + 0.33 \times 10^{-3}(t - 70°F)].$$

The net heat flux could be now calculated from Eqs. (42), (43), and (44) to give

$$q''_{\text{net}} = 20.9 I^2 R_e - 1400 h_{fg} \rho_g \phi \left(\frac{p_v}{p_T - p_v} \right)_{t_g}$$

$$-3600 \phi \rho_g (c_p)_g (t_w - t_{inlet})_g. \tag{45}$$

Since it was found in Appendix B that the local heat flux at inside-wall thermocouple locations was about 3.5% less than average heat flux due to nonhomogeneous heating, the net heat flux of Eq. (45) was multiplied by 0.965 when net fluxes for these thermocouple locations were calculated.

Fluid Bulk Temperature

The bulk temperature of the fluid was calculated at various positions along the length of the heated tube by adding the temperature increase produced in the fluid due to heat addition, to the inlet-liquid temperature; i.e.,

$$t_b = t_{\ell(\text{at inlet})} + \frac{q'' \pi DL}{(c_p)_\ell W_\ell}. \tag{46}$$

Only the liquid-heat capacity was considered in the calculation because the heat capacity of air present was relatively negligible.

Heat-transfer Coefficient

The local heat-transfer coefficient was calculated for all experiments using

$$h = \frac{q''_{net}}{(t_w - t_b)}, \tag{47}$$

with heat flux and temperature values determined from Eqs. (45), (46), and (39). For zero-injection and liquid-heat-transfer tests, the air-heating and latent-heat transport corrections did not have to be made.

Gas-bubbling Rate and Superficial Gas Velocity

When the pressure inside the tube of the heated test section was uniform along its length, the gas-injection rates were also uniform along its length and could be calculated using gas density values determined from pressure measurements as

$$\phi = \frac{W_g}{3600 \rho_g A_T} = \frac{W_g}{3600 \rho_g \pi \cdot 0.625 \cdot 10.5},$$

$$\phi = 7.0 \frac{W_g}{\rho_g}. \tag{48}$$

Figure 44 is a calibration curve for uniform gas injection obtained when there was no liquid in the heated-section tube, and the pressure in it was one atmosphere. This curve gives the pressure drop required across the insulated wall of the tube to achieve a given gas-injection rate.

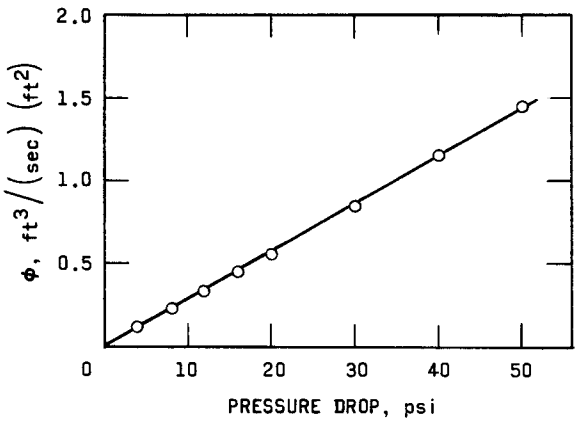

Fig. 44. Pressure Drop across Wall of Heated-section Tube

Since there was some static-pressure drop along the tube for all the two-phase flow experiments, and since the pressure in the air plenum was the same throughout, the gas-injection rate varied somewhat along the length of the tube. This variation occurred because a certain pressure difference across the wall of the tube produced a given injection rate (Fig. 44), and, consequently increasing pressure differences due to static-pressure drop produced increasing gas-injection rates along the tube. The magnitude of this injection non-uniformity was limited to small values by proper experiment-design criteria. The local gas-injection rates and superficial gas velocities were calculated, however, taking these variations of ϕ into account.

The deviation of local gas-injection rate from average ϕ for the test section was determined using the linear pressure drop versus ϕ relationship of Fig. 44, and assuming that the static-pressure drop in the test section is linear. The local superficial gas velocity was determined from the total gas input up to the local point in consideration as

$$U_g = \frac{W_g}{3600\,\rho_g(\pi/4)D^2}. \tag{49}$$

In Eq. (40), W_g is the sum of gas input into the mixer section, up to the point of calculation along the length of the heated section, the gas input in the heated section being determined using the average ϕ only for the length of the test section under consideration.

APPENDIX D

Accuracy of Heat-transfer Results

Since the purpose of the heat-transfer tests was to study the general behavior of two-phase heat transfer for various liquid and air flow conditions (rather than to determine average heat-transfer rates for design purposes), the precision and accuracy of the results were examined. Precision at a particular measurement point for a given test series was significant because, in this study, the relative variations in heat-transfer coefficient with a change of hydrodynamic conditions for a given test series were just as important as the absolute values.

All the errors involved were treated as uncertainties with consistent deviation limits and were combined statistically[65] to keep the initial and final deviation limits uniform. Since the individual errors were calculated for the most inaccurate or extreme experimental conditions, which did not necessarily occur together, they reflect the worst accuracy and precision that could be encountered, rather than normal values for average experimental conditions.

Heat-flux Error

Power input was calculated from current readings and resistance measurements of the test section. The calculations were checked by wattmeter and voltmeter measurements, and by heat-balance calculations on the fluid flowing through the test section. The maximum deviation of wattmeter measurements was 3%. Since the temperature rise of the fluid in many experiments was only several degrees Fahrenheit, some of the heat balances deviated by as much as 12% from power-input calculations.

The error in the net heat flux was calculated for the worst possible experimental conditions. The ammeter at the minimum reading was accurate to 1%, and the resistance measurements were also within 1%. The air heating and heat of vaporization losses were limited to 7% of the heat flux, and the local inhomogeneous heating effects were calculated to be about 3.5%. Assuming that these influences on heat flux could be determined with an accuracy of 20%, additional errors of 1.4 and 0.7%, respectively, could occur. Including the $\pm\frac{1}{3}\%$ fluctuation in power supply, the individual uncertainties were combined to give a total error of

$$\text{Error}_{\text{net heat flux}} = (2^2 + 1^2 + 1.4^2 + 0.7^2 + 0.33^2)^{1/2} = 2.75\%.$$

For relative-error, or precision, calculation the resistance and inhomogeneity uncertainties could be excluded, resulting in a combined error of only 2.5%.

Temperature Errors

The calibration accuracy of the liquid-inlet thermocouple, added to the potentiometer uncertainty, gave a possible error of 0.8°F in reading of liquid-inlet temperatures. For a maximum temperature rise of 15°F encountered in the test section, the calculated temperature rise could be in error by 0.5°F, because of the heat-flux and liquid-flow uncertainties, resulting in a combined error in local bulk temperature of 0.95°F.

The temperatures of the tube at its inside diameter were calculated from inside-wall thermocouple measurements. The reading error for these thermocouples was 0.8°F, due to the calibration and potentiometer inaccuracies. Results of Table II indicated that, due to error in location of the inside-wall thermocouple junction, the actual temperature difference between the junction and the I.D. surface could differ from the calculated value by as much as 20%. At the high heat flux of 8×10^4 Btu/(hr)(ft^2) used in the experiments, the location uncertainty could give an error of 2.4°F, resulting in an error of 2.5°F for surface temperatures.

The error in calculating the fluid-film temperature drop could therefore be

$$\text{Error}_{(t_w - t_b)} = (2.5^2 + 0.95^2)^{1/2} = 2.7°\text{F}.$$

This 2.7°F error results in a 9% accuracy error in calculating $(t_w - t_b)$ values for the minimum film temperature drops of 30°F encountered at heat fluxes of 8×10^4 Btu/(hr)(ft^2).

However, the precision for a given inside-wall thermocouple for the same conditions would be within 1.2°F, because the error due to junction location would not have to be considered. The resulting precision error in calculating $(t_w - t_b)$ values would therefore be only 4%.

Error in Heat-transfer Coefficient

Since the heat-transfer coefficient was calculated from

$$h = \frac{q''_{net}}{t_w - t_b},$$

the heat-flux and film-temperature-drop errors were combined to determine the accuracy and precision of heat-transfer-coefficient results. The accuracy and precision were found to be within 9.3 and 4.5%, respectively.

Flow-rate Errors

Air and liquid flow rates to the test sections were calculated as outlined in Appendix A. Since the error in orifice flow coefficient could be 2%, and the maximum manometer error for experimental conditions encountered could also be 2%, the accuracy of flow rate calculations was within 2.2%.

The gas-injection rate and superficial gas velocity were calculated as outlined in Appendix C. Combining the possible error of 2% in gas-density calculation, with the 2.2% flow-rate error, resulted in a combined error of 3% for both ϕ and U_g calculations. The accuracy of U_g/U_ℓ calculations was, consequently, within 3.7%.

Comparison of Water Heat-transfer Coefficients

Experimental forced-convection water heat-transfer coefficients found in the present tests were compared to published heat-transfer correlations to check the overall accuracy of the equipment and instrumentation.

The experimental water h_L values at thermocouple positions Nos. 2 and 3 were obtained when air flow to the test sections was shut off temporarily in the air-water tests. Measurements were made in the range of 5000 to 50,000 Reynolds' numbers for the water-flow rates used in the air-injection experiments.

The Sieder and Tate equation,

$$\frac{h_L D}{k_\ell} = 0.023(Re_L)^{0.8}(Pr_L)^{1/3}\left(\frac{\mu_b}{\mu_w}\right)^{0.14}, \qquad (50)$$

was used for calculating the liquid heat-transfer coefficient values for $Re_L > 10{,}000$. For $Re_L \sim 5000$, correlation curves recommended by Sieder and Tate[67] were used. The heat-transfer coefficients obtained from Sieder and Tate relationships were multiplied by Aladyev's[66] local-to-infinite L/D heat-transfer coefficient ratios to account for the entrance effects on heat transfer. Aladyev's results were used for the entrance-region corrections because his measurements were made for water flowing in a circular tube.

All the experimental heat-transfer coefficients obtained, as shown in Fig. 45, were found to be within 15% of the predicted values. Since the Sieder and Tate correlations predict heat-transfer rates only within ±20%, the comparison presented in Fig. 45 can be considered as good. Consequently, the overall accuracy of the heat-transfer experiments should be expected to be approximately within the limits specified.

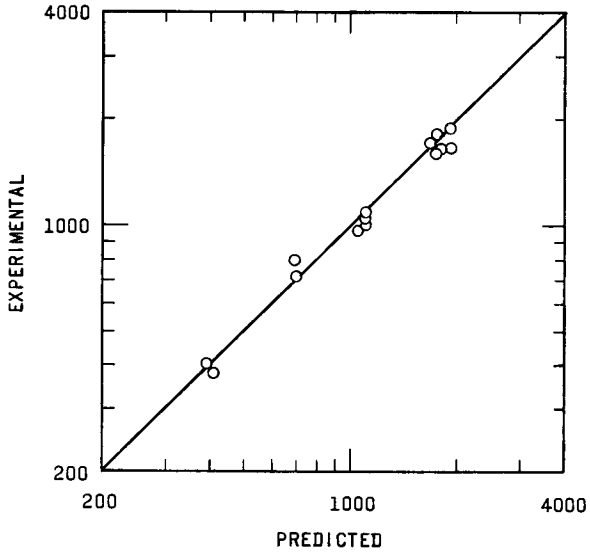

Fig. 45

Comparison of h_L's for Water

APPENDIX E

Heat-transfer Data

Table III

DATA FOR AIR-WATER STUDY WITH ø = 0

W_ℓ lb/hr	W_g Mixing Section lb/hr	q''_{net} x 10^{-4} Btu/(hr)(ft^2)	t_ℓ Inlet °F	t_w No. 2 °F	t_w No. 3 °F	P_{static} (Exit Heated Section) psia	Flow Pattern
480	48.5	4.95	72.4	105.1		16.7	annular
480	29.5	4.95	72.6	109.2		15.7	annular
480	22.0	4.95	72.5	111.7		15.5	annular
480	15.5	4.95	72.5	114.0		15.2	annular
480	9.9	4.95	72.7	115.6		15.0	slug
480	6.5	4.95	73.0	112.1		15.0	slug
480	5.15	4.95	72.4	111.9		15.0	slug
480	4.18	4.95	72.4	113.8	115.5	15.0	bubble
480	2.05	4.95	72.5	118.4	120.0	15.0	bubble
480	3.04	4.95	72.2	116.3	117.5	15.0	bubble
2160	68.5	7.13	71.3	99.8	101.2	27.7	annular
2160	56.0	6.10	73.6	97.8		23.7	annular
2160	43.0	6.10	73.4	98.7		22.7	annular
2160	30.4	6.10	73.8	99.8		20.7	annular
2160	21.0	6.10	73.9	100.4		19.7	froth
2160	13.3	6.10	73.9	103.1		19.2	froth
2160	9.0	6.10	73.9	107.6		18.7	froth
2160	3.75	6.10	74.1	109.7		17.2	bubble
2160	0.83	6.10	74.3	118.6		16.7	bubble
4320	1.11	6.0	74.6	106.6		19.7	bubble
4320	1.90	6.0	74.8	105.3		20.2	bubble
4320	3.24	6.0	74.1	103.6		20.7	froth
4320	4.68	6.0	74.1	102.4		21.7	froth
4320	6.24	6.0	74.1	101.9		22.4	froth

Table IV

DATA FOR AIR-ETHYLENE GLYCOL STUDY WITH ø = 0

q''_{net} = 1.77 x 10^4 Btu/(hr)(ft^2)

W_ℓ lb/hr	W_g Mixing Section lb/hr	t_ℓ Inlet °F	t_w No. 2 °F	t_w No. 3 °F	P_{static} (Exit Heated Section) psia	Flow Pattern
540	48.5	73.4	136.3	134.3	17.7	annular
540	36.7	73.1	139.1	138.1	17.2	annular
540	29.7	72.5	141.7	141.7	16.7	annular
540	22.0	72.9	146.6	145.7	16.5	annular
540	15.6	73.0	149.1	148.3	16.2	slug
540	9.85	73.2	146.6	147.1	16.1	slug
540	6.40	73.4	149.1	149.9	15.9	slug
540	5.20	72.8	150.8	150.8	15.7	slug
540	4.10	72.8	151.3	152.4	15.7	slug
540	3.04	73.0	152.8	153.2	15.7	bubble
540	1.87	73.2	157.1		15.7	bubble
540	0	73.1	272.1	263.1	15.7	-
2400	54.5	78.6	131.8	130.6	27.7	annular
2400	42.3	79.1	134.5	133.5	25.7	annular
2400	30.0	78.8	138.4	137.6	23.7	annular
2400	20.4	78.6	141.5	140.9	22.2	annular
2400	13.5	78.8	146.2	145.0	20.7	froth
2400	9.0	78.5	149.5	148.7	19.9	froth
2400	3.67	78.5	162.4	161.3	18.5	bubble
2400	0.80	78.6	174.1	171.3	17.9	bubble
2400	0	78.8	210.7	204.9	17.7	-

Table V

DATA FOR STUDY OF MASS VELOCITY EFFECTS

Liquid	W_ℓ lb/hr	W_g Mixing Section lb/hr	W_g Heated Section lb/hr	q''_{net} x 10^{-4} Btu/(hr)(ft^2)	t_ℓ Inlet °F	t_w No. 2 °F	t_w No. 3 °F	P_{static} Heated Section psi	P_{static} (Exit Heated Section) psia	Flow Pattern
Water	956	0.432	0.123	6.0	68.8	110.4	113.4	0.44	15.0	bubble
	1480	0.900	0.123	6.0	69.7	108.3	110.6	0.57	15.9	bubble
	1920	1.57	0.130	6.0	72.0	108.1	110.2	0.68	16.4	bubble
	2400	2.48	0.142	6.0	73.1	107.1	109.0	0.83	17.2	bubble
	2980	3.60	0.154	6.0	73.7	105.1	107.7	1.06	18.5	froth
	3580	5.07	0.169	6.0	74.1	103.4	106.1	1.25	20.3	froth
	4320	6.55	0.187	6.0	75.2	102.8	106.3	1.50	22.7	froth
Ethylene Glycol	1045	0.505	1.22	1.77	76.6	137.0	139.2	0.6	16.2	bubble
	1585	0.935	1.22	1.77	79.6	134.3	136.6	0.73	16.7	bubble
	1765	1.51	1.31	1.77	81.8	132.8	135.9	0.84	17.2	bubble
	2650	2.48	1.44	1.77	82.4	130.3	132.3	0.96	18.1	froth
	3220	3.42	1.55	1.77	82.7	128.5	130.2	1.1	19.3	froth
	3180	0	0	1.77	83.0	173.6	171.8	-	-	-
	3650	4.71	1.66	1.77	83.2	125.9	127.1	1.25	20.7	froth
	4230	5.40	1.75	1.77	83.4	125.8	127.2	1.4	23.2	froth
	4230	0	0	1.77	83.6	162.8	157.4	-	-	-

Table VI

DATA FOR STUDY OF AIR-ETHYLENE GLYCOL FLOW RATIO EFFECTS

W_g Mixing Section lb/hr	W_g Heated Section lb/hr	q''_{net} x 10^{-4} Btu/(hr)(ft^2)	t_ℓ Inlet °F	t_w No. 2 °F	t_w No. 3 °F	Δp_{static} Heated Section psi	p_{static} (Exit Heated Section) psia	Flow Pattern
			W_ℓ = 540 lb/hr					
48.5	1.51	1.77	73.4	121.4	122.5	0.73	17.9	annular
36.7	1.50	1.77	73.1	122.4	123.9	0.60	17.2	annular
29.7	1.46	1.77	72.5	123.5	125.1	0.52	16.8	annular
22.0	1.46	1.77	72.9	125.4	127.6	0.47	16.5	annular
15.6	1.46	1.77	73.0	127.2	129.3	0.42	16.2	slug
9.85	1.46	1.77	73.2	129.3	131.4	0.40	16.2	slug
6.40	1.46	1.77	73.4	130.8	132.2	0.40	16.0	slug
5.20	1.46	1.77	72.8	131.4	132.6	0.40	15.7	slug
4.10	1.46	1.77	72.8	131.1	132.4	0.40	15.7	slug
3.04	1.46	1.77	73.0	131.7	131.8	0.40	15.7	slug
1.87	1.46	1.77	73.2	133.6	134.6	0.40	15.7	bubble
0	1.46	1.77	73.1	139.9	141.6	0.42	15.7	bubble
0.74	8.3	1.74	73.3	120.2	122.3	0.50	16.2	slug
3.4	8.3	1.74	73.3	119.3	121.5	0.50	16.2	slug
6.05	8.3	1.74	73.2	118.5	120.6	0.52	16.2	slug
10.40	8.3	1.74	73.1	117.4	119.4	0.54	16.2	slug
18.0	8.3	1.74	73.1	116.1	118.3	0.65	16.6	annular
35.0	8.6	1.74	73.1	113.8	115.8	0.85	17.4	annular
48.0	8.7	1.74	73.2	113.5	115.5	1.05	18.2	annular
			W_ℓ = 2400 lb/hr					
54.5	2.34	1.77	78.6	118.6	119.5	1.38	27.7	annular
42.3	2.10	1.77	79.1	119.7	120.6	1.23	25.7	annular
30.0	1.95	1.77	78.8	121.1	122.7	1.10	23.7	annular
20.4	1.82	1.77	78.6	121.8	123.2	1.03	22.2	annular
13.5	1.78	1.77	78.8	123.6	125.3	0.97	20.7	froth
9.0	1.73	1.77	78.5	124.1	126.2	0.86	19.9	froth
3.67	1.57	1.77	78.5	128.1	129.8	0.87	18.5	froth
0.80	1.57	1.77	78.6	129.9	131.7	0.935	17.9	bubble
0	1.57	1.77	78.8	131.0	133.1	0.915	17.7	bubble
0.80	10.2	1.74	78.5	116.6	121.0	1.54	19.7	froth
3.80	10.2	1.74	78.3	117.0	121.0	1.45	20.2	froth
6.65	10.2	1.74	78.4	116.1	120.0	1.44	20.7	annular
10.1	10.4	1.74	78.6	116.2	119.3	1.45	21.4	annular
16.6	10.8	1.74	78.8	116.1	118.9	1.60	24.7	annular
31.0	11.2	1.74	79.0	116.2	118.2	1.74	25.9	annular
56.5	11.9	1.74	79.2	115.3	116.6	1.95	29.5	annular

Table VII

DATA FOR STUDY OF AIR-WATER FLOW RATIO EFFECTS

W_g Mixing Section lb/hr	W_g Heated Section lb/hr	I amps	t_ℓ Inlet °F	t_w No. 2 °F	t_w No. 3 °F	t_w No. 6 °F	t_w No. 7 °F	Δp_{static} Heated Section psi	p_{static} (Exit Heated Section) psia	Flow Pattern
				W_ℓ = 480 lb/hr						
48.5	1.51	3.92	72.4	101.8	102.8	91.3	91.3	0.60	17.2	annular
29.5	1.48	3.92	72.6	103.4	104.6	93.3	93.7	0.35	16.2	annular
22.0	1.47	3.92	72.5	105.3	106.6	95.3	95.7	0.31	15.9	annular
15.5	1.47	3.92	72.5	106.6	108.1	96.7	97.0	0.28	15.7	annular
9.9	1.47	3.92	72.7	109.7	110.8	98.7	98.0	0.28	15.5	slug
6.5	1.44	3.92	73.0	112.1	112.1	99.0	97.3	0.40	15.0	slug
5.15	1.44	3.92	72.4	111.0	111.0	98.7	98.0	0.40	15.0	slug
4.18	1.44	3.92	72.4	111.8	112.1	100.2	98.7	0.40	15.0	slug
2.05	1.44	3.92	72.5	111.7	112.6	101.6	101.3	0.30	15.0	bubble
0	1.44	3.92	72.4	114.6	116.0	106.5	108.4	0.28	15.0	bubble
8.2	8.3	3.92	69.2	109.0	110.9	98.0	97.7	0.5	15.3	annular
18.0	8.3	3.92	69.2	106.3	105.9	93.8	94.3	0.54	15.7	annular
1.13	8.3	4.34	70.2	121.1	121.5	105.8	107.4	0.4	15.0	slug
3.4	8.3	4.34	71.0	123.0	123.7	106.9	106.3	0.45	15.0	slug
6.0	8.3	4.34	71.0	121.3	123.7	106.5	105.8	0.50	15.0	annular
8.1	8.3	4.34	69.7	117.7	119.9	104.7	105.0	0.50	15.7	annular
18.0	8.3	4.34	70.6	115.6	115.6	100.9	101.5	0.45	15.8	annular
42.2	8.4	4.34	70.2	111.3	111.2	96.7	97.9	0.83	17.2	annular
86.0	8.4	4.34	69.4	108.7	107.9	93.9	92.9	1.4	21.0	annular
				W_ℓ = 2160 lb/hr						
56.0	2.22	4.37	73.6	100.4	101.6	90.2	91.6	1.18	24.7	annular
43.0	2.17	4.37	73.4	101.3	102.6	91.0	92.2	0.97	23.2	annular
30.4	1.91	4.37	73.8	101.6	102.9	91.6	93.2	0.79	21.5	annular
21.0	1.75	4.37	73.9	101.7	103.3	92.3	94.8	0.80	19.7	annular
13.3	1.72	4.37	73.9	107.3	110.6	96.1	98.1	1.30	19.3	froth
9.0	1.70	4.37	73.9	108.9	111.9	97.8	99.3	1.16	18.7	froth
3.75	1.56	4.37	74.1	108.4	110.5	99.0	101.0	0.90	17.3	froth
0.83	1.56	4.37	74.3	109.3	111.2	102.0	104.1	0.73	16.7	bubble
0	1.56	4.37	74.5	110.5	112.3	103.6	106.5	0.70	16.7	bubble
10.6	10.4	4.56	70.6	120.1	118.8	102.2	101.8	2.10	19.1	froth
16.6	10.4	4.56	70.2	115.3	115.9	100.2	100.7	1.95	19.2	annular
31.5	10.8	4.56	70.6	111.6	109.4	96.2	95.2	2.10	21.2	annular
63.6	11.4	4.62	70.6	112.0	107.2	94.5	91.7	2.06	33.7	annular
1.12	10.1	4.62	70.6	114.3	113.0	100.6	101.5	1.71	18.7	froth
3.8	10.1	4.62	70.6	118.2	116.6	102.7	102.0	1.35	19.2	froth
6.74	10.3	4.62	70.6	119.6	118.4	102.9	101.9	1.95	19.3	froth
				W_ℓ = 4320 lb/hr						
1.11	1.75	4.32	74.6	101.1	104.1	95.2	98.5	1.12	19.7	bubble
1.90	1.75	4.32	74.8	101.8	105.3	95.5	98.7	1.15	20.2	bubble
3.24	1.82	4.32	74.1	101.5	104.8	94.8	98.1	1.23	20.7	froth
4.68	1.85	4.32	74.1	101.9	105.3	94.5	97.5	1.33	21.7	froth
6.24	1.93	4.32	74.1	101.9	105.4	94.7	97.6	1.44	22.4	froth

Table VIII

DATA FOR STUDY OF INJECTION EFFECTS IN ETHYLENE GLYCOL

W_g Mixing Section lb/hr	W_g Heated Section lb/hr	q''_{net} x 10^{-4} Btu/(hr)(ft^2)	t_ℓ Inlet °F	t_w No. 2 °F	t_w No. 3 °F	Δp_{static} Heated Section psi	P_{static} (Exit Heated Section) psia	Flow Pattern
			W_ℓ = 540 lb/hr					
0	2.27	1.77	73.1	130.1	130.2	0.47	15.7	bubble
0.51	1.73	1.77	73.4	133.3	134.0	0.47	15.7	bubble
0.84	1.21	1.77	72.0	135.1	135.3	0.42	15.7	bubble
1.22	0.75	1.77	72.0	137.6	139.2	0.42	15.7	bubble
1.82	0	1.77	72.1	154.3	159.0		15.7	bubble
27.5	0	1.77	72.6	140.2	138.8	0.50	16.7	annular
25.8	1.95	1.77	72.6	119.9	119.2	0.50	16.7	annular
23.5	4.56	1.75	72.6	115.8	115.0	0.60	16.7	annular
21.8	6.76	1.75	72.6	113.5	113.2	0.64	16.7	annular
20.0	9.50	1.72	72.5	110.1	110.6	0.70	16.7	annular
16.2	14.0	1.72	72.5	107.4	108.3	0.73	16.7	annular
11.9	18.6	1.72	72.6	105.3	106.0	0.73	16.7	annular
8.6	23.4	1.69	72.6	104.0	104.4	0.75	16.7	annular
			W_ℓ = 2400 lb/hr					
0	2.53	1.77	81.3	129.3	131.1	1.06	17.7	froth
0.72	1.74	1.77	81.5	131.0	132.6	0.96	17.5	froth
1.08	1.30	1.77	81.1	132.2	134.7	0.90	17.4	froth
1.52	0.76	1.77	81.4	135.3	138.0	0.82	17.4	froth
2.16	0	1.77	81.6	165.3	165.1	0.80	17.7	bubble
28.1	0	1.77	78.7	136.8	137.2	1.02	23.4	annular
26.7	1.82	1.77	78.7	121.7	122.8	1.15	23.2	annular
25.5	3.60	1.77	78.7	119.0	120.6	1.35	23.1	annular
23.1	6.55	1.77	78.7	117.7	120.0	1.43	23.1	annular
21.0	9.15	1.75	78.5	115.6	117.8	1.58	23.2	annular
18.3	12.40	1.73	78.5	113.6	116.6	1.68	23.2	annular
13.3	18.20	1.70	78.5	109.5	113.7	1.80	23.4	annular
8.2	24.70	1.67	78.5	106.6	110.6	1.98	23.9	annular
3.35	28.8	1.65	78.7	104.8	108.6	2.24	23.6	annular

Table IX

DATA FOR STUDY OF INJECTION EFFECTS IN WATER

W_g Mixing Section lb/hr	W_g Heated Section lb/hr	t_ℓ Inlet °F	t_w No. 2 °F	t_w No. 3 °F	t_w No. 6 °F	t_w No. 7 °F	Δp_{static} Heated Section psi	P_{static} (Exit Heated Section) psia	Flow Pattern
			W_ℓ = 1080 lb/hr		I = 4.32 Amps				
17.7	32.4	69.3	100.2	103.7	91.8	98.5	1.7	19.7	annular
25.6	25.3	69.5	103.1	106.8	92.4	98.5	1.6	19.7	annular
30.4	18.0	69.3	105.9	109.0	93.9	97.6	1.5	19.2	annular
34.2	12.7	68.9	108.1	108.9	95.0	96.3	1.4	19.2	annular
38.2	8.1	68.9	108.3	107.8	92.5	94.6	1.25	19.2	annular
3.35	8.9	68.9	117.5	116.1	102.1	101.7	1.05	19.2	froth
43.0	4.45	68.6	104.6	104.3	92.9	92.0	1.15	19.1	froth
12.8	0	68.9	107.6	110.1	96.1		0.55	16.3	froth
11.9	0.91	69.3	107.9	110.4	96.6	97.7	0.50	16.3	froth
11.4	1.28	69.3	108.7	111.2	97.1	97.7	0.60	16.2	froth
10.3	3.13	69.1	111.6	111.4	97.3	96.5	0.90	16.3	froth
7.9	6.22	69.3	116.1	114.4	100.3	98.2	1.12	16.7	froth
5.15	10.10	70.0	116.1	114.8	100.9	100.8	1.14	16.4	froth
0.9	15.8	70.0	106.4	108.7	97.0	100.4	1.0	16.7	froth
0.36	3.4	69.7	109.4	110.7	100.8	102.3	0.65	15.9	bubble
0.80	2.34	69.7	109.9	111.5	101.5	102.3	0.55	15.7	bubble
1.62	1.25	70.0	109.6	112.3	101.6	102.7	0.45	15.9	bubble
1.96	0.78	70.2	110.4	113.7	102.9	103.8	0.45	15.7	bubble
2.50	0	70.2	115.6	119.4	105.1		0.45	15.7	bubble
			W_ℓ = 480 lb/hr		I = 3.92 Amps				
0	2.9	71.0	111.0	111.2	101.9	105.4	0.36	15.0	bubble
0.74	2.02	71.4	111.9	112.5	102.6	102.2	0.34	15.0	bubble
1.37	1.21	71.3	110.9	112.5	102.0	101.9	0.30	15.0	bubble
1.80	0.75	71.3	110.5	112.5	101.7	101.7	0.28	15.0	bubble
2.34	0	71.5	116.7	118.4			0.30	15.0	bubble
			W_ℓ = 4320 lb/hr		I = 4.32 Amps				
0	2.5	72.8	99.7	101.9	92.7	95.9	1.27	20.2	froth
0.86	1.56	72.9	99.3	103.0	93.8	97.2	1.1	19.4	froth
1.21	1.05	73.0	99.1	103.2	94.4	98.2	1.0	19.4	froth
2.11	0	73.0	103.5	107.5			1.0	19.7	froth
			W_ℓ = 2160 lb/hr		I = 4.35 Amps				
0	2.6	71.2	107.4	108.4	99.8	101.5	0.86	15.0	bubble
0.76	1.75	70.7	107.0	108.4	98.9	101.0	0.76	16.7	bubble
1.08	1.3	70.6	106.9	108.7	99.2	101.1	0.70	16.7	bubble
1.55	0.76	70.5	106.5	109.1	99.6	101.9	0.65	16.7	bubble
2.12	0	70.4	111.1	-	-	-		16.7	bubble
			W_ℓ = 1080 lb/hr		I = 4.30 Amps				
0.36	3.40	69.7	109.4	110.7	100.8	102.3	0.65	16.0	bubble
0.79	2.36	69.7	109.9	111.5	101.5	102.3	0.55	16.0	bubble
1.62	1.25	70.0	109.6	112.3	101.6	102.7	0.45	16.0	bubble
1.96	0.75	70.2	110.4	113.7	102.9	103.8	0.45	16.0	bubble
2.47	0	70.2	115.6	119.4	105.1	-	0.45	16.0	bubble

Table X

DATA FOR LIQUID WATER TESTS

W_ℓ lb/hr	$q''_{net} \times 10^{-4}$ Btu/(hr)(ft^2)	t_ℓ Inlet °F	t_w No. 2 °F	t_w No. 3 °F
480	4.95	72.4	207.4	213.1
1080	7.9	72.6	180.8	190.3
2160	6.0	71.3	128.7	133.8
2160	6.1	74.5	110.5	112.3
4280	7.5	82.3	124.0	130.1
4300	7.4	69.2	112.2	116.3
4320	6.0	74.1	109.1	113.3

APPENDIX F

Void-fraction Data

Table XI

VOID-FRACTION DATA AT W_ℓ = 480 lb/hr

Position*	W_g Mixing Section lb/hr	W_g Heated Section lb/hr	Constants in Eq. (1) $\bar{\alpha}$	d	a	b	c
1	0	1.57	0.560	0.462	-1.31	4.58	-3.1
2			0.616	0.765	-0.18	-2.23	2.0
1	0	1.06	0.440	0.8	2.0	-6.14	5.6
			0.545	0.537	1.06	-4.77	4.27
1	0	4.64	0.780	0.38	3.16	-7.21	4.9
2			0.800	0.99	0.01	-1.47	1.2
3	0	1.30	0.573	0.83	-0.028	0.033	-1.02
1	3.85	1.54	0.770	0.71	1.74	-3.92	1.96
2			0.605	0.91	-0.67	0.60	-0.67
1	12.7	4.28	0.923	0.91	0.75	-2.08	1.33
2			0.855	0.93	0.103	-1.38	1.32
1	1.08	1.05	0.753	0.90	-0.64	0.11	0.54
2			0.710	1.23	-3.22	7.84	-6.09
1	3.25	3.28	0.830	-	-	-	-
2			0.865	0.767	3.72	-12.5	9.57
1	6.4	4.8	0.785	0.74	1.8	-4.6	2.73
2			0.770	1.09	-1.47	3.44	-3.04

Table XII

VOID-FRACTION DATA AT W_ℓ = 1080 lb/hr

Position*	W_g Mixing Section lb/hr	W_g Heated Section lb/hr	Constants in Eq. (1) $\bar{\alpha}$	d	a	b	c
3	0	0.57	0.240	0.26	-1.4	6.1	-5.4
1	0	2.26	0.450	-0.063	2.18	-3.5	2.35
2			0.590	0.432	1.66	-4.28	3.01
1	1.65	1.62	0.566	-	-	-	-
2			0.570	0.57	0.312	-2.7	2.90
1	1.67	1.65	0.557	0.38	1.92	-5.33	4.0
2			0.574	0.77	-0.47	0.76	-0.906
1	3.8	1.50	0.670	0.59	1.14	-2.66	1.56
2			0.675	1.04	-1.12	2.0	-1.98
1	4.9	4.7	0.755	0.66	1.04	-1.3	-0.041
2			0.785	1.11	-1.5	1.8	-0.76
1	12.9	12.5	0.836	0.97	-1.35	2.03	-0.54
2			0.864	0.99	-0.23	-0.097	0.003
1	6.3	6.3	0.800	0.883	-1.08	3.68	-3.07
2			0.763	0.90	-0.21	-0.28	0.25
1	25.3	4.35	0.900	0.916	0.88	-2.44	1.41
2			0.854	0.96	-0.72	2.0	-1.64
1	1.15	1.15	0.584	0.566	-0.383	0.074	0.74
2			0.575	0.84	-1.97	6.31	-5.54

Table XIII

VOID-FRACTION DATA AT W_ℓ = 2160 lb/hr

Position*	W_g Mixing Section lb/hr	W_g Heated Section lb/hr	Constants in Eq. (1) $\bar{\alpha}$	d	a	b	c
3	0	1.67	0.377	0.205	0.433	1.6	-2.3
1	0	2.20	0.484	0.046	1.69	-2.85	2.18
2			0.340	-0.11	3.15	-8.0	6.15
1	0	2.20	0.320	-0.01	1.65	-0.86	0.1
2			0.412	0.103	0.94	-0.238	-0.331
1	0	10.8	0.548	-0.010	1.64	-0.865	0.097
2			0.740	0.514	1.72	-4.63	3.63
1	0	4.40	0.321	0.37	-5.82	25.5	-22.6
2			0.541	0.34	-0.474	2.81	-2.00
1	0	6.18	0.374	0.338	-5.03	23.3	-20.9
2			0.620	0.367	1.36	-2.96	2.22
1	1.72	1.50	0.393	0.185	0.31	1.32	-1.55
2			0.382	0.35	-0.53	3.32	-3.27
1	6.40	4.75	0.703	0.53	0.84	-1.03	0.38
2			0.709	0.94	-1.63	5.5	-5.05
1	12.5	6.25	0.786	0.687	0.322	0.66	-1.13
2			0.780	0.92	-0.048	-1.13	0.96
1	18.9	12.5	0.834	0.802	-0.122	0.209	0.10
2			0.836	0.97	-0.09	-0.47	0.17
1	15.7	12.9	0.855	0.673	0.524	0.364	-0.785
2			0.835	0.805	0.033	-0.7	1.08
1	3.12	3.23	0.573	0.527	-0.55	1.81	-1.13
2			0.640	0.755	-1.42	5.1	-4.4

Table XIV

VOID-FRACTION DATA AT W_ℓ = 4320 lb/hr

Position*	W_g Mixing Section lb/hr	W_g Heated Section lb/hr	Constants in Eq. (1) $\bar{\alpha}$	d	a	b	c
3	0	1.17	0.200	0.112	-0.23	2.25	-2.13
1	0	4.55	0.221	0.29	-4.16	18.5	-16.6
2			0.392	0.141	-0.69	4.51	-3.62
1	12.7	4.65	0.693	0.517	0.177	1.47	-1.60
2			0.735	0.80	-1.68	5.12	-3.7
1	23.9	6.20	0.743	0.566	0.414	0.944	-1.37
2			0.745	0.90	-1.68	5.44	-4.56
1	1.61	1.53	0.335	0.235	-0.49	2.88	-2.45
2			0.338	0.138	0.35	2.46	-3.18
1	3.45	2.23	0.450	0.312	-0.30	4.25	-4.47
2			0.461	0.306	-0.152	3.45	-3.71
1	7.30	4.70	0.635	0.504	-1.24	7.0	-6.3
2			0.658	0.547	0.552	-0.43	-0.08
1	3.92	3.95	0.471	0.392	-1.26	3.60	-1.95
2			0.525	0.471	-0.25	2.4	-2.5

* The positions used for void-fraction tests were as follows:

No. 1: 4-1/4 in. from entrance to heated section (No. 6 thermocouple position).
No. 2: 9-7/8 in. from entrance to heated section (No. 2 thermocouple position).
No. 3: 9 in. after exit from heated section (in the observation section).

ACKNOWLEDGMENTS

This study was carried out with the financial support of the United States Atomic Energy Commission at Argonne National Laboratory under the Associated Midwest Universities program.

The author gratefully acknowledges the help he received during the course of this study, especially from the following persons: Professor V. E. Bergdolt, who initiated and encouraged this study; Dr. Michael Petrick, who aided with valuable suggestions and helpful criticisms; Professor R. J. Grosh, for taking over as major professor; Professor P. W. McFadden, for his helpful suggestions and patient review of the study.

The author is especially grateful to Jay Norco and also George Lambert for the fine job of constructing the apparatus, and for valuable help with experiments and data reduction. He is also grateful to Leonard Indykiewicz for his help in taking data, and to the other members of the Heat Engineering Section of Argonne National Laboratory's Reactor Engineering Division, for their readiness to help and assist him at all times.

Thanks are also due to Sue Catilavas, for her valuable aid with the computer programs, and to Michael Sims, for his expert help in preparing and editing the illustrations.

The author extends his thanks to Mrs. Marjorie Luebs for typing the manuscript.

BIBLIOGRAPHY

1. N. Zuber and E. Fried, Two-phase Flow and Boiling Heat Transfer to Cryogenic Liquids, Am. Rocket Soc. J., 32, 1332-1341 (1962).
2. G. B. Wallis, The Analogy between the Bubbling of Air into Water and Nucleate Boiling at Saturation Temperature, UKAEA Report, AEEW-R28 (1960).
3. G. B. Wallis, A Gas-liquid Analogue of Nucleate Boiling, Nuclear Power, 5, 99-101 (1960).
4. N. Zuber, Hydrodynamic Aspects of Boiling Heat Transfer, AECU-4439 (1959).
5. J. G. Collier, A Review of Two-phase Heat Transfer (1935-1957), UKAEA Report, AERE CE/R-2496 (1958).
6. P. A. Lottes et al., Boiling Water Reactor Technology - Status of the Art Report - Vol. I. Heat Transfer and Hydraulics, ANL-6561 (1962).
7. J. W. Westwater, "Things We Don't Know about Boiling Heat Transfer," Research in Heat Transfer, Pergamon Press, London, 61-72 (1963).
8. J. A. R. Bennett, Two-phase Flow in Gas-liquid Systems - A Literature Survey, UKAEA Report, AERE CE/R-2497 (1958).
9. W. A. Gresham et al., Review of the Literature on Two-phase (Gas-liquid) Fluid Flow in Pipes, WADC-TR-55-422 (1955).
10. J. Jacobs, Heat Transfer and Fluid Flow, TID-3305 (1958).
11. G. B. Wallis, Some Hydrodynamic Aspects of Two-phase Flow and Boiling, Proc. 1961 International Heat Transfer Conference, Part II, Am. Soc. Mech. Engrs., New York, 1961, 319-340.
12. F. O. Mixon, W. Y. Chon, and K. O. Beatty, Jr., The Effect of Electrolytic Gas Evolution on Heat Transfer, Chem. Eng. Progr., 55, 49-53 (1959).
13. E. E. Gose, A. Acrivos, and E. E. Petersen, Heat Transfer to Liquids with Gas Evolution at the Interface, Mexico City meeting, Am. Inst. Chem. Engrs. (1960).
14. G. E. Sims, U. Akturk, and K. O. Evans-Lutterodt, Simulation of Pool Boiling Heat Transfer by Gas Injection at the Interface, Int. J. Heat and Mass Transfer, 6, 531-535 (1963).
15. S. S. Kutateladze, Heat Transfer in Condensation and Boiling, AEC-tr-3770 (1952).
16. J. H. Vohr, Flow Patterns of Two-phase Flow - A Survey of Literature, TID-11514 (1960).

17. Y. Y. Hsu and R. W. Graham, A Visual Study of Two-phase Flow in a Vertical Tube with Heat Addition, NASA-TN-D-1564 (1963).

18. E. R. Hosler, Visual Study of Boiling at High Pressure, AICHE Preprint No. 10, presented at the Sixth Nat. Heat Transf. Conf., Boston (1963).

19. G. B. Wallis and P. Griffith, Liquid and Gas Distributions in a Two-phase Boiling Analogy, Mass. Inst. Techn. Tech. Rept. No. 13 (1958).

20. H. Verschoor and S. Stemerding, Heat Transfer in Two-phase Flow, Proc. General Discussion on Heat Transfer, Inst. Mech. Engrs., London, 201-204 (1951).

21. H. Groothuis and W. P. Hendal, Heat Transfer in Two-phase Flow, Chem. Eng. Science, 11, 212-220 (1959).

22. R. F. Knott et al., An Experimental Study of Heat Transfer to Nitrogen-Oil Mixtures, Ind. and Eng. Chemsitry, 51, 1369-1372 (1959).

23. H. A. Johnson and A. H. Abou-Sabe, Heat Transfer and Pressure Drop for Turbulent Flow of Air-Water Mixtures in a Horizontal Pipe, Trans. Am. Soc. Mech. Engrs., 74, 977-987 (1952).

24. H. A. Johnson, Heat Transfer and Pressure Drop for Viscous-Turbulent Flow of Oil-Air Mixtures in a Horizontal Pipe, Trans. Am. Soc. Mech. Engrs., 77, 1257-1264 (1955).

25. M. Jakob, Heat Transfer, 1, Chaps. 26 and 29, John Wiley and Sons, New York (1959).

26. F. C. Gunther and F. Kreith, Photographic Study of Bubble Formation in Heat Transfer to Subcooled Water, Heat Transfer and Fluid Mechanics Institute, Berkeley, Calif. (1949).

27. W. M. Rohsenow and J. A. Clark, A Study of the Mechanism of Boiling Heat Transfer, Trans. Am. Soc. Mech. Engrs., 73, 609-620 (1951).

28. N. Zuber, Nucleate Boiling. The Region of Isolated Bubbles and the Similarity with Natural Convection, Int. J. Heat and Mass Transfer, 6, 53-78 (1963).

29. K. Nishikawa and K. Yamagata, On the Correlation of Nucleate Boiling Heat Transfer, Int. J. Heat and Mass Transfer, 1, 219-235 (1960).

30. K. Engelberg-Forster and R. Greif, Heat Transfer to a Boiling Liquid - Mechanism and Correlations, Trans. Am. Soc. Mech. Engrs., J. of Heat Transfer, 81, 43-53 (1959).

31. H. J. Ivey and D. J. Morris, On the Relevance of the Vapor-Liquid Exchange Mechanism for Subcooled Boiling Heat Transfer at High Pressure, UKAEA Report, AEEW-R137 (1962).

32. F. D. Moore and R. B. Mesler, The Measurement of Rapid Surface Temperature Fluctuations during Nucleate Boiling of Water, Am. Inst. Chem. Engrs. J., 7, 620-624 (1961).

33. S. G. Bankoff, A Note on Latent Heat Transport in Nucleate Boiling, Am. Inst. Chem. Engrs. J., 8, 63-65 (1962).

34. J. F. Mumm, Heat Transfer to Boiling Water Forced through a Uniformly Heated Tube, ANL-5276 (1954).

35. V. V. Bogdanov, Investigation of the Effect of the Rate of Motion of the Water Current on the Heat Exchange Coefficient on Boiling in an Inclined Tube, Izvest. Akad. Nauk, Otdelenie Tekn. Nauk, No. 4, 136-140 (1955); UKAEA Translation, AERE-596 (1955).

36. L. S. Sterman and N. G. Styushin, Investigation of Heat Exchange in the Boiling of a Liquid in Pipes, Teploperedacha I Aerodinakika, Trudy UKTI, 21 (1951); taken from (5).

37. L. S. Sterman, Investigation of Heat Exchange in the Boiling of a Liquid in Pipes, Zhurnal Tekn. Fiziki, 24, 2046-2053 (1954); UKAEA Translation, AERE-565 (1955).

38. G. H. Anderson, G. G. Haselden, and B. G. Mantzouranis, Two-phase (Gas-Liquid) Flow Phenomena - IV, Chem. Eng. Sci., 17, 751-769 (1962).

39. S. A. Guerrieri and R. D. Talty, A Study of Heat Transfer to Organic Liquids in Single-tube, Natural-circulation, Vertical-tube Boilers, Chem. Eng. Progr. Symp. Series, No. 18, 52, 69-72.

40. J. G. Collier and D. J. Pulling, Heat Transfer to Two-phase Gas-Liquid Systems, UKAEA Report, AERE-R3809 (1962).

41. J. F. Marchaterre and B. M. Hoglund, Correlation for Two-phase Flow, Nucleonics, 20, 142 (1962).

42. M. Petrick, A Study of Vapor Carryunder and Associated Problems, ANL-6581 (1962).

43. H. Christensen, Power-to-void Transfer Functions, ANL-6385, (1961).

44. S. G. Bankoff, A Variable Density Single-fluid Model for Two-phase Flow with Particular Reference to Steam-Water Flow, Trans. ASME, J. Heat Transfer, 82, Series C, 265-272 (1960).

45. H. S. Isbin et al., Heat Transfer to Steam-Water Flows, Proc. 1961 Heat Transfer and Fluid Mechanics Institute, Stanford Univ. Press, 70 (1961).

46. E. R. Bartle, Preparation for Mass Transfer Cooling Experiments in a Turbulent Boundary Layer, Convair Sci. Res. Lab. Memorandum, June, 1959.

47. H. H. Hooker and G. F. Popper, A Gamma-ray Attenuation Method for Void Fraction Determinations in Experimental Boiling Heat Transfer Test Facilities, ANL-5766 (1958).

48. M. Petrick and B. S. Swanson, Radiation Attenuation Method of Measuring Density of a Two-phase Fluid, Rev. Sci. Instr., 29, 1079-1085 (1958).

49. Glycols, Union Carbide Chemicals Co., New York, Form-4763G (1961).

50. B. L. Richardson, Some Problems in Horizontal Two-phase Flow, ANL-5949 (1958).

51. G. F. Hewitt et al., Burnout and Nucleation in Climbing Film Flow, UKAEA Report, AERE-R4374 (1963).

52. J. G. Knudsen and D. L. Katz, Fluid Dynamics and Heat Transfer, McGraw-Hill Book Co., New York, 394 (1958).

53. R. W. Lockhart and R. C. Martinelli, Proposed Correlation of Data for Isothermal Two-phase, Two-component Flow in Pipes, Chem. Eng. Progr., 45, 39-48 (1949).

54. C. F. Gunther, Photographic Study of Surface-boiling Heat Transfer to Water with Forced Convection, Trans. Am. Soc. Mech. Engrs., 73, 115-123 (1951).

55. W. Siemes and E. Borchers, On Bubble Sizes in Bubble Columns, Chem. Eng. Sci., 12, 77-87 (1960).

56. M. Hirata, Diameters and Slip Velocities of Air Bubbles Injected from a Hole into Water Flow in a Horizontal Channel, Univ. of Minnesota Heat Transfer Lab. Rept., HTL TR No. 53 (Aug 1963).

57. R. F. Gaertner, Photographic Study of Nucleate Pool Boiling on a Horizontal Surface, Am. Soc. Mech. Engrs. Paper No. 63-WA-76 (1963).

58. N. Zuber and J. Hench, Steady State and Transient Void Fractions of Bubbling Systems and Their Operation Limits, Part I: Steady State Operation, General Electric Report, 62 GL 100 (July 1962).

59. W. H. McAdams, Heat Transmission, 3rd. Ed., McGraw-Hill Book Co., 378 (1954).

60. R. F. Gaertner and J. W. Westwater, Novel Method for Determining Nucleate Boiling Sites, Chem. Eng. Progr., 55, 58-61 (1959).

61. W. R. Gambill and R. D. Bundy, High-flux Heat-transfer Characteristics of Pure Ethylene Glycol in Axial and Swirl Flow, Am. Inst. Chem. Engrs. J., 9, 55-59 (1963).

62. Fluid Meters - Their Theory and Application, Am. Soc. Mech. Engrs., New York (1959).

63. P. Grootenhuis, R. W. Powell, and R. P. Tye, Thermal and Electrical Conductivity of Porous Metals Made by Powder Metallurgy Methods, Proc. Phys. Soc. London, 65, Sect. B., 502-511 (1952).

64. P. Grootenhuis, The Mechanism and Application of Effusion Cooling, J. Roy. Aeronaut. Soc., 63, 73-89 (1959).

65. S. J. Kline and F. A. McClintock, Describing the Uncertainties in Single-sample Experiments, Mech. Eng., 75, 3-8 (1953).

66. Ref. 52, p. 400.

67. Ref. 52, p. 395.

Price $2.50 . *Available from the Office of Technical Services, Department of Commerce, Washington 25, D.C.*